RADC-TR-72-109
Technical Report
May 1972

A DETAILED ANALYTICAL AND EXPERIMENTAL INVESTIGATION OF AN INCLINED END FIRE RECEIVING RHOMBIC ANTENNA ARRAY

Approved for public release;
distribution unlimited.

Rome Air Development Center
Air Force Systems Command
Griffiss Air Force Base, New York

R99

UNCLASSIFIED

Security Classification

DOCUMENT CONTROL DATA - R & D

(Security classification of title, body of abstract and indexing annotation must be entered when the overall report is classified)

1 ORIGINATING ACTIVITY (Corporate author)

Rome Air Development Center (OCTA)
Griffiss Air Force Base, New York 13440

2a. REPORT SECURITY CLASSIFICATION

Unclassified

2b. GROUP

N/A

3 REPORT TITLE

A DETAILED ANALYTICAL AND EXPERIMENTAL INVESTIGATION OF AN INCLINED END FIRE RECEIVING RHOMBIC ANTENNA ARRAY

4 DESCRIPTIVE NOTES (Type of report and inclusive dates)

Final - 1969 - 1970 In-House

5 AUTHOR(S) (First name, middle initial, last name)

Edward J. Christopher

6 REPORT DATE	7a. TOTAL NO OF PAGES	7b. NO OF REFS
May 1972	93	7

8a Job Order Number	9a. ORIGINATOR'S REPORT NUMBER(S)
45060000	RADC-TR-72-109
b.	
c.	9b. OTHER REPORT NO(S) (Any other numbers that may be assigned this report)
d.	

10 DISTRIBUTION STATEMENT

Approved for public release; distribution unlimited.

11 SUPPLEMENTARY NOTES	12 SPONSORING MILITARY ACTIVITY
RADC Project Engineer Edward J. Christopher Area Code 315 330-2443	Rome Air Development Center (OCTA) Griffiss Air Force Base, New York 13440

13 ABSTRACT

This report provides an account of a new rhombic antenna array design and the resultant effect upon the antenna pattern resulting from this design.

The intent of this effort was twofold, first to reduce the deep nulls in the vertical profile that existed with a horizontal single rhombic in order to obtain smooth vertical coverage from 2° to 24° in elevation and secondly, to reduce the first side lobe levels in the horizontal plane pattern of a single rhombic antenna. The first objective was obtained by inclining the rhombic antenna approximately 8°. The factors responsible for the nulls in the vertical profile, i.e. cancellation of signal energy that results when the ground reflected wave arrives 180° out of phase with the direct wave at a distant point, still exist; however the amplitude of the reflected wave is less than it was prior to inclining. Therefore the degree of signal cancellation is much less than in the horizontal configuration. Available experimental data indicates that maximum null depths on the order of 17 dB which existed in the vertical profile of the horizontal rhombic, have been reduced by as much as 12 to 15 dB in the inclined rhombic configuration. The second objective was accomplished by physically separating the two rhombic elements such that the first end fire null of the array factor was coincident with the first side lobes of the element pattern, thereby reducing the first side lobe levels of the array pattern. The available experimental data indicates first side lobe levels that are 8 to 10 dB down from the peak of the main beam, as compared to side lobe levels of 5 dB obtained for a single horizontal rhombic.

The rhombic antennas as installed now provide reduced side lobe levels and the

(Over)

DD FORM 1 NOV 1473

UNCLASSIFIED

Security Classification

14 KEY WORDS	LINK A		LINK B		LINK C	
	ROLE	WT	ROLE	WT	ROLE	WT
Antennas H. F. Antennas Rhombic Antenna Antenna Radiation Patterns						

Abstract continued

smoother vertical coverage required to achieve the desired propagation characteristics to make use of a greater number of propagation modes.

As of the date of this report several operational high frequency antenna installations, using inclined rhombic arrays of the type described herein have been installed as part of Project 673A.

A DETAILED ANALYTICAL AND EXPERIMENTAL INVESTIGATION OF AN INCLINED END FIRE RECEIVING RHOMBIC ANTENNA ARRAY

E. J. Christopher

FOREWORD

This in-house technical report, prepared under Job Order Number 45060000, has been reviewed by the Information Office (OI) and is releasable to the National Technical Information Service (NTIS).

The author wishes to acknowledge the guidance and technical assistance provided by Mr. Carmen Malagisi, Antenna Section, in the preparation of this report, and also Mr. Nicholas Internicola, Antenna Section, for his valuable assistance in the reduction and preparation of the pattern data.

This technical report has been reviewed and is approved.

Approved: ARTHUR J. FROHLICH
Chief, Techniques Branch
Surveillance & Control Division

Approved: JAMES L. RINNING
Colonel, USAF
Chief, Surveillance and
Control Division

FOR THE COMMANDER:

FRED I. DIAMOND
Actg. Chief, Plans Office

A B S T R A C T

This report provides an account of a new rhombic antenna array design and the resultant effect upon the antenna pattern resulting from this design.

The intent of this effort was twofold, first to reduce the deep nulls in the vertical profile that existed with a horizontal single rhombic in order to obtain smooth vertical coverage from 2° to 24° in elevation and secondly, to reduce the first side lobe levels in the horizontal plane pattern of a single rhombic antenna. The first objective was obtained by inclining the rhombic antenna approximately 8°. The factors responsible for the nulls in the vertical profile, i.e. cancellation of signal energy that results when the ground reflected wave arrives 180° out of phase with the direct wave at a distant point, still exist; however the amplitude of the reflected wave is less than it was prior to inclining. Therefore the degree of signal cancellation is much less than in the horizontal configuration. Available experimental data indicates that maximum null depths on the order of 17 dB which existed in the vertical profile of the horizontal rhombic, have been reduced by as much as 12 to 15 dB in the inclined rhombic configuration. The second objective was accomplished by physically separating the two rhombic elements such that the first end fire null of the array factor was coincident with the first side lobes of the element pattern, thereby reducing the first side lobe levels of the array pattern. The available experimental data indicates first side lobe levels that are 8 to 10 dB down from the peak of the main beam, as compared to side lobe levels of 5 dB obtained for a single horizontal rhombic.

The rhombic antennas as installed now provide reduced side lobe levels and the smoother vertical coverage required to achieve the desired propagation characteristics to make use of a greater number of propagating modes.

As of the date of this report several operational high frequency antenna installations, using inclined rhombic arrays of the type described herein have been installed as part of Project 673A.

Table of Contents

SECTION I

INTRODUCTION

This report outlines the results of a detailed analytical and experimental investigation of an inclined end fire receiving rhombic antenna array.

The following comments are presented with the intent of outlining the basic design factors and principle of operation of the rhombic antenna. The rhombic is an HF antenna using the traveling wave principle in its mode of operation. It is best suited for long distance, low angle transmission and reception. The antenna shown in Figure I-1 has a two-wire transmission line running from the transmitter to the long wire radiating curtain. As shown, this diagram indicates a unidirectional radiating capability; however a bidirectional capability can be achieved by a standard switching arrangement which interchanges feed and terminal points. The terminal dissipation line serves as a load for power not radiated. Each leg of the rhombic has a radiation pattern which is the result of an attenuated traveling wave. The overall pattern is due to the interference between the four legs and their images. The height above ground H, the length of the legs L, and the included angle A are the parameters that control the pattern for each frequency.

Figure I-2 represents the generally accepted antenna configuration that had been used up to the time that this program was initiated to accomplish vertical coverage at the HF frequencies. The configuration shown was designed to operate over a frequency range of from 8 - 24 MHz. Complete vertical coverage of from 2° to 30° was achieved by switching from one rhombic to the other, i.e. from the high to the low rhombic. The

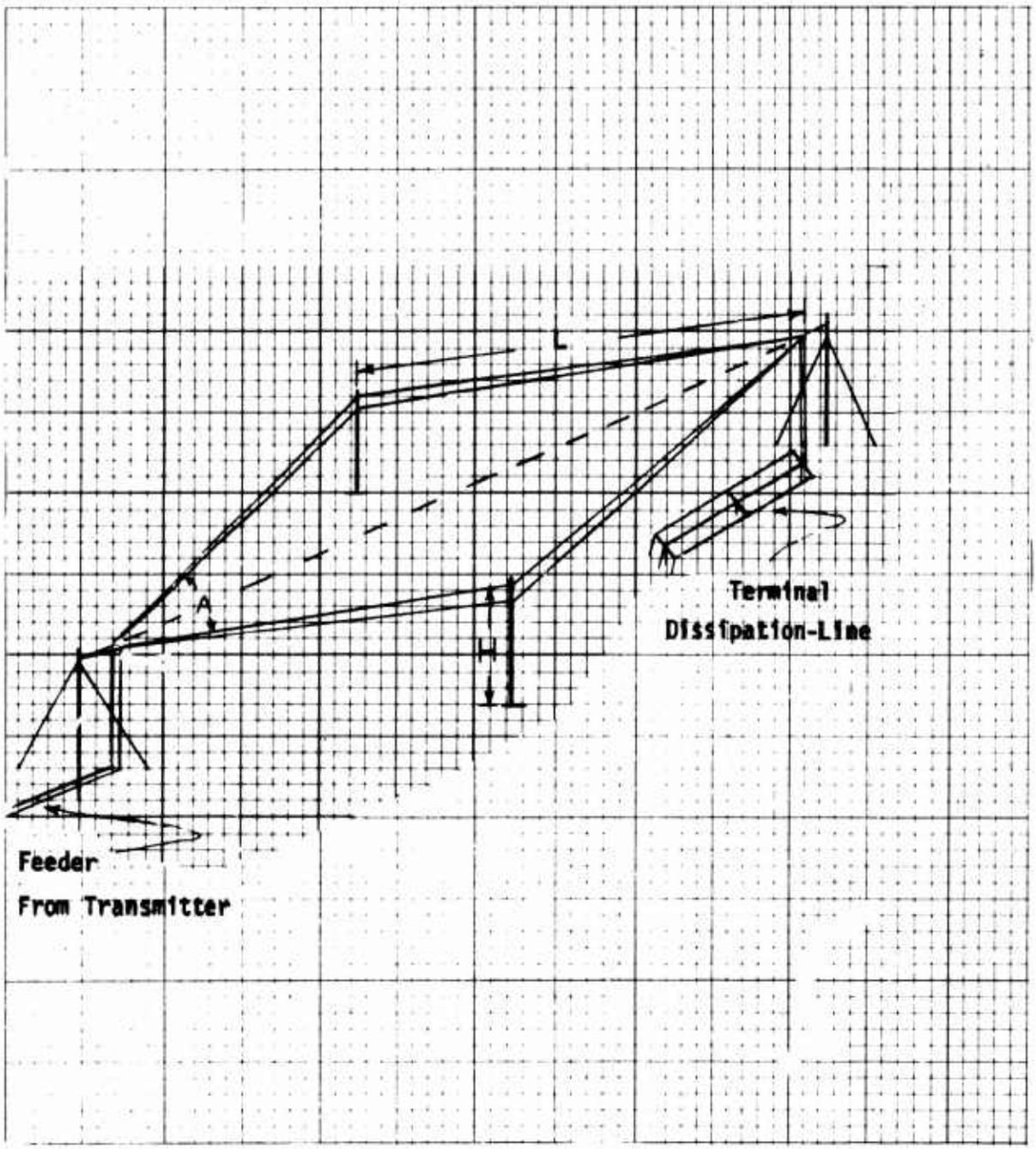

Figure I-1

HORIZONTAL RHOMBIC

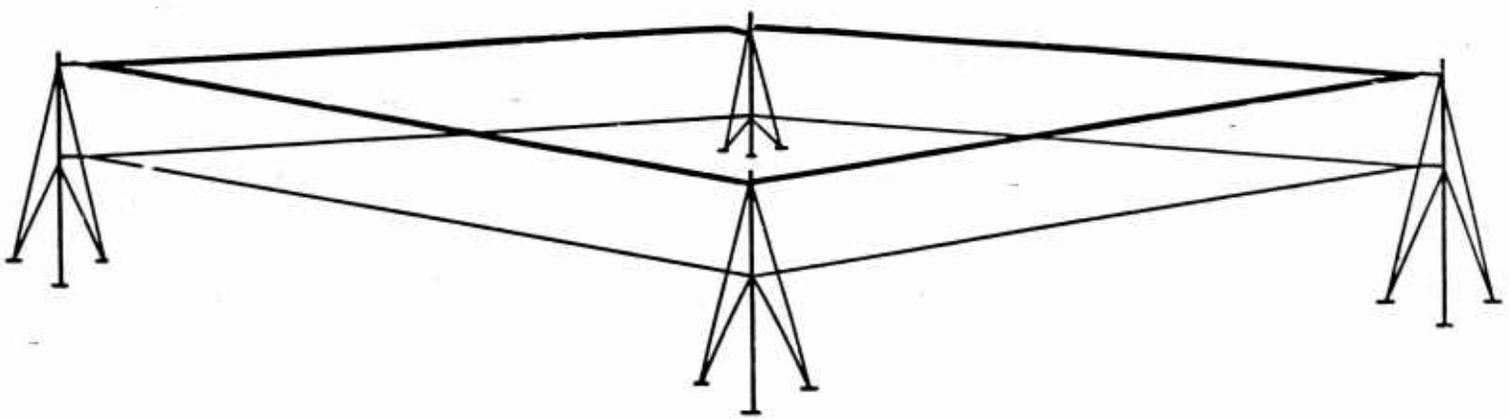

LOW ANGLE COVERAGE ———
HIGH ANGLE COVERAGE ———

FIGURE I-2

lower antenna provided coverage from approximately 10° to 25° in elevation and the upper provided coverage from 2° to 10° in elevation. A computer program was set up to determine what the vertical profile would be for the antennas shown in Figure I-2. Pertinent rhombic antenna parameters such as leg lengths, included angle and height above ground, similar to those to be used in the array to be installed, were used in this program, thereby allowing a more valid pattern comparison to be made between the conventional configuration and the alternate configuration to be discussed. The computed vertical profile of the antennas shown in Figure I-2 is plotted in Figure I-3. This figure reveals undesirable deep nulls in the vertical profile which are attributed to the cancellation of signal energy that results when the ground reflected wave arrives 180° out of phase with the direct wave at a distant point. This horizontal configuration does not adequately provide the vertical coverage required to achieve the desired propagation characteristics.

The first objective of this program was to reduce these nulls to a minimum in order to obtain a smoother vertical profile, thereby allowing for the reception of a greater number of propagating modes. This was accomplished by inclining the rhombic antenna approximately 8°, as shown in Figure I-4. The factors responsible for the nulls in the vertical profile still exist, and the resultant vertical array pattern obtained from the rhombic element and its image still has null positions at the same location as prior to inclining; however the amplitude of the reflected wave is much less than in the horizontally positioned rhombics shown in Figure I-2. The degree to which this cancellation of

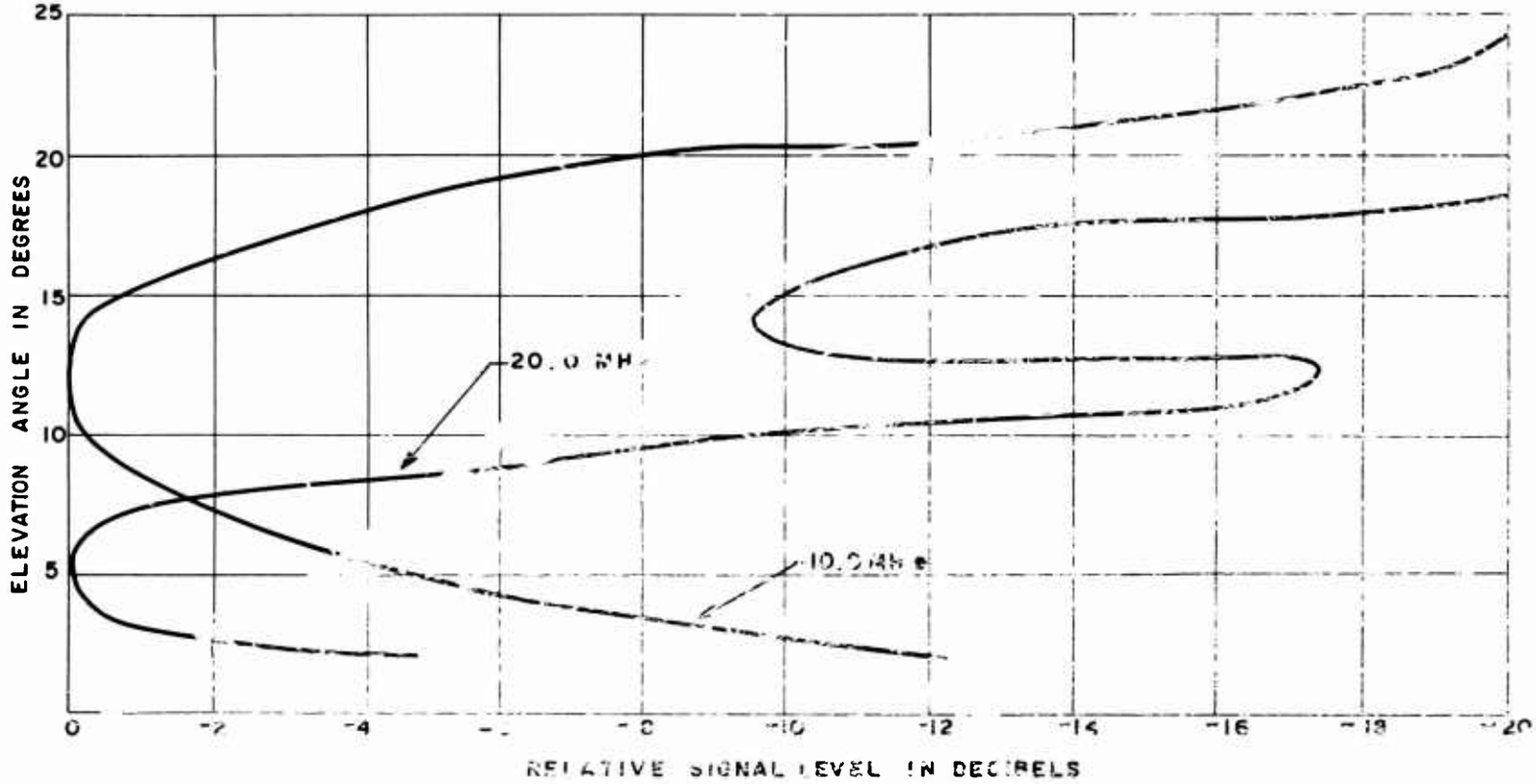

COMPUTED VERTICAL PROFILE PRIOR TO MODIFICATION

Figure 1-1 COMPUTED VERTICAL PROFILE PRIOR TO MODIFICATION

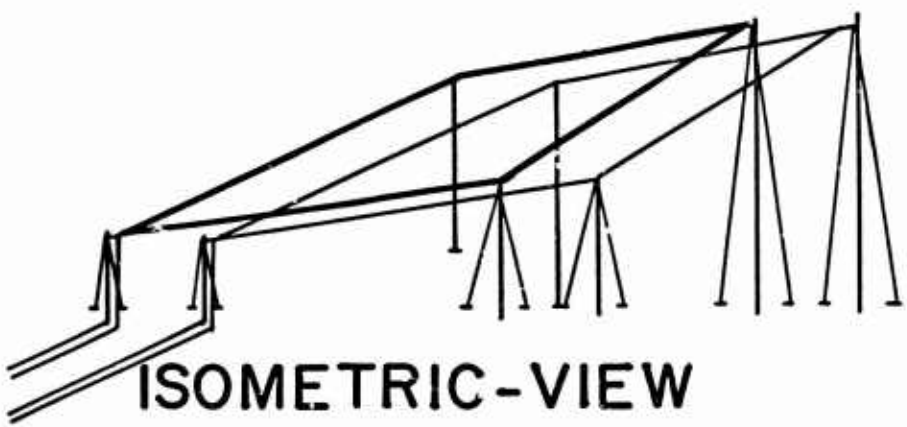

ISOMETRIC-VIEW

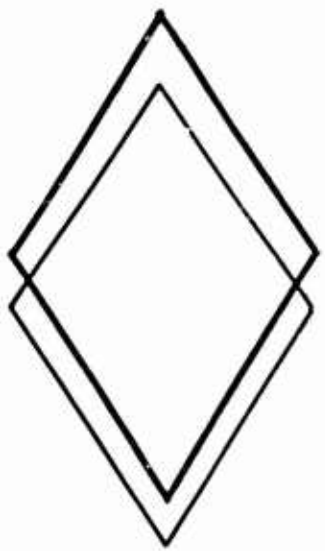

TOP-VIEW

Figure I-4

signal energy was minimized is demonstrated by reduced null depths as seen in Figures I-5 and I-6. These figures show a reduction of from 12 to 15 dB in the maximum null depths that existed in the vertical profile of Figure I-2. This modification will allow maximum use of a greater number of propagating modes, which in the horizontal rhombic case were incident upon null positions that existed in the vertical pattern profile. The inclined arrangement of Figure I-4 was optimumly designed for the highest operating frequency in order to allow for its use at all frequencies below the upper limit.

The arrayed configuration as shown in Figure I-4 allowed for the accomplishment of the second objective of the program which was to reduce the first side lobe levels in the horizontal plane of the antenna pattern. These lobes are usually down only about 5.0 to 5.5 dB from the peak of the main beam. The two rhombic antenna elements were physically separated such that the first end fire null of the array factor was coincident with the peaks of the first side lobe levels of the element pattern, thereby reducing the first side lobe levels of the resultant array pattern. It might be worth while to mention that this approach for reducing side lobe levels provides the added flexibility of being able to steer the far out nulls of the array pattern. This may be accomplished by changing the frequency of operation or in an analogous way by physically varying the length of line between the array elements. Frequency variations only slightly alter the shape of the main beam and first side lobe levels; however the far out lobes are

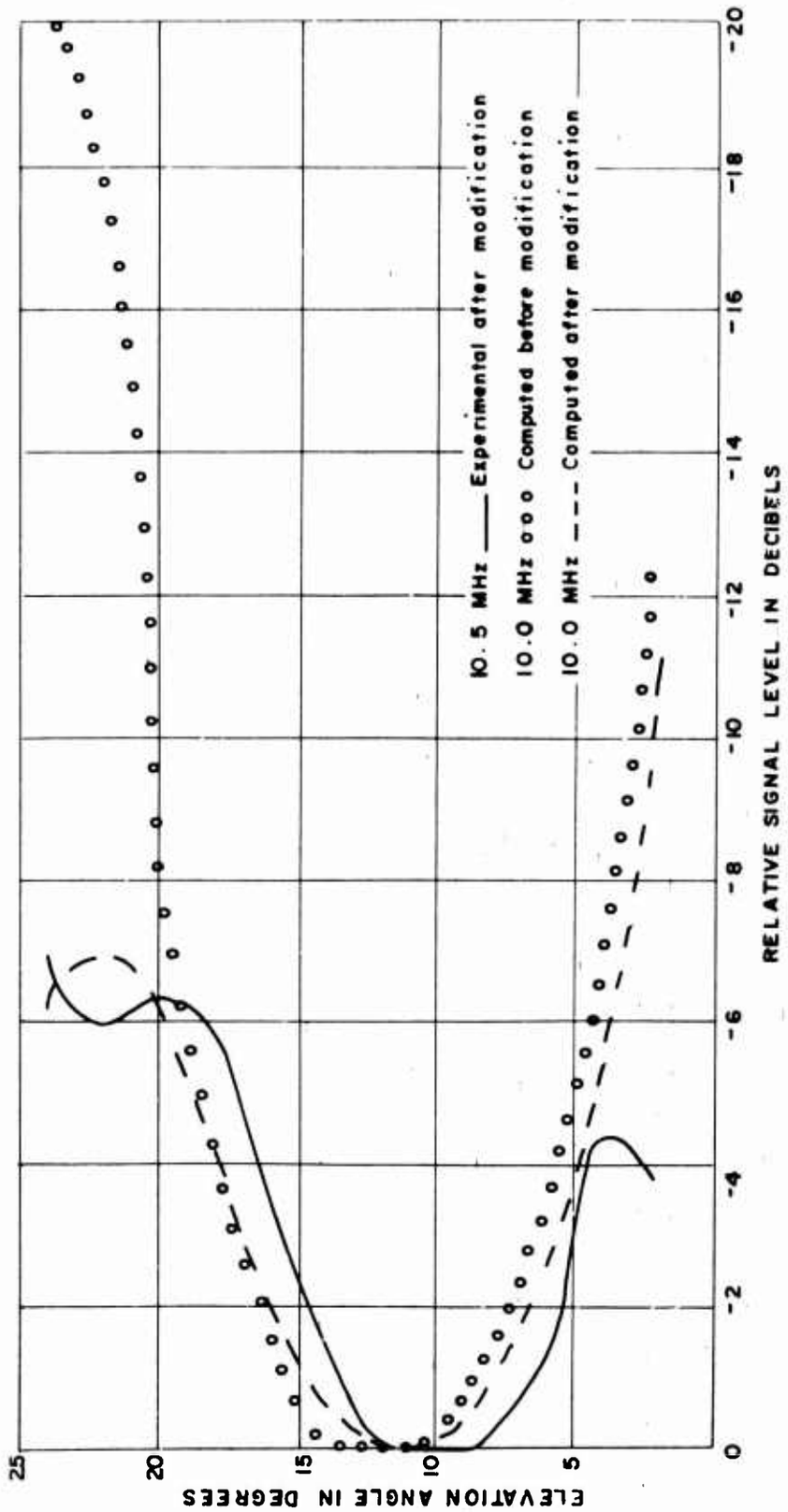
10.5 MHz —— Experimental after modification
10.0 MHz o o o Computed before modification
10.0 MHz - - - Computed after modification
RELATIVE SIGNAL LEVEL IN DECIBELS
-20
-18
-16
-14
-12
-10
-8
-6
-4
-2
0
ELEVATION ANGLE IN DEGREES
25
20
15
10
5

Figure I-5

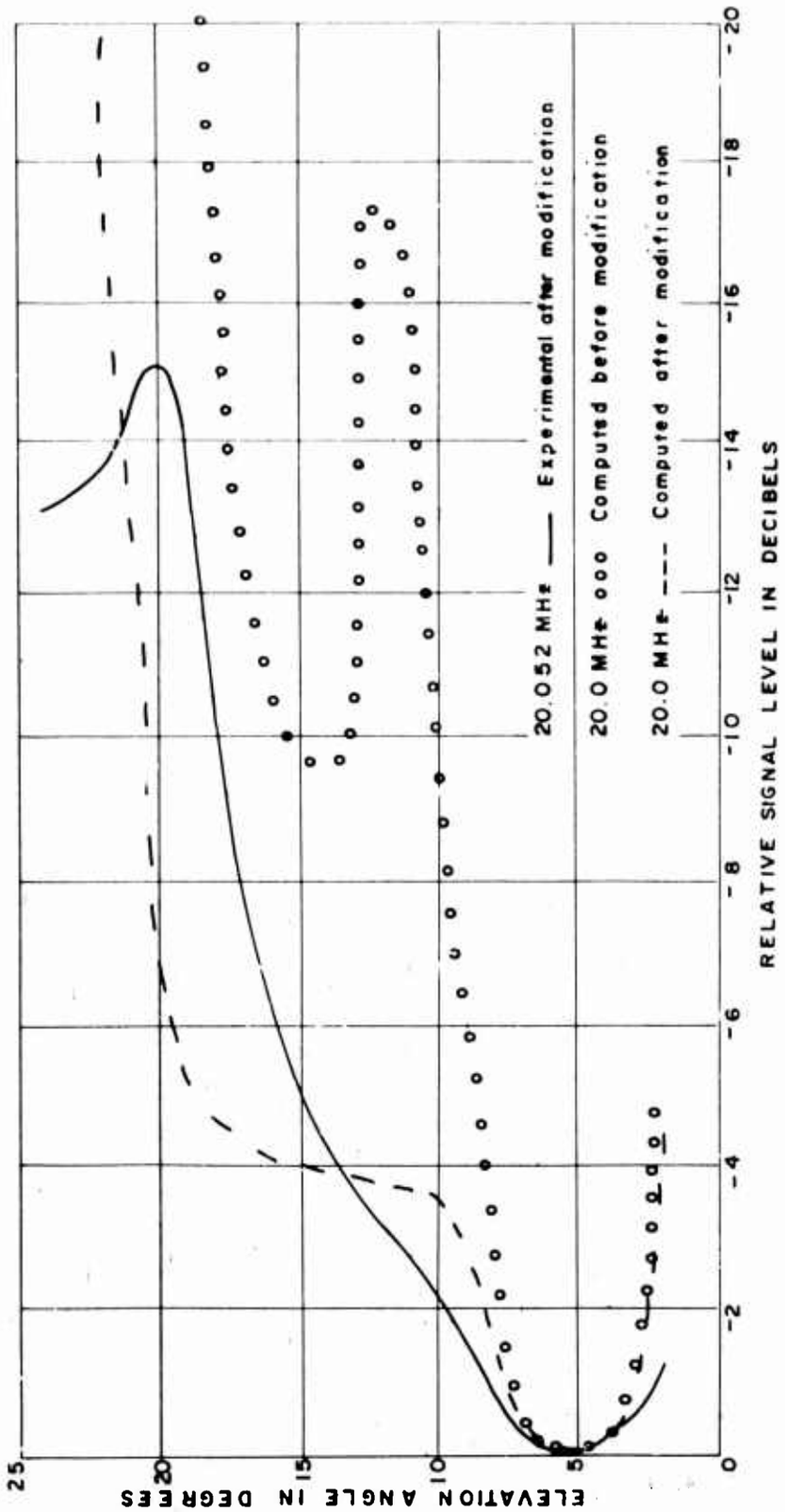
ELEVATION ANGLE IN DEGREES
25
20
15
10
5
0
-2
-4
-6
-8
-10
-12
-14
-16
-18
-20
RELATIVE SIGNAL LEVEL IN DECIBELS
20.052 MHz —— Experimental after modification
20.0 MHz ooo Computed before modification
20.0 MHz --- Computed after modification

Figure I-6

shifted appreciably. Such a flexibility provides the capability of nulling out interfering signals in the region of the far out secondary lobes. The extent of available frequency excursion depends upon the amount of main beam degradation that is tolerable for the intended application. This null steering capability was mentioned only as a point of interest and is not to be interpreted as an intentional design feature of the antenna under discussion, but merely as being available, if required. Hereafter reference will be made to the antennas before and after modification, where this latter designation refers to the inclined rhombic elements and the former refers to the assumed generally accepted configuration of Figure I-2.

SECTION II

PROCEDURE

Use was made of a portion of the AN/ASM-13* Airborne Antenna Pattern Analyzer System installed aboard a C-131 aircraft. The system was designed to measure radiation patterns of both fixed and rotating ground antennas in their actual operational environment. The automatic range control portion of the system was used in making the rhombic antenna pattern measurements. This portion of the system is coupled to the aircraft's automatic pilot system to provide for constraining the aircraft to any desired slant range between 5 and 25 nautical miles. This equipment has had a range accuracy of $\pm$ 750 feet and the precision with which a selected path can be maintained is $\pm$ 100 feet. The aircraft's altitude is held constant by using the aircraft's standard altimeter and auto-pilot. The aircraft altitude is established to the degree of accuracy required for the system by assistance from a theodolite and wide angle finder scope which are located at the site and are operated by the ground crew. The pilot established an approximate altitude and after the aircraft is flying under control of the automatic range control system, it is again observed by the ground theodolite. The pilot is then given voice instruction as to what altitude corrections to make to attain the precise altitude required. The auto-pilot will then maintain the aircraft at this altitude for

*This system has since been replaced by the FSM-17.

the duration of the pass through the antenna pattern without serious deviation.

On numerous occasions two runs were made at the same elevation angle and resulted in successful duplication of the pattern, thereby providing further confidence in the stability of the aircraft.

A triggering device, which was controlled by the ground crew member observing the aircrafts azimuthal position through the wide angle scope, was connected to the pattern recorder. As the aircraft passed through the vertical cross hair of the scope, the device was triggered and a line was strobed onto the recorded pattern at every 10° in azimuth. The graduated circle on the theodolite was then used to allow the operator to rotate the scope until the vertical cross hair was positioned at a point 10° displaced from the previous location. During the reduction of the pattern data the accuracy achieved by this technique was on the order of $\pm$ 1.5° over a 360° arc, as compared to computed array patterns.

Complete orbital flights of 360° were made at elevation angles varying from 2° to 24° in 2° increments, for a slant range of 5 nautical miles. This corresponds to vertical coverage of approximately 1100 to 13,000 feet.

Figure II-1 is a block diagram of the receiving, recording and calibrating equipment. The receiver and recorder shown were calibrated with a HP 608B signal generator.

Stepped calibration curves were made at 3 distinct frequencies, 10.5, 15.0 and 20.052 MHz, prior to and after each complete set of

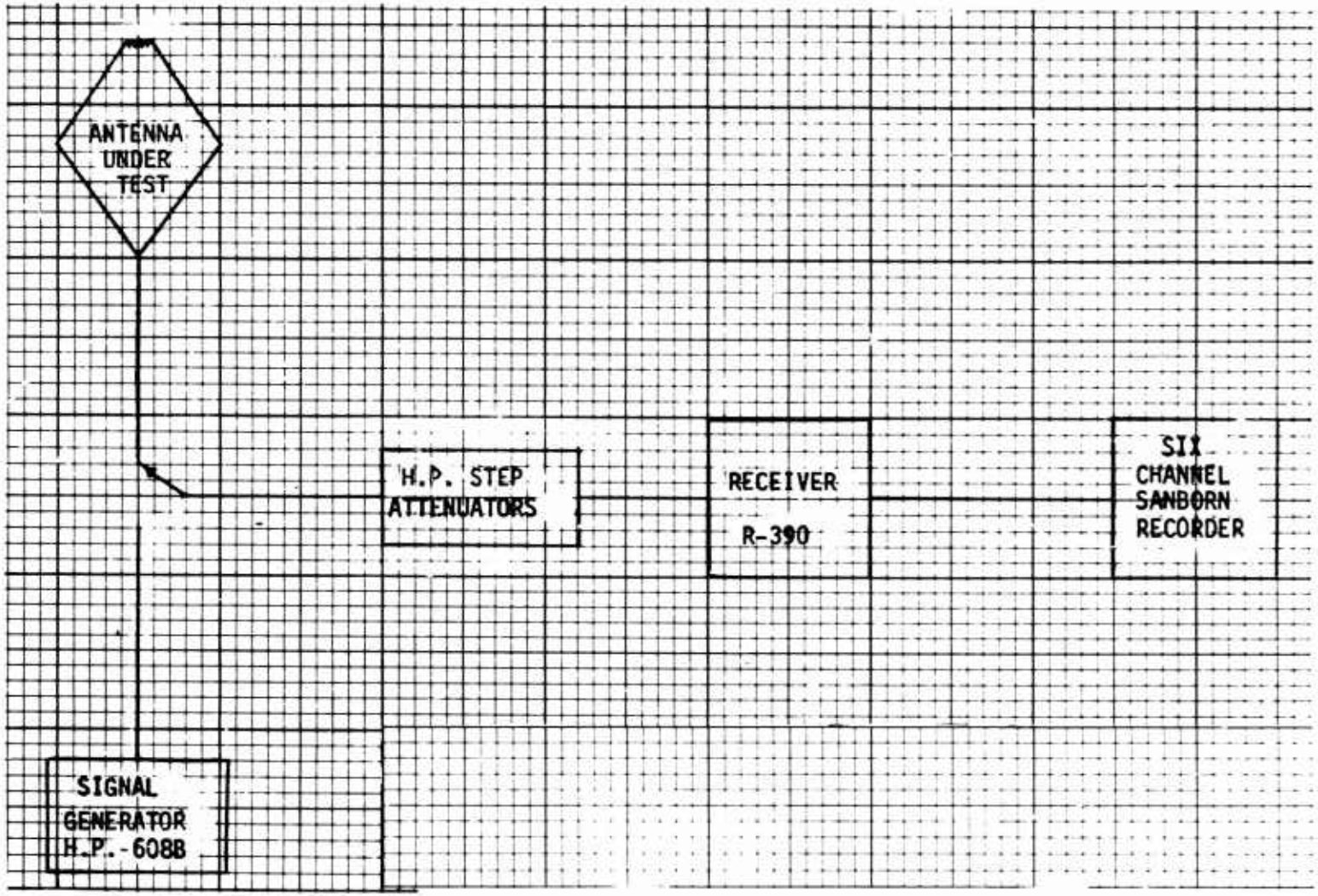

RECEIVING-RECORDING AND CALIBRATING EQUIPMENT

Figure II-1

vertical coverage patterns from 2° to 24° were obtained. These comparative curves did not vary more than ± 0.5 dB throughout the tests. In the reduction of all data obtained, use was made of the calibration charts since linearity was not assumed to exist throughout the dynamic range of the receiving equipment.

In an attempt to minimize the undesirable effects resulting from variations in radiated power, caused by drifting in the transmitter frequency, the following measures were taken. A Hanson synthesizer was used as a transmitter. The frequency stability of the synthesizer is one part in 10^9 per day. No power output change was noticed by the transmitter operator on the aircraft. A transmitter-receiver stability test conducted in the laboratory for a period of 36 hours provided variations on the order of ± 0.5 dB in the radiated signal level. With the maintenance of a constant frequency level, repeatable calibration curves and a constant current on the transmitting loop antenna, it was reasonably assumed that at each particular frequency of operation the radiated power output was constant.

Transformer terminations had been incorporated into the Stockbridge rhombics which allow for the reception of either a horizontally or vertically polarized signal or both simultaneously.*[1] Throughout the

*[1]This can be visualized in the following way, when the rhombic, which is a conducting curtain, is fed in an unbalanced manner, i.e. both sides of the curtain are fed in phase and against ground, it receives only vertical polarization. Its mode of operation is analogous to the conventional Beverage antenna, which is simply a long radiating wire fed against ground. When fed with a balanced line, i.e. both sides of the curtain are fed out of phase, only horizontal polarization is received.

tests the rhombics were used in the receive mode for a transmitted signal of horizontal polarization, i.e. receivers were placed at the horizontal output ports of the antenna. Figure II-2 depicts the antenna configuration and arrangement of the transformer terminations. From this figure it is apparent that a bidirectional receiving capability is available, i.e. the antenna can receive in either of two directions separated by 180°.

It is essential that the polarity of the transmitting antenna be precisely known and maintained. The orientation of the transmitting loop as shown in Figure II-3 provides a transmitted signal that is horizontally polarized. This loop operation was used throughout the flight tests. Figure II-4 represents a superposition of both the horizontal and vertical components of the signal received on two separate channels of the Sanborn recorder for a transmitting loop orientation as shown in Figure II-3. Use was made of two separate receivers located at both the horizontal and vertical output ports, as shown in Figure II-2. From this figure, polarization isolation on the order of 24 dB is achieved in the end fire direction, i.e. in the direction of beam maxima. This figure is indicative of good antenna balance for horizontal polarization and also provides an excellent indication as to how well the transmitting loop antenna is radiating an essentially pure horizontally polarized signal.

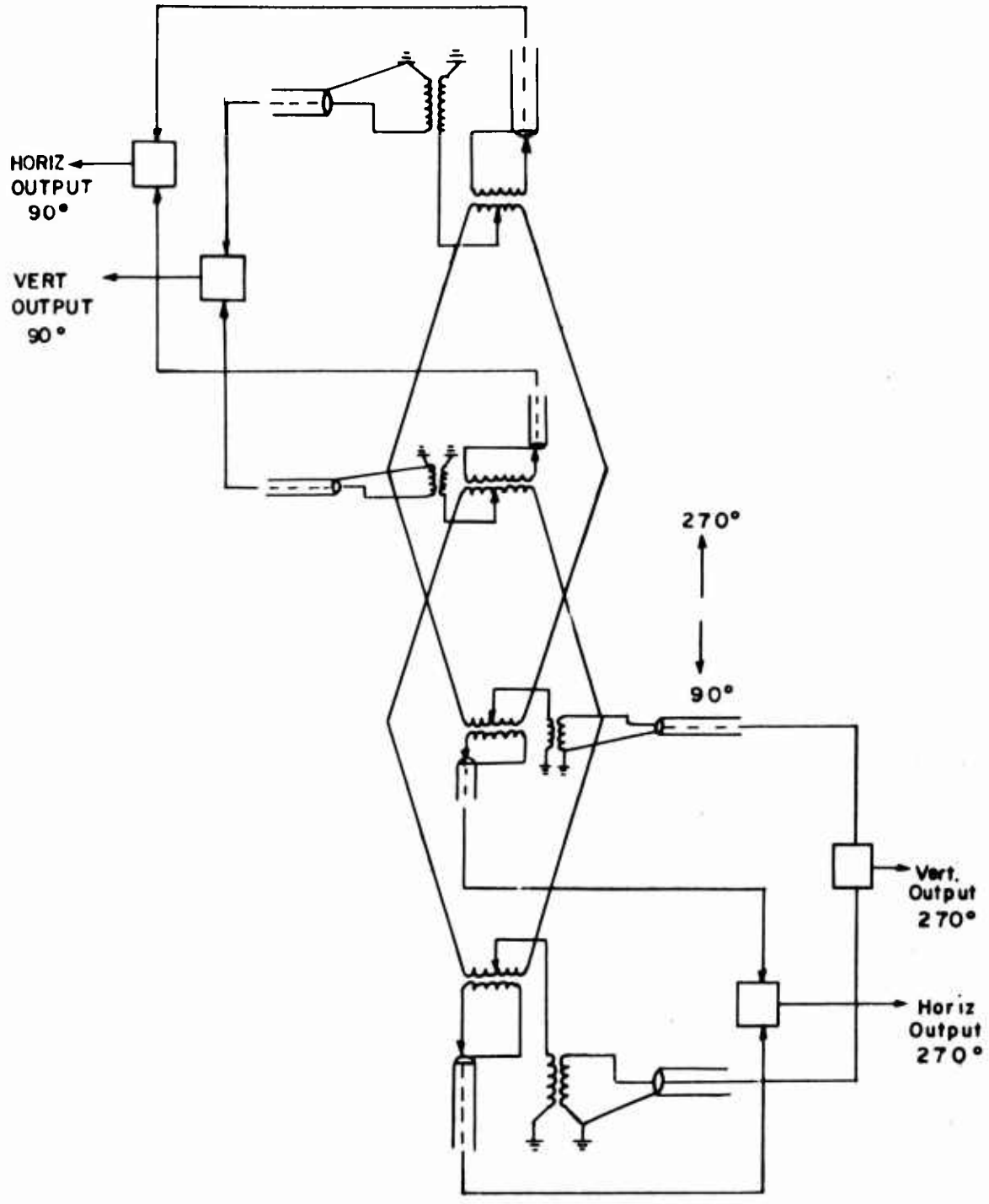

ARRAY TRANSFORMER CONFIGURATION

Figure II-2

APPAY TRANSFORMER CONFIGUPATION

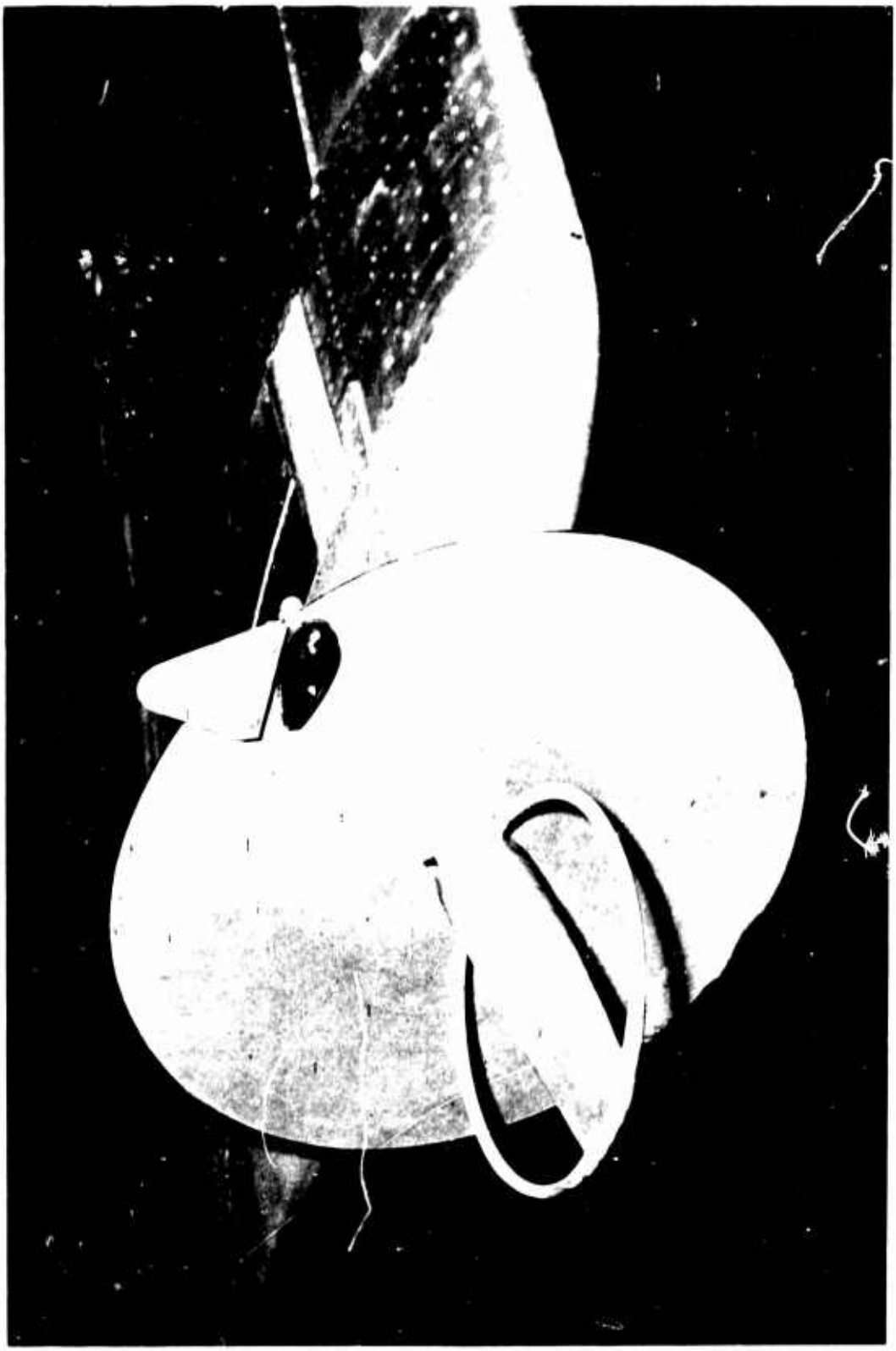

Figure II-3

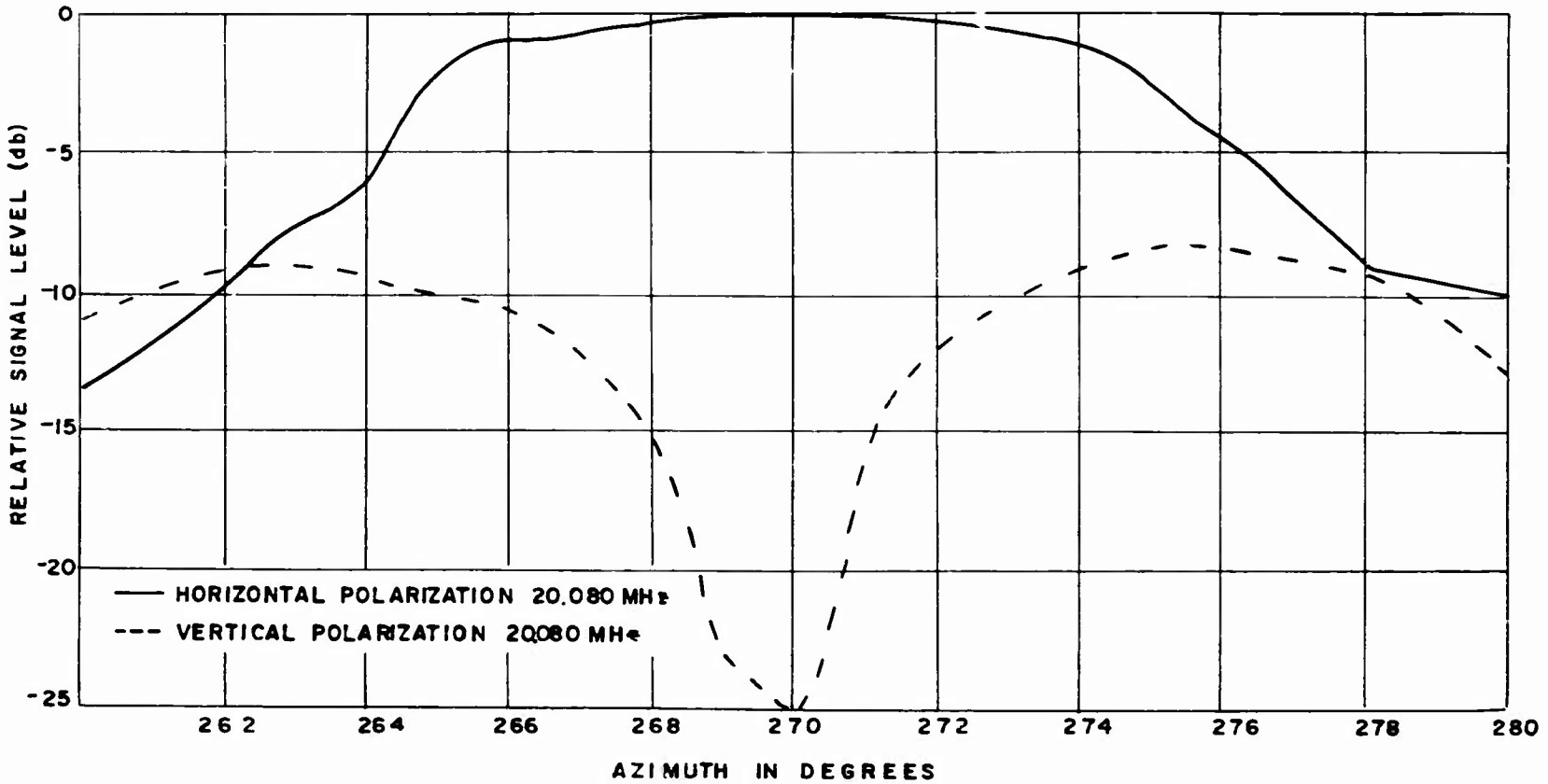

POLARIZATION — ISOLATION

Figure II-4 POLARIZATION - ISOLATION

SECTION III

EVALUATION

In the data to be presented use was made of the results of the computer program conducted under Contract AF 30(602)-2881. A UNIVAC 1130A Computer was used for this program. Computed patterns were provided for the horizontaliy polarized field, the vertically polarized field and the total field at frequencies of 10.0, 15.0 and 20.0 MHz for 360° azimuthal coverage and for elevation angles of from 0° to 40°. The horizontally polarized computed patterns obtained were compared to the experimental patterns to determine the degree of success achieved in properly designing and evaluating the inclined rhombic array.

The pattern data obtained using the Sanborn recorder as shown in Figure II-1 was reduced to the polar plots contained in this report. Figures III-1 through III-32 represent superpositions of both the computed and experimental horizontal antenna patterns for elevation angles of from 2° to 24°. The data of Figures III-1 through III-32 has been normalized to 0 dB at the peak of the main beam for both the computed and experimental data. However, as indicated in the legend of each of the plots, the peak (Pk) of the computed patterns at various elevation angles, relative to the peak in the vertical profile, have been denoted at each frequency of operation. The experimental pattern data has been plotted in a similar manner. For example, at a test (experimental) frequency of 10.5 MHz the peak of the vertical profile is at the 8° elevation angle and is denoted in Figure III-4 by Pk = 0 dB. Also in this same figure the peak of the

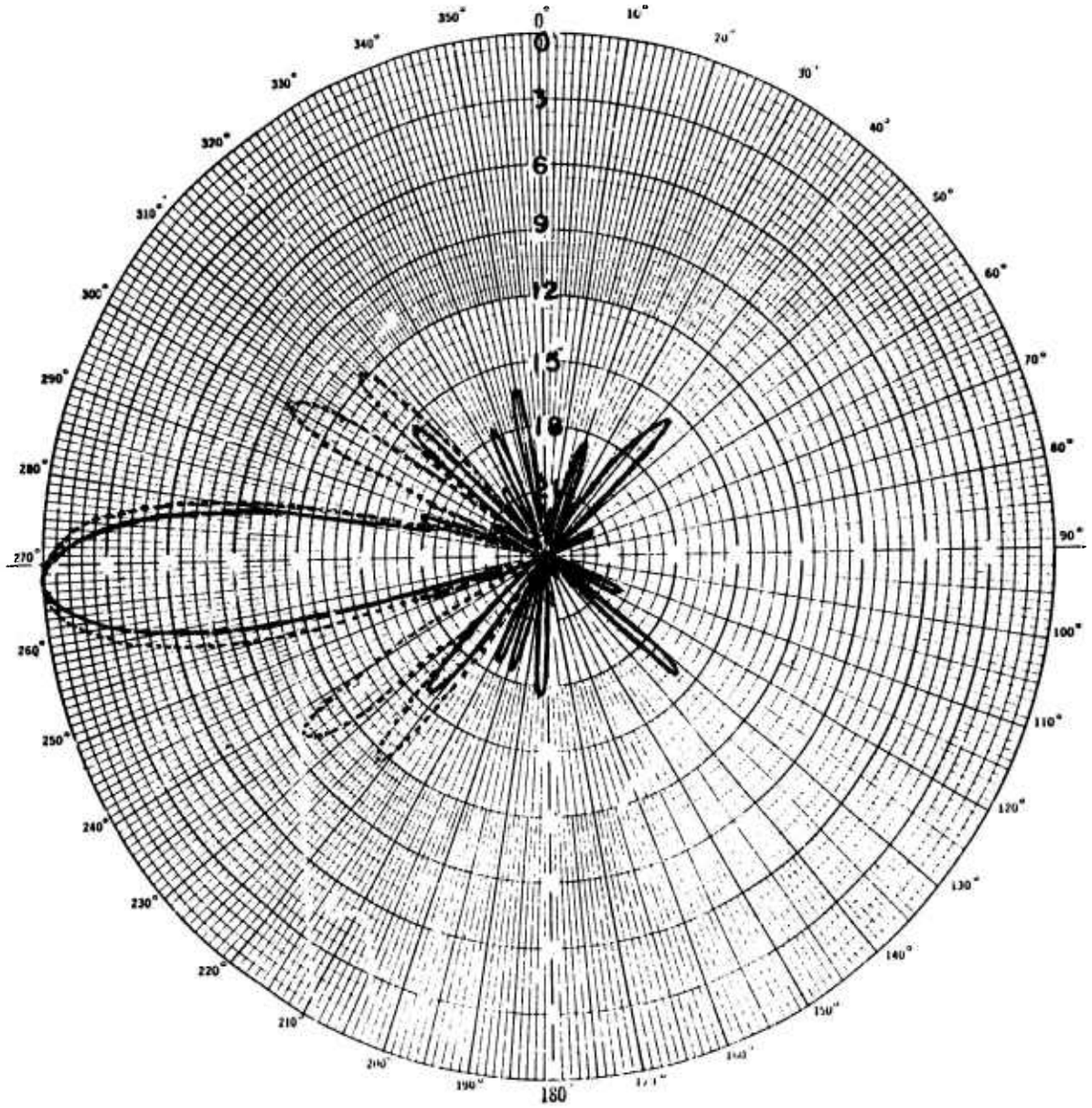

Figure III-1

WEST RHOMBIC
HORIZONTAL POLARIZATION

Elevation 2°

—— Experimental Freq. 10.5 MHz Pk = -3.8 dB

---- Computed Freq. 10.0 MHz Pk = -11.1 dB

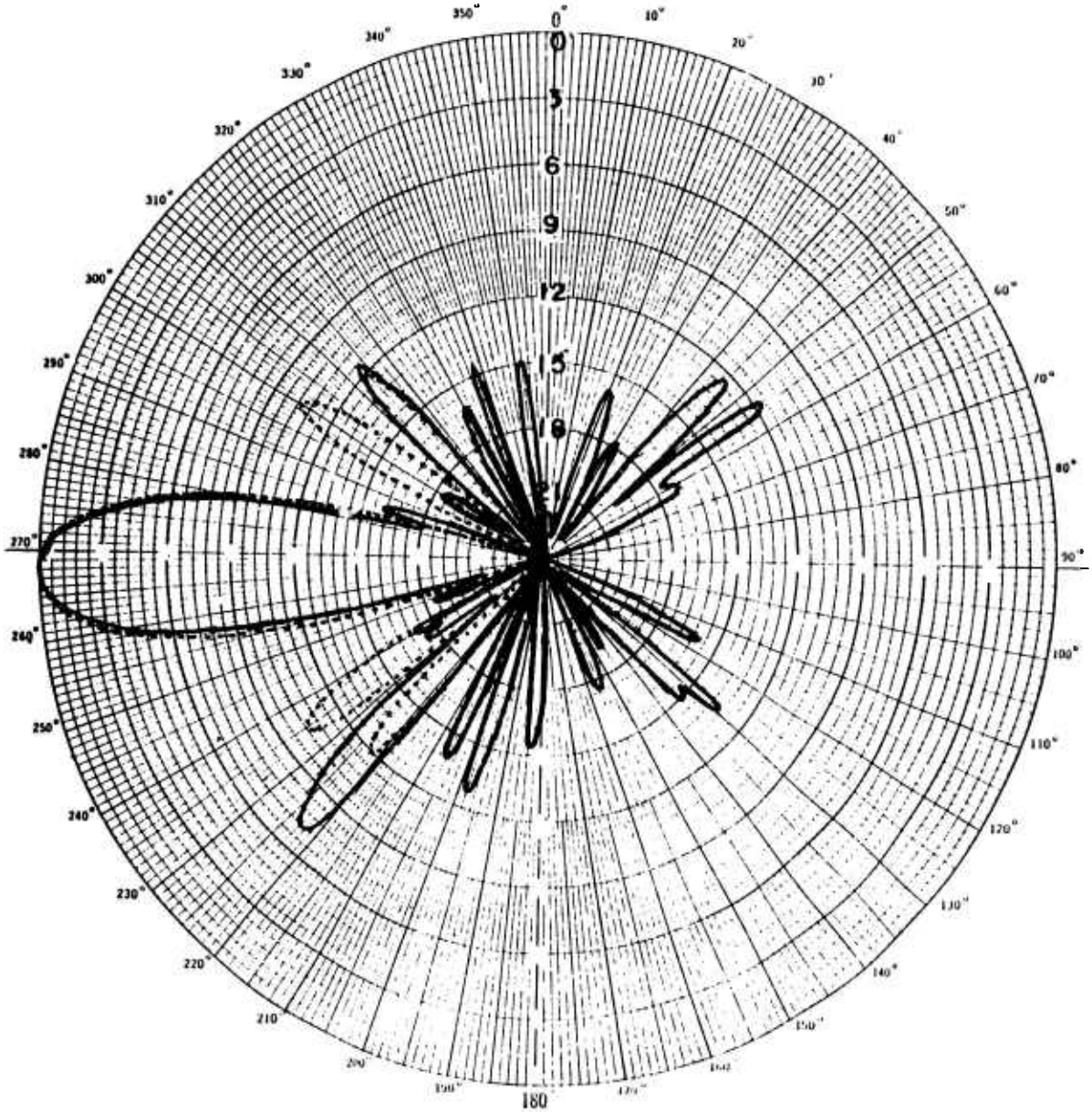

Figure III-2

WEST RHOMBIC
HORIZONTAL POLARIZATION

Elevation 4°

—— Experimental Freq. 10.5 MHz

Pk = -4.0 dB

---- Computed Freq. 10.0 MHz

Pk = -11.1 dB

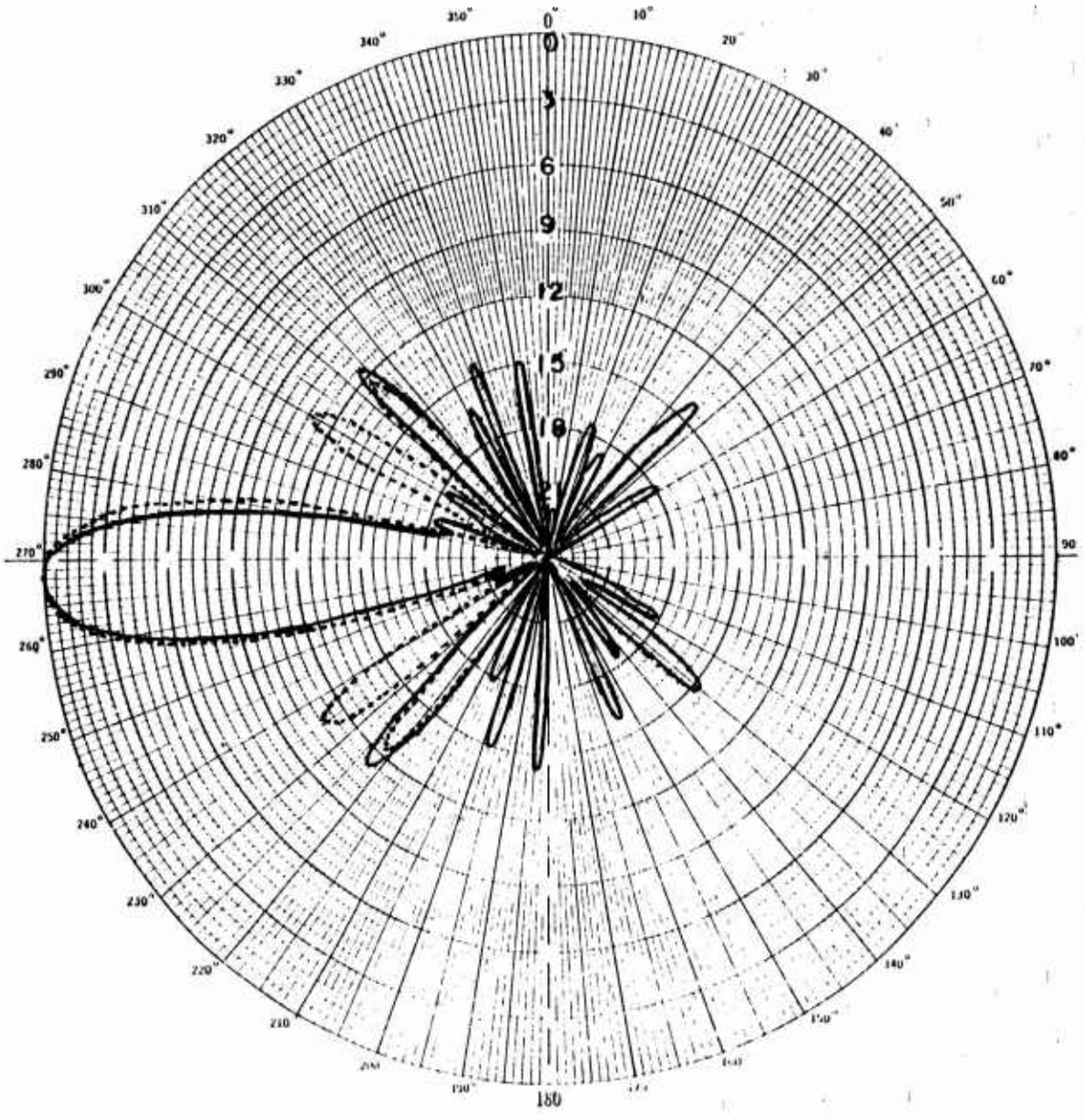

Figure III-3

WEST RHOMBIC
HORIZONTAL POLARIZATION

Elevation 6°

—— Experimental Freq. 10.5 MHz Pk = -1.3 dB

---- Computed Freq. 10.0 MHz Pk = -2.5 dB

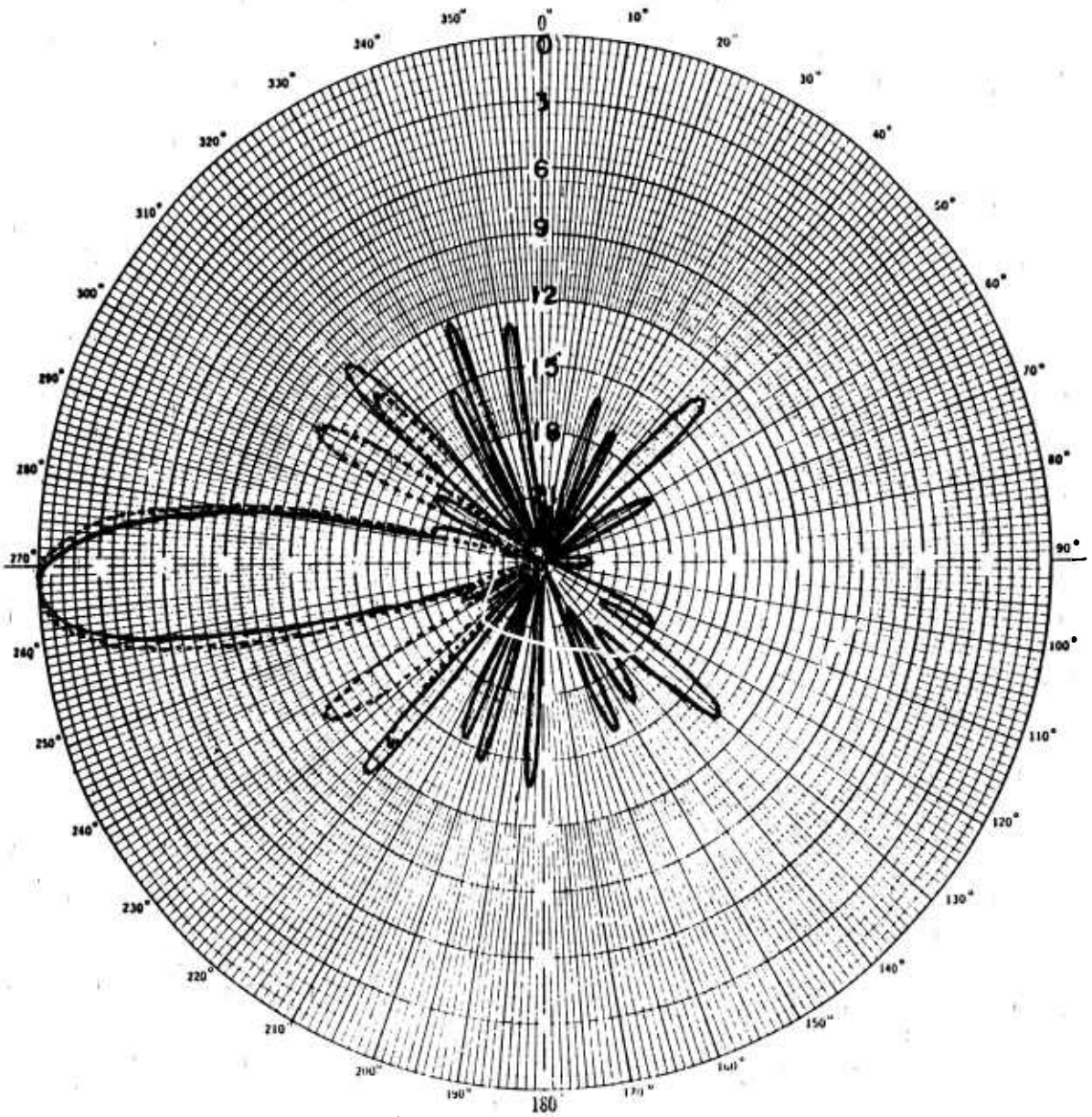

Figure III-4

WEST RHOMBIC
HORIZONTAL POLARIZATION

Elevation 8°

—— Experimental Freq. 10.5 MHz ---- Computed Freq. 10.0 MHz

Pk = 0 dB Pk = -.9 dB

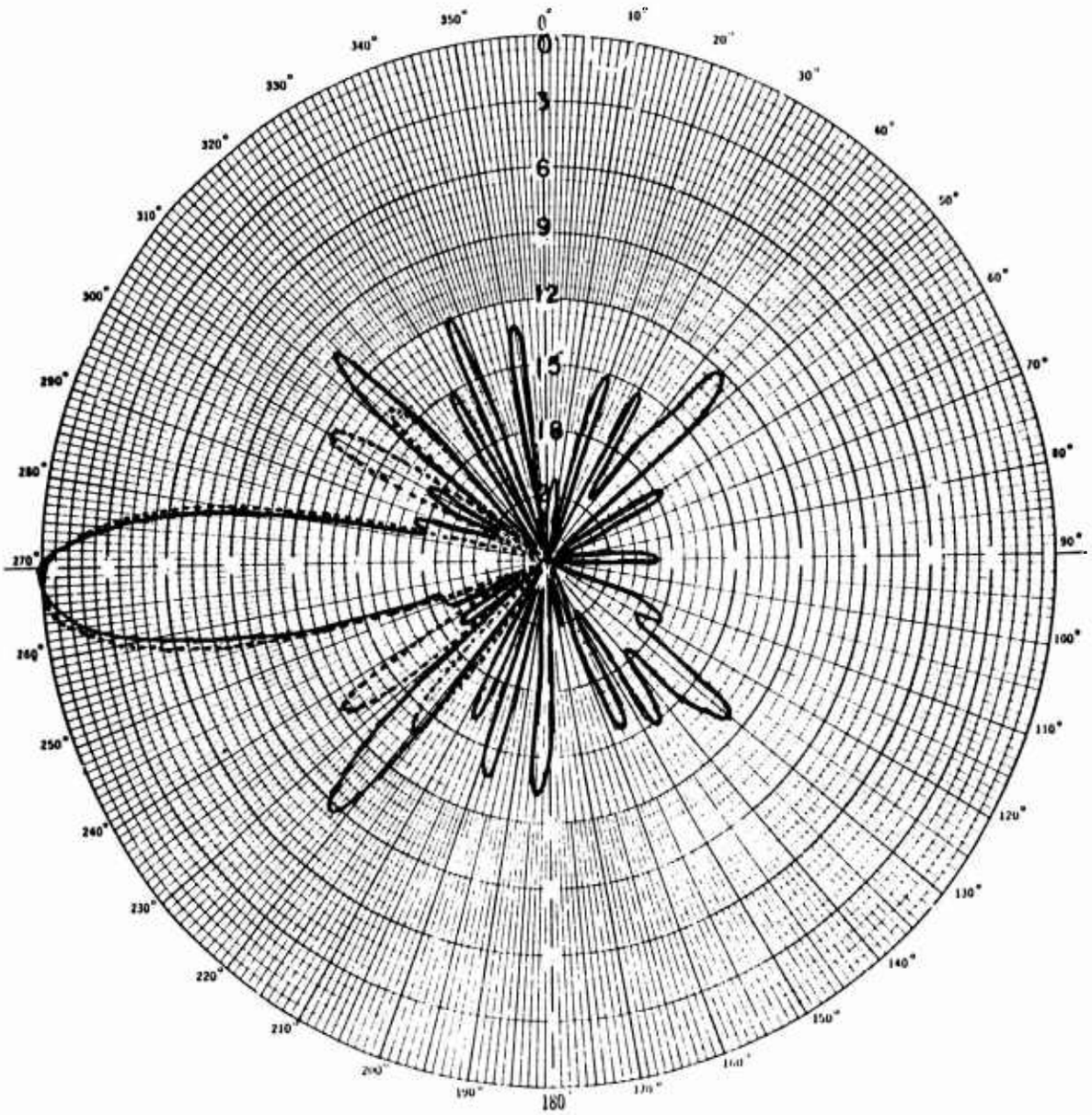

Figure III-5

WEST RHOMBIC
HORIZONTAL POLARIZATION

Elevation 10°

—— Experimental Freq. 10.5 MHz

Pk = -.2 dB

---- Computed Freq. 10.0 MHz

Pk = -.1 dB

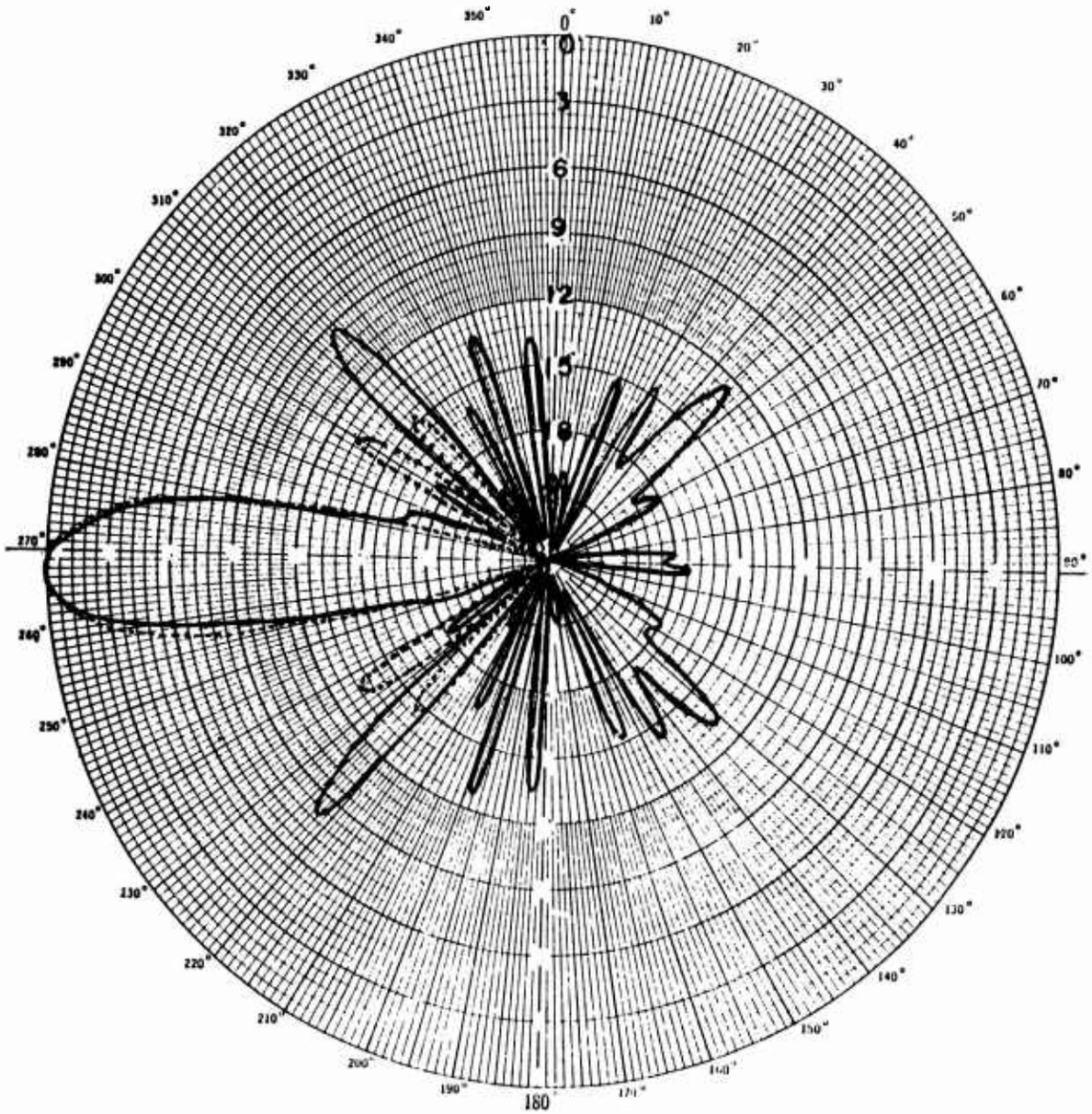

Figure III-6

WEST RHOMBIC
HORIZONTAL POLARIZATION

Elevation 12°

_____ Experimental Freq. 10.5 MHz

Pk = -.4 dB

---- Computed Freq. 10.0 MHz

Pk = 0 dB

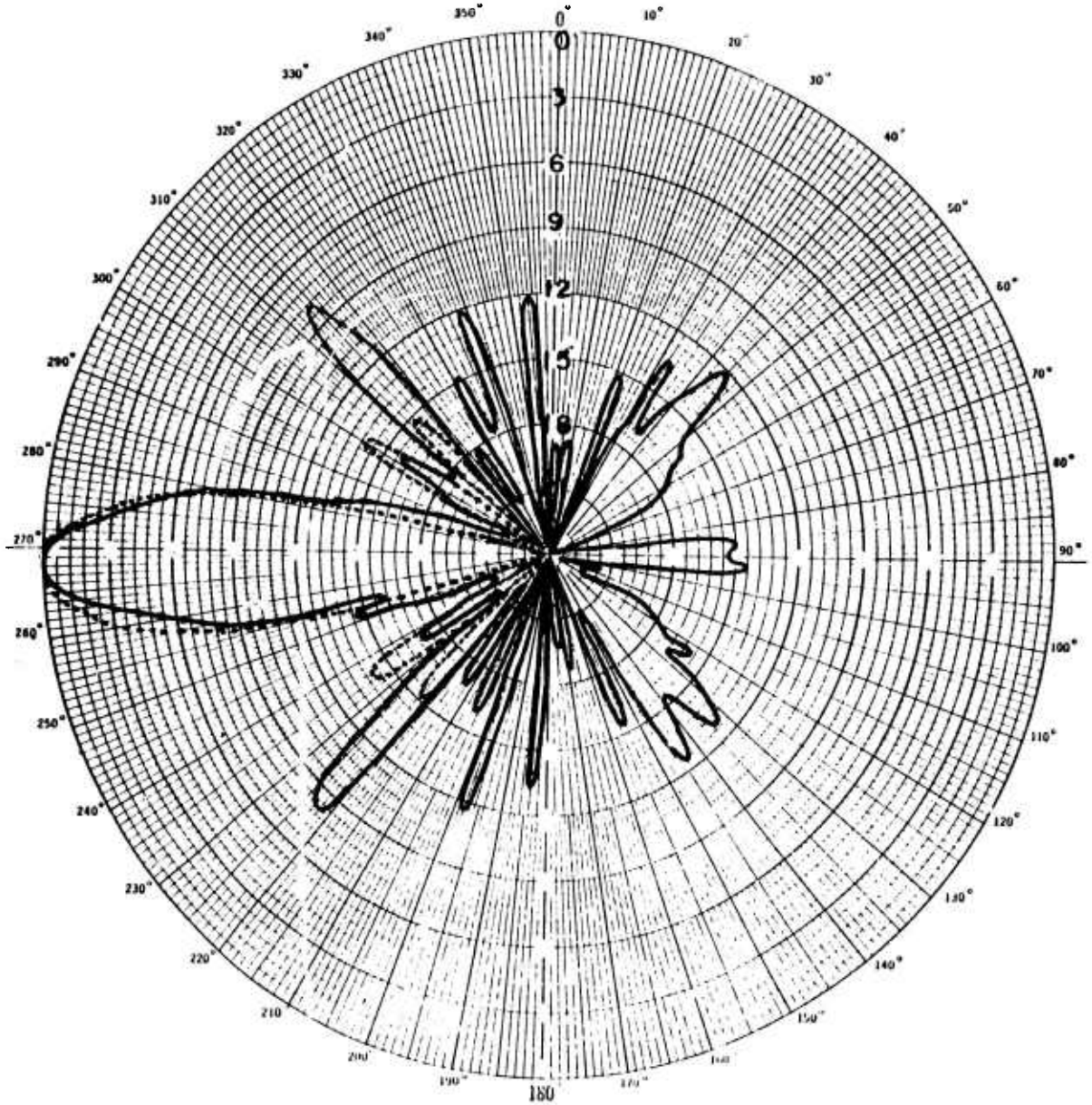

Figure III-7

WEST RHOMBIC
HORIZONTAL POLARIZATION

Elevation 14°

_____ Experimental Freq. 10.5 MHz

Pk = -1.4 dB

---- Computed Freq. 10.0 MHz

Pk = -.7 dB

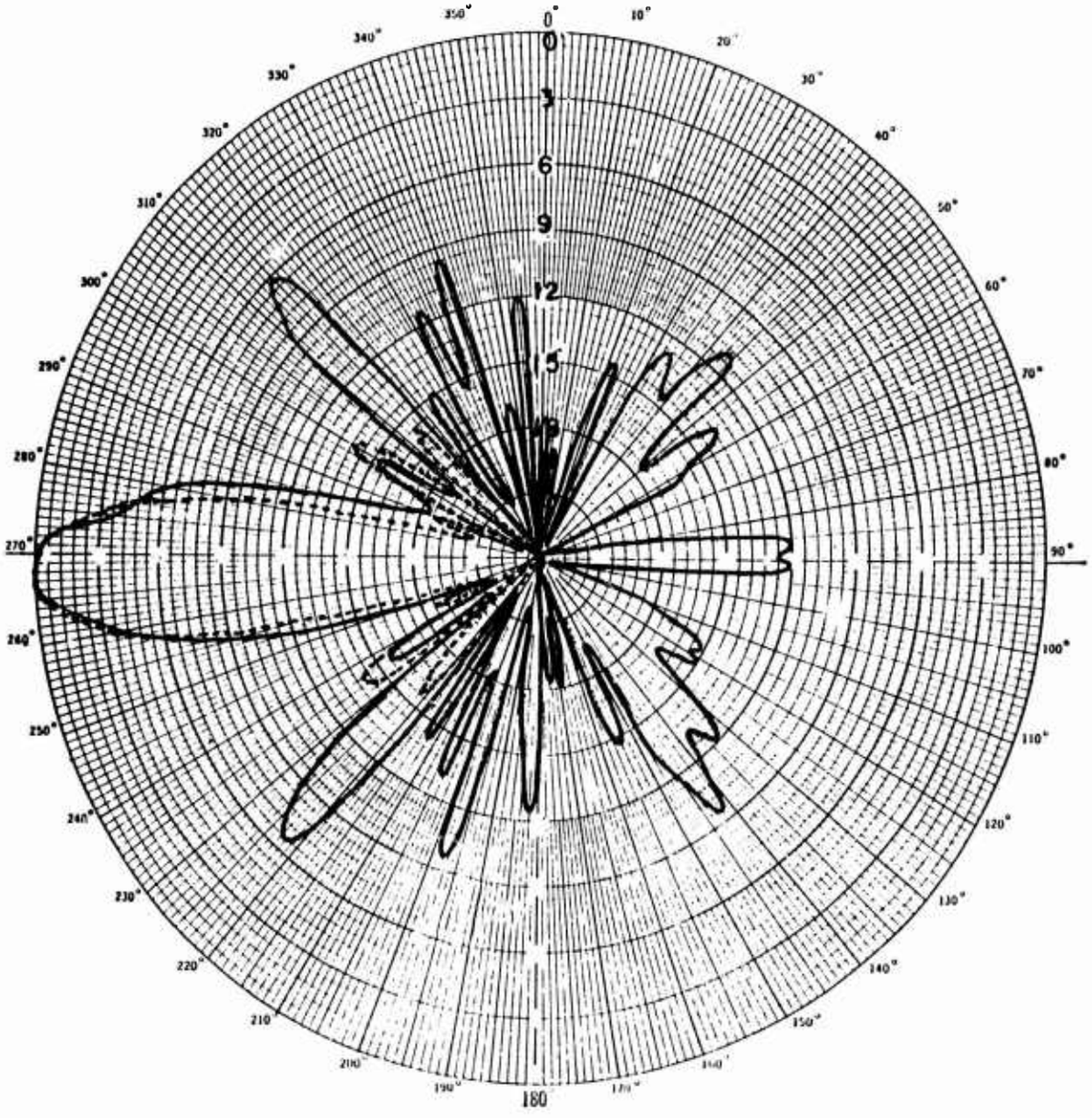

Figure III-8

WEST RHOMBIC
HORIZONTAL POLARIZATION

Elevation 16°

—— Experimental Freq. 10.5 MHz

Pk = -3.4 dB

---- Computed Freq. 10.0 MHz

Pk = -2.1 dB

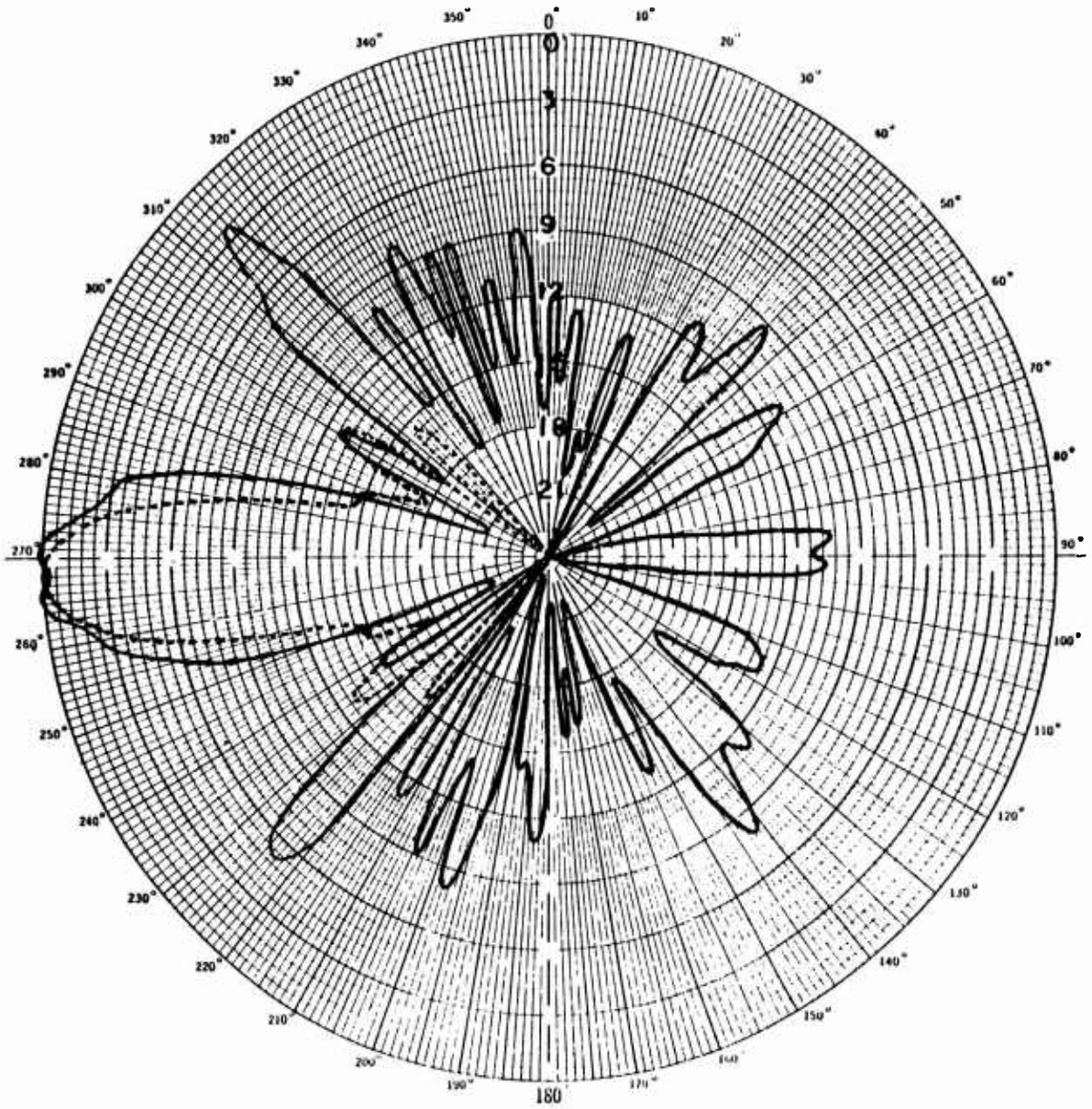

Figure III-9

WEST RHOMBIC
HORIZONTAL POLARIZATION

Elevation 18°

——— Experimental Freq. 10.5 MHz

Pk = -5.8 dB

---- Computed Freq. 10.0 MHz

Pk = -4.2 dB

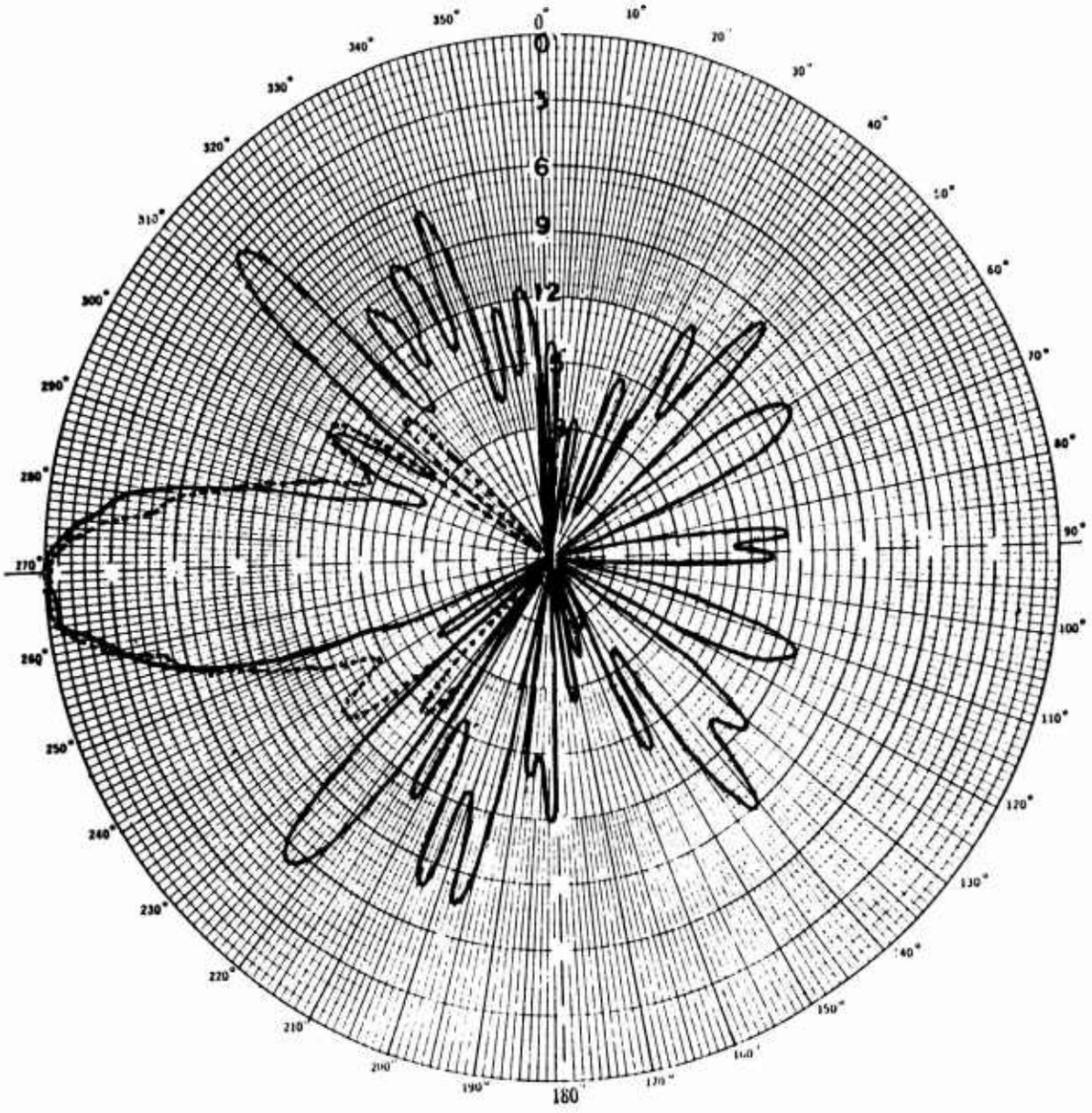

Figure III-10

WEST RHOMBIC
HORIZONTAL POLARIZATION

Elevation 20°

—— Experimental Freq. 10.5 MHz

Pk = -6.3 dB

---- Computed Freq. 10.0 MHz

Pk = -6.4 dB

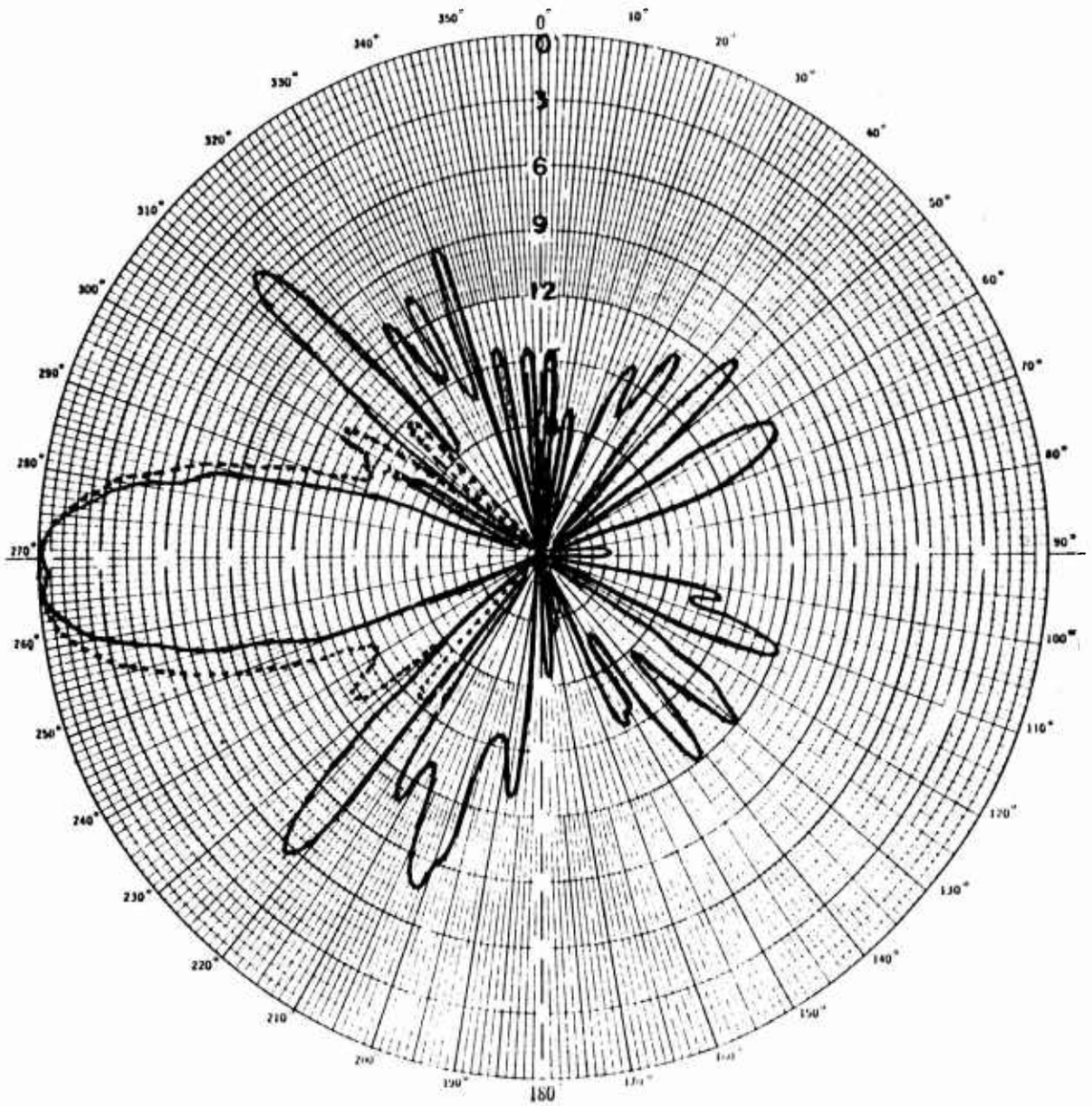

Figure III-11

WEST RHOMBIC
HORIZONTAL POLARIZATION

Elevation 22°

—— Experimental Freq. 10.5 MHz

Pk = -6.0 dB

---- Computed Freq. 10.0 MHz

Pk = -7.0 dB

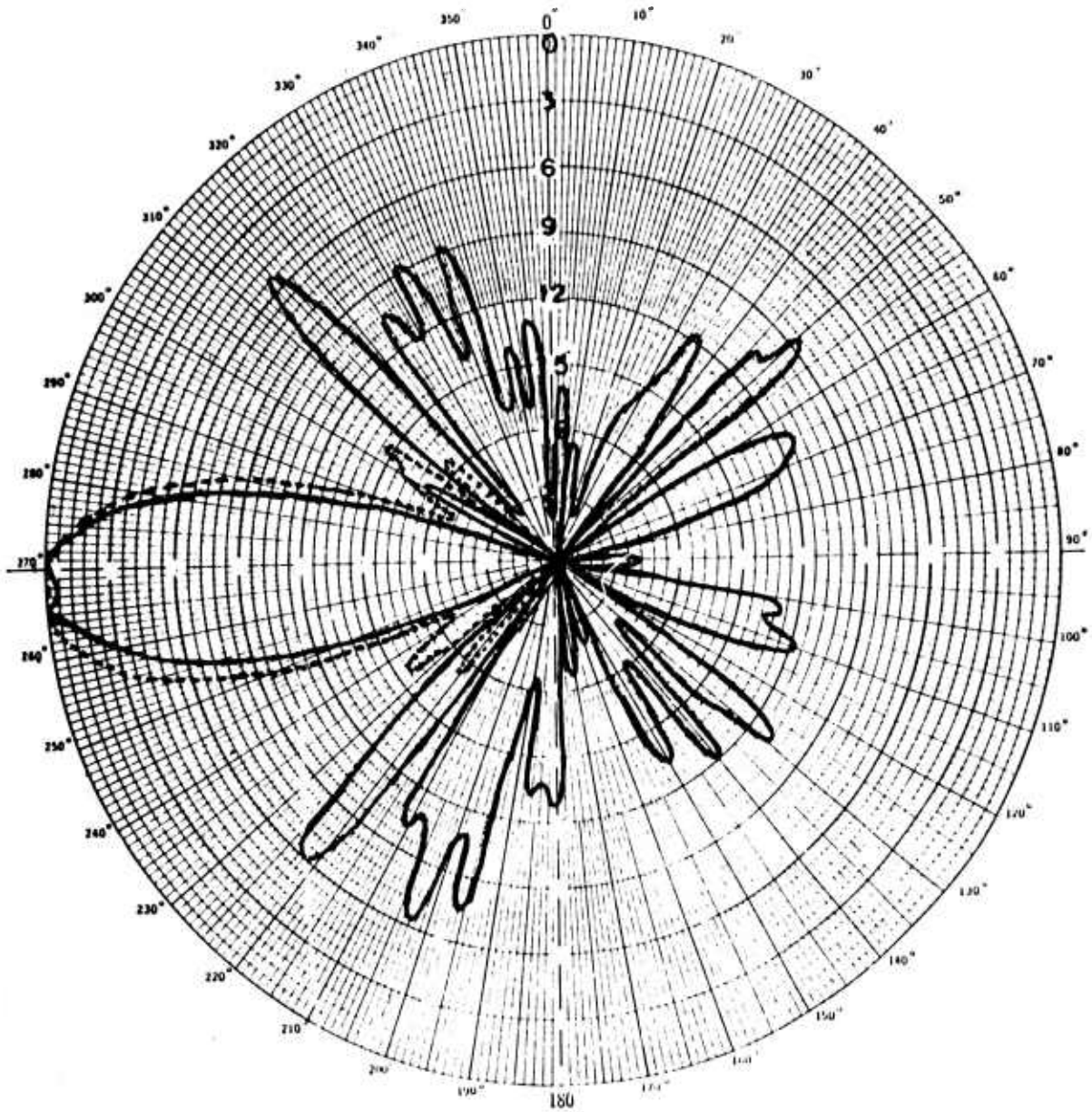

Figure III-12

WEST RHOMBIC
HORIZONTAL POLARIZATION

Elevation 24°

—— Experimental Freq. 10.5 MHz

Pk = -7.0 dB

---- Computed Freq. 10.0 MHz

Pk = -6.2 dB

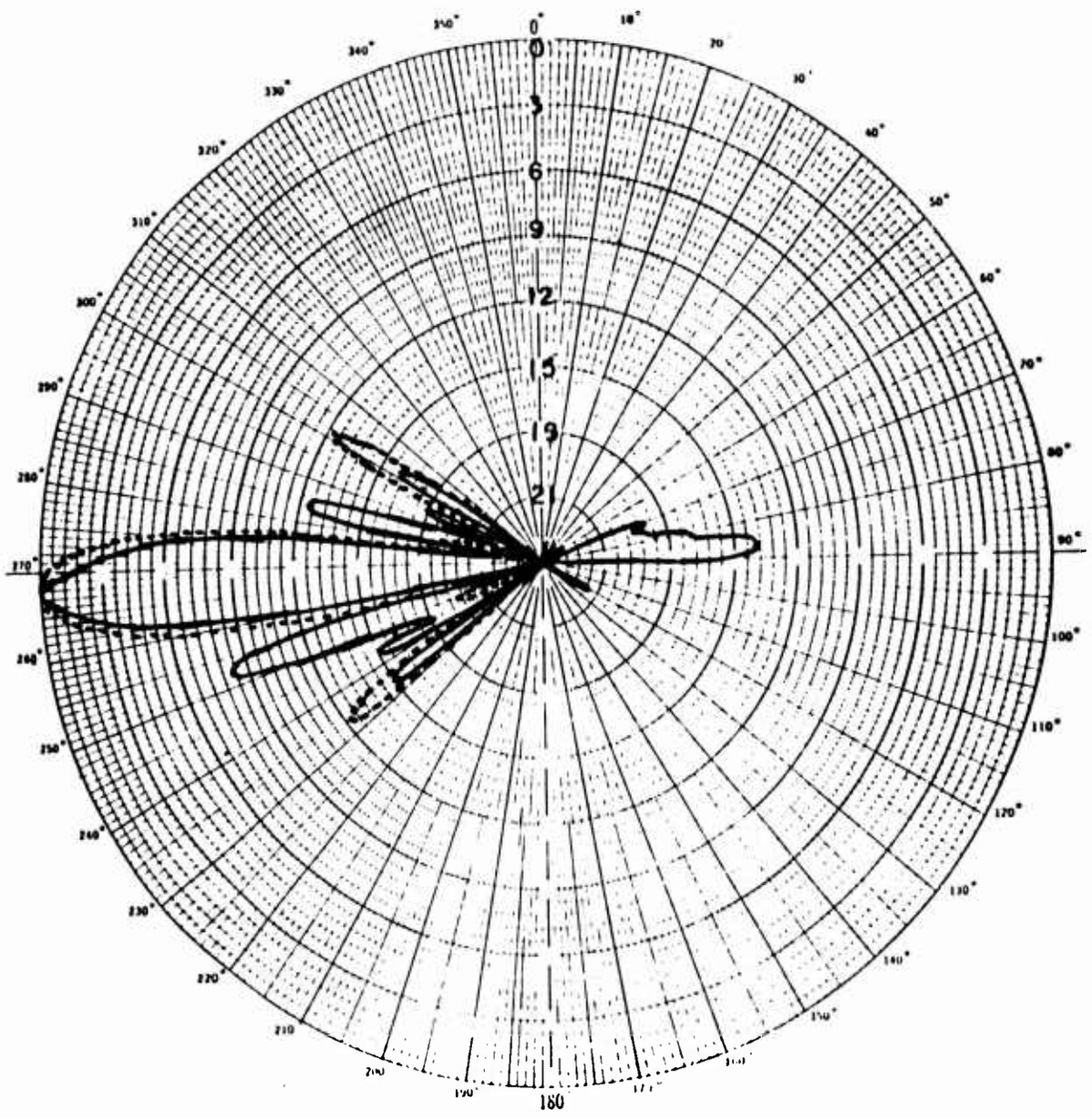

Figure III-13

WEST RHOMBIC
HORIZONTAL POLARIZATION

Elevation 2°

—— Experimental Freq. 15.093 MHz ---- Computed Freq. 15.0 MHz

Pk = -2 dB Pk = -6.92 dB

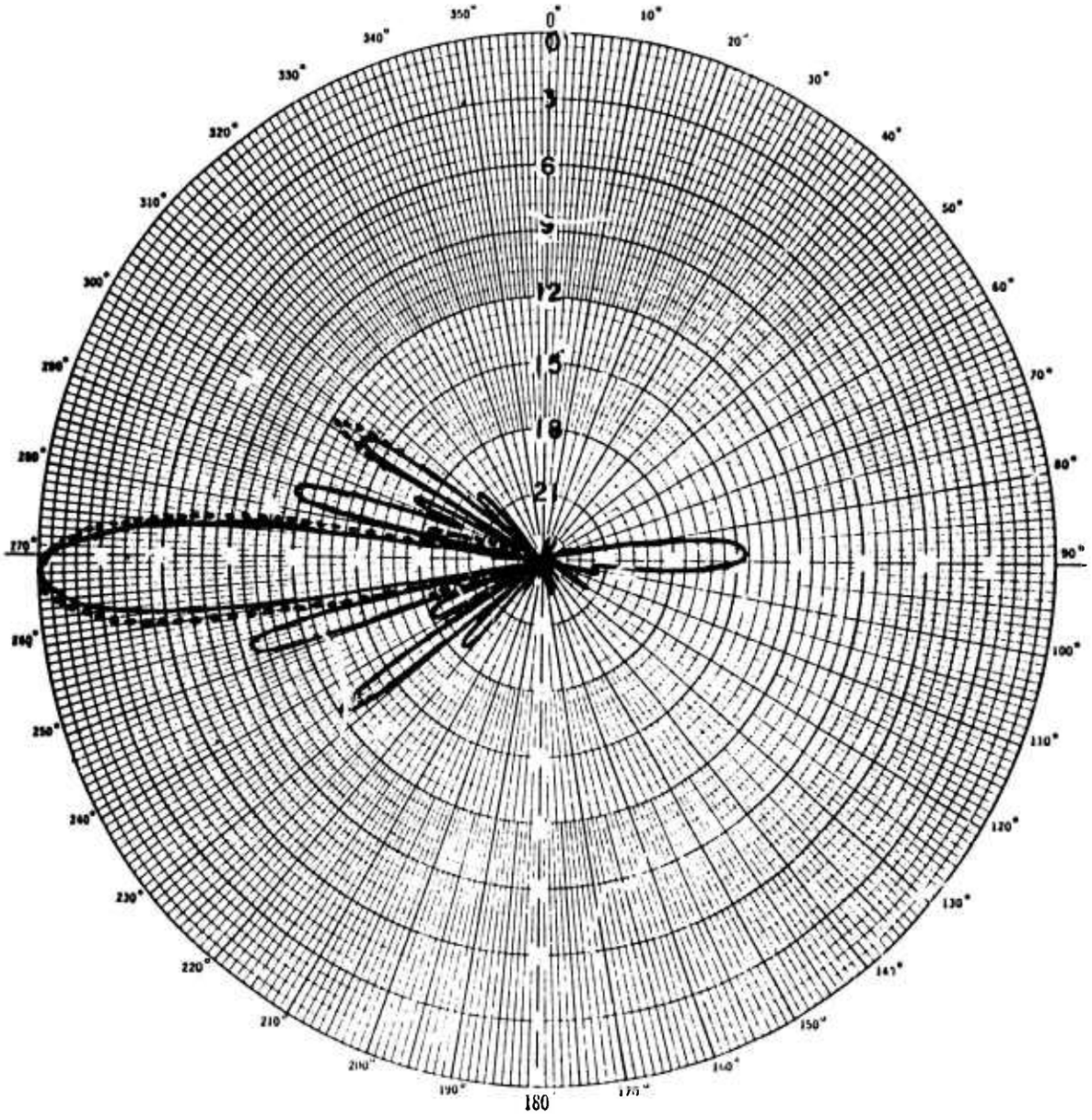

Figure III-14

WEST RHOMBIC
HORIZONTAL POLARIZATION

Elevation 4°

—— Experimental Freq. 15.093 MHz

Pk = -.3 dB

---- Computed Freq. 15.0 MHz

Pk = -1.9 dB

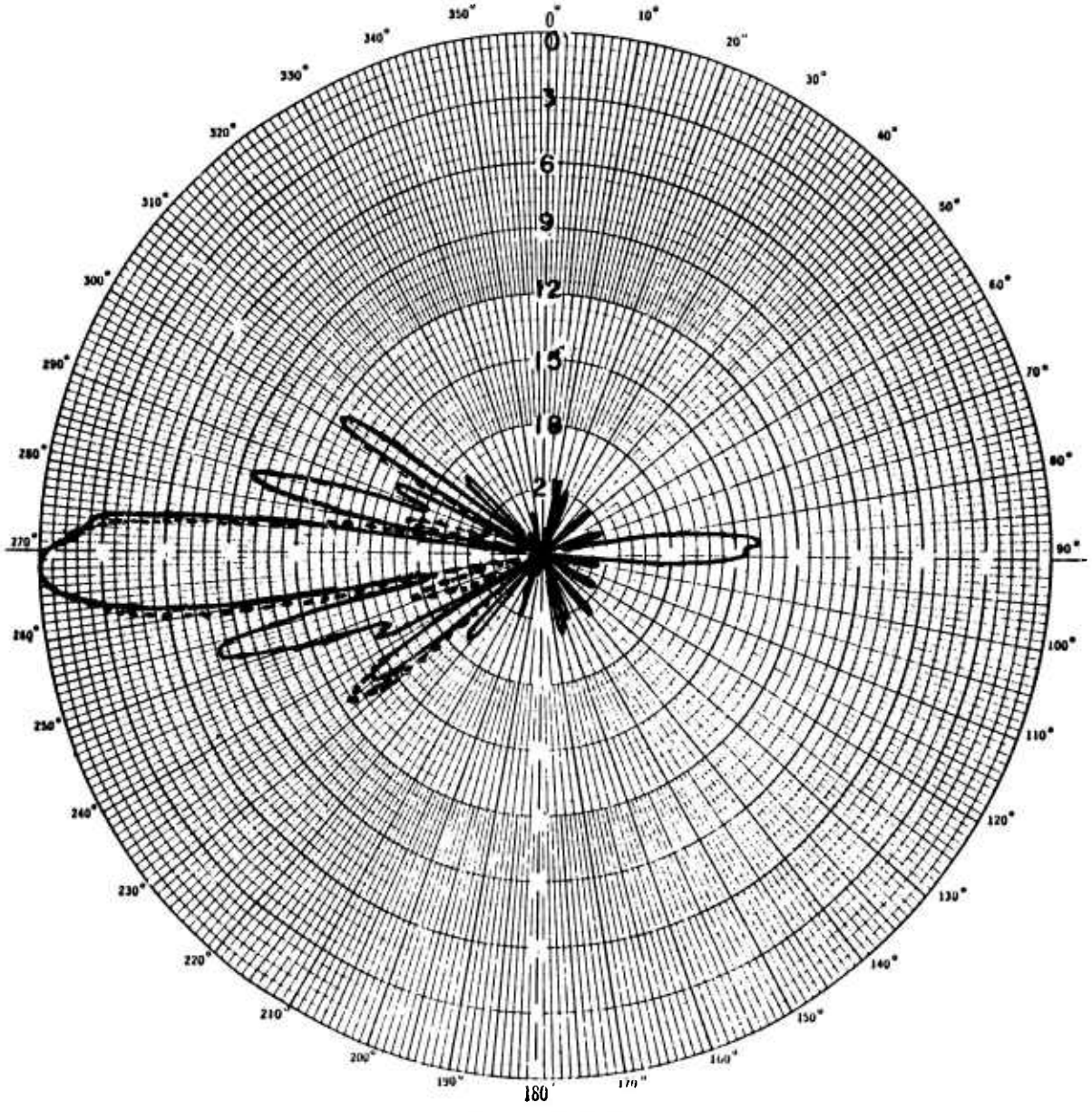

Figure III-15

WEST RHOMBIC
HORIZONTAL POLARIZATION

Elevation 6°

—— Experimental Freq. 15.093 MHz

Pk = 0. dB

---- Computed Freq. 15.0 MHz

Pk = -.03 dB

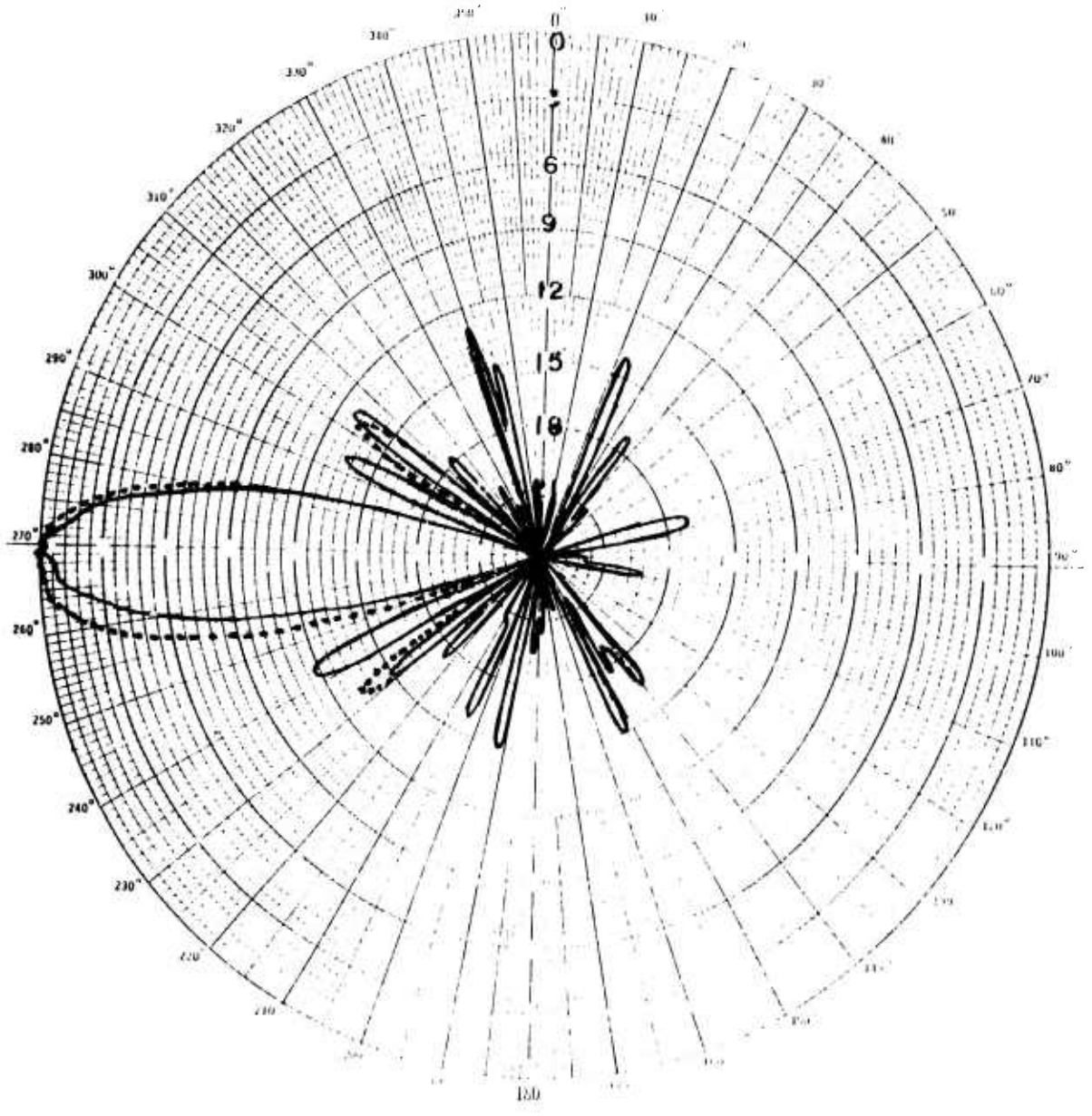

Figure III-16

WEST RHOMBIC
HOPIZONTAL POLARIZATION

Elevation 16°

—— Experimental Freq. 15.093 MHz

Pk = -4. dB

---- Computed Freq. 15.0 MHz

Pk = -5.7 dB

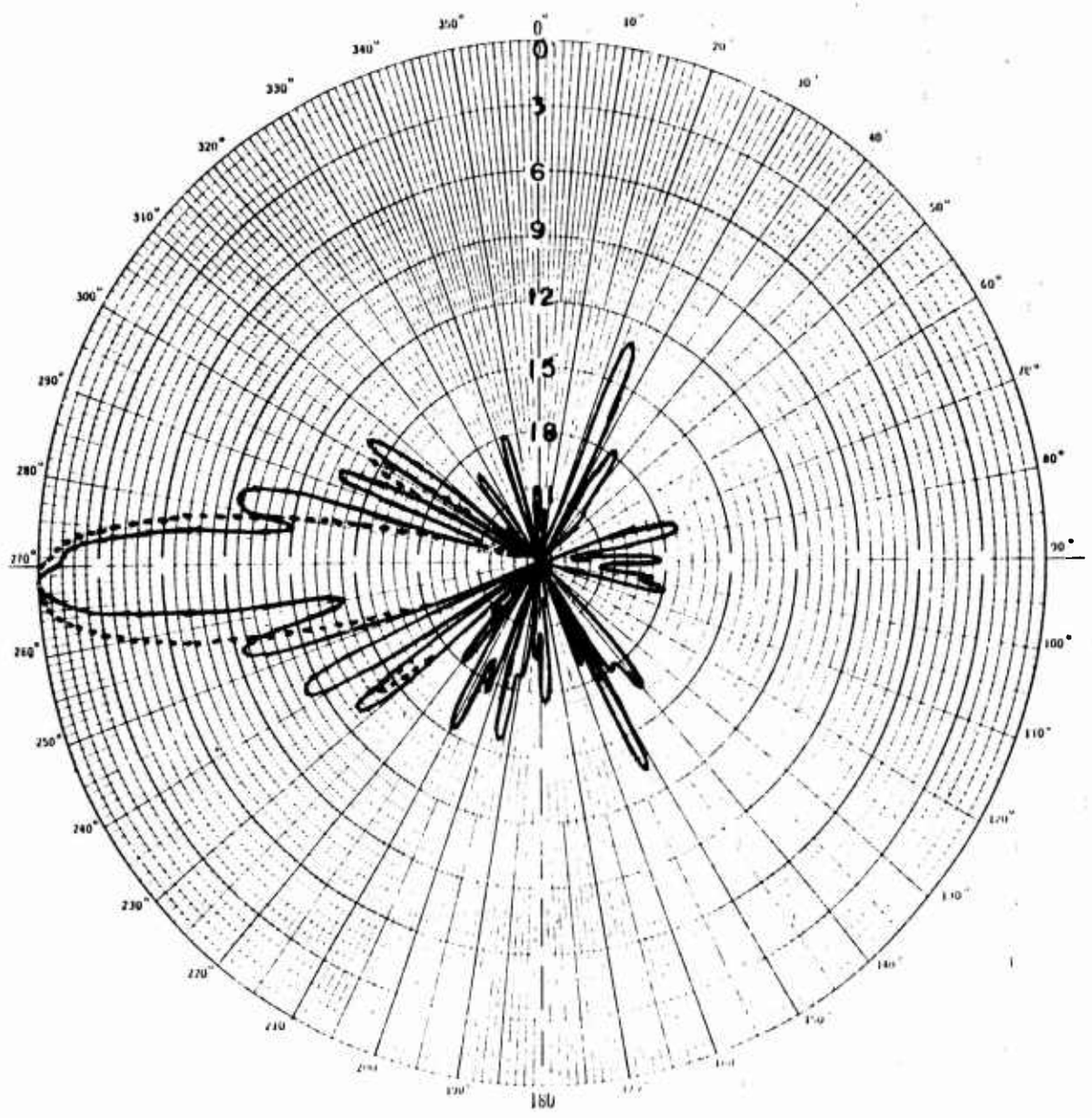

Figure III-17

WEST RHOMBIC
HORIZONTAL POLARIZATION

Elevation 18°

—— Experimental Freq. 15.093 MHz ---- Computed Freq. 15.0 MHz

Pk = -4.5 dB Pk = -5.16 dB

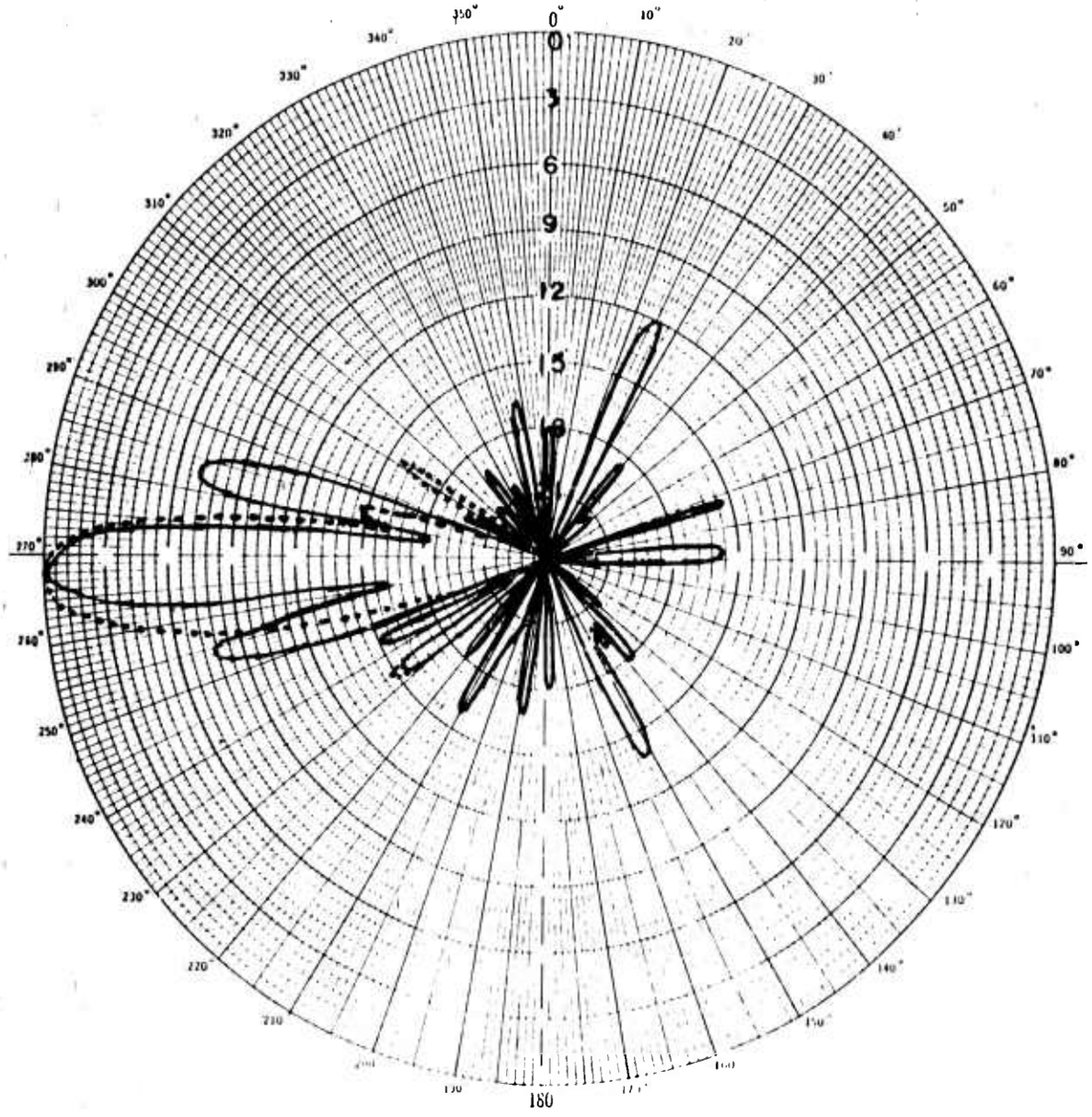

Figure III-18

WEST RHOMBIC
HORIZONTAL POLARIZATION

Elevation 20°

—— Experimental Freq. 15.093 MHz

Pk = -4.8 dB

---- Computed Freq. 15.0 MHz

Pk = -5.42 dB

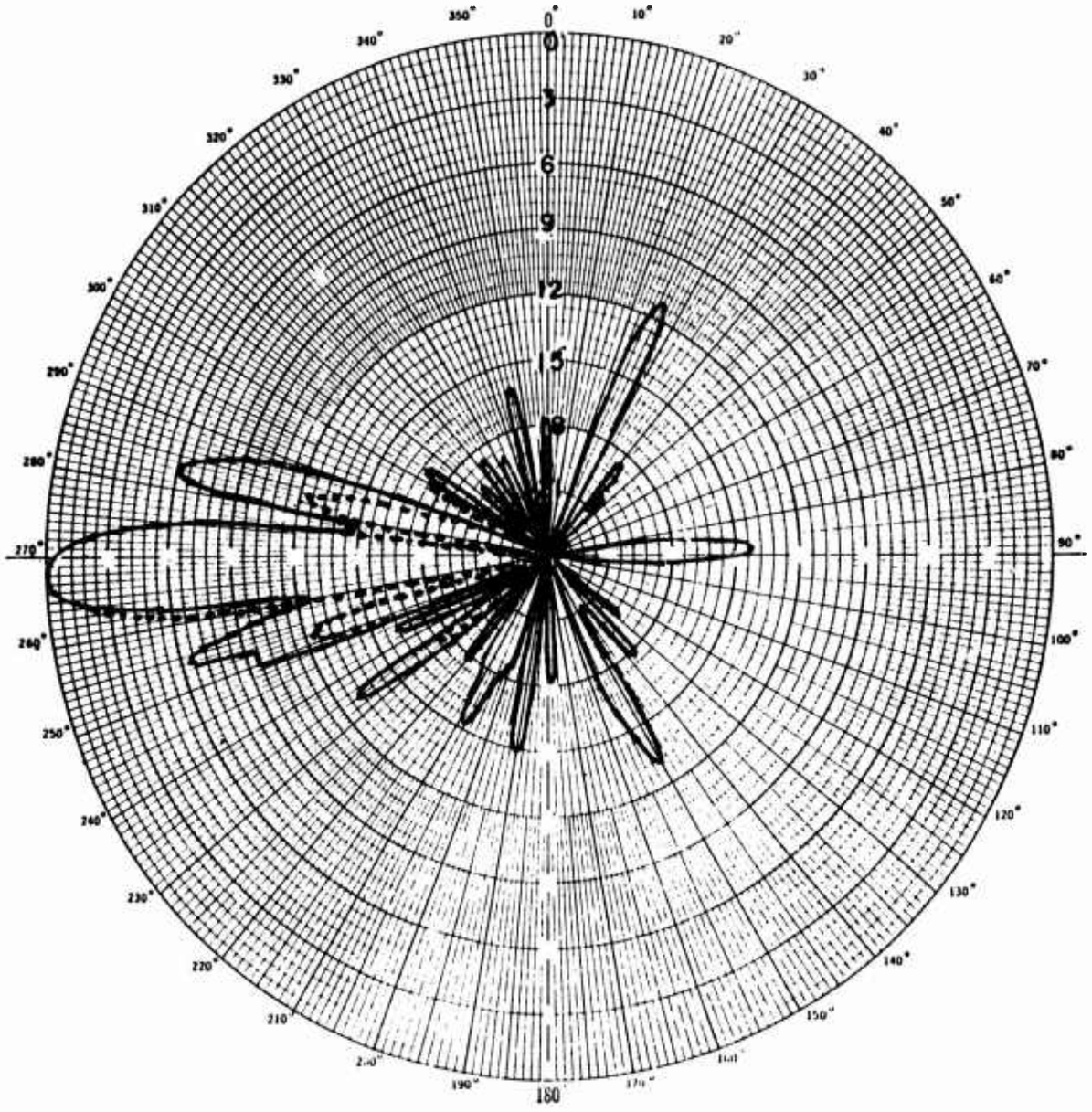

Figure III-19

WEST RHOMBIC
HORIZONTAL POLARIZATION

Elevation 22°

—— Experimental Freq. 15.093 MHz

Pk = -5.3 dB

---- Computed Freq. 15.0 MHz

Pk = -5.85 dB

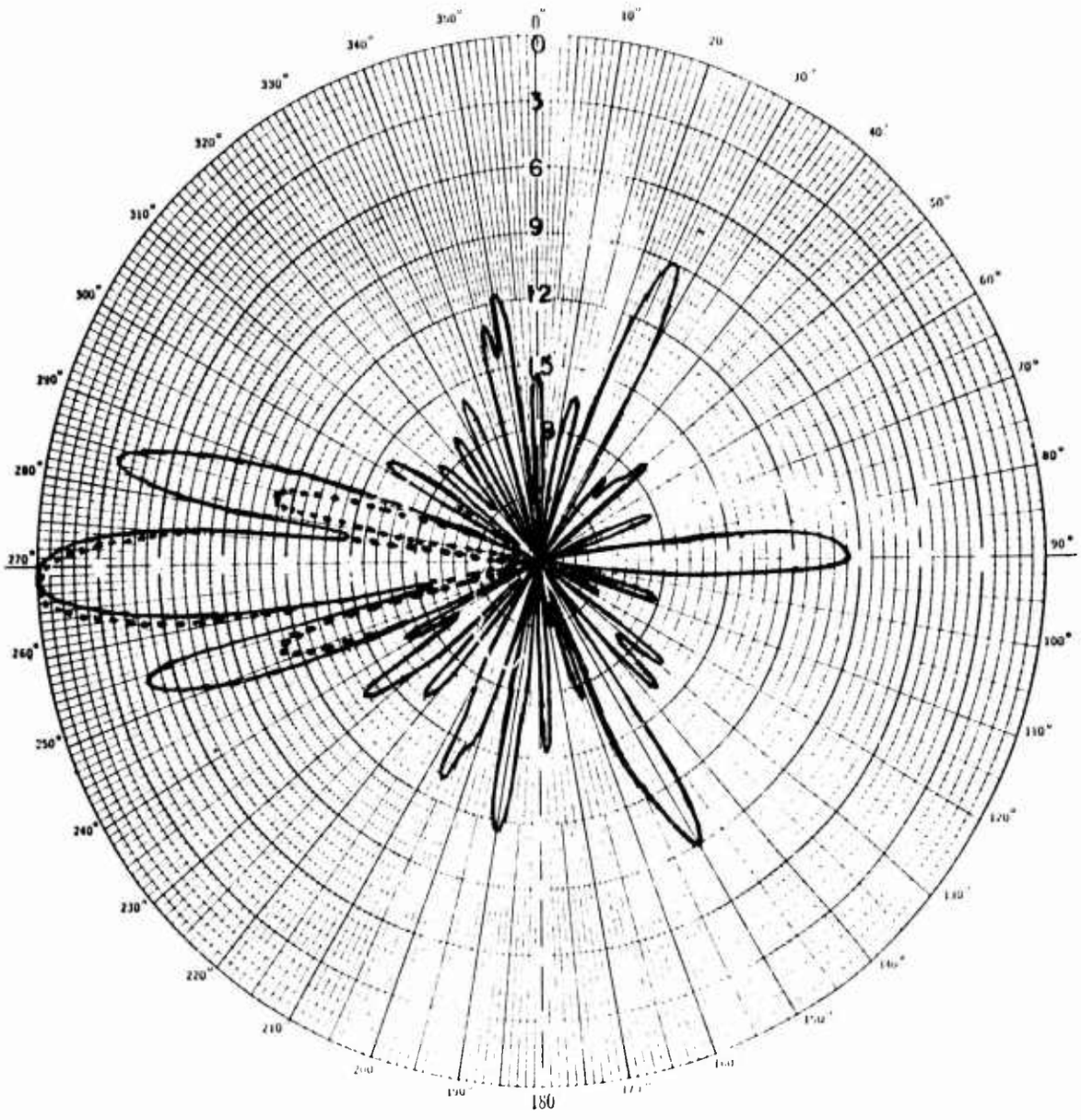

Figure III-20

WEST RHOMBIC
HORIZONTAL POLARIZATION

Elevation 24°

—— Experimental Freq. 15.093 MHz ---- Computed Freq. 15.0 MHz

Pk = -8.3 dB Pk = -6.44 dB

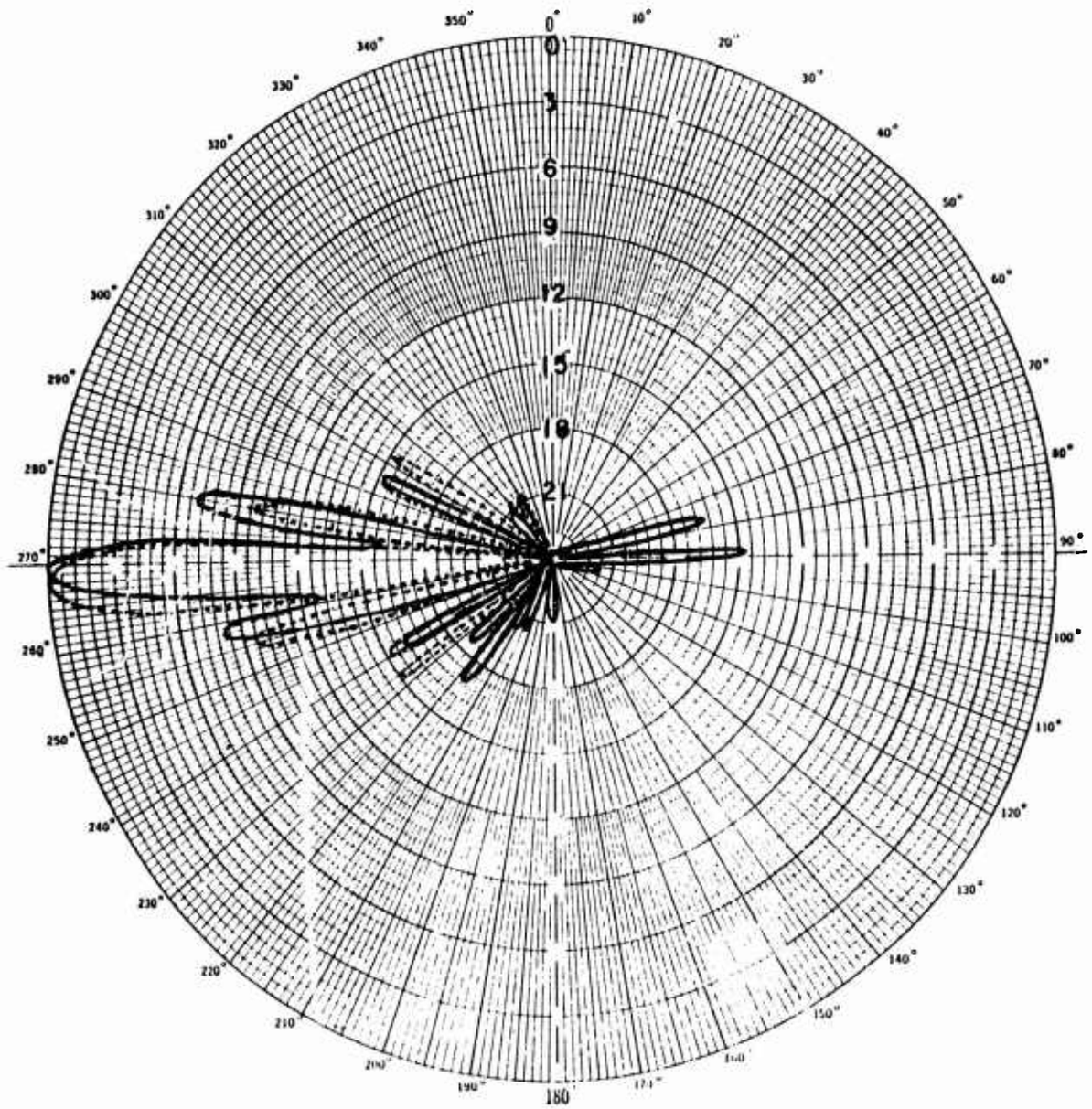

Figure III-21

WEST RHOMBIC
HORIZONTAL POLARIZATION

Elevation 2°

_____ Experimental Freq. 20.052 MHz ---- Computed Freq. 20.0 MHz

Pk = -1.2 dB Pk = -4.5 dB

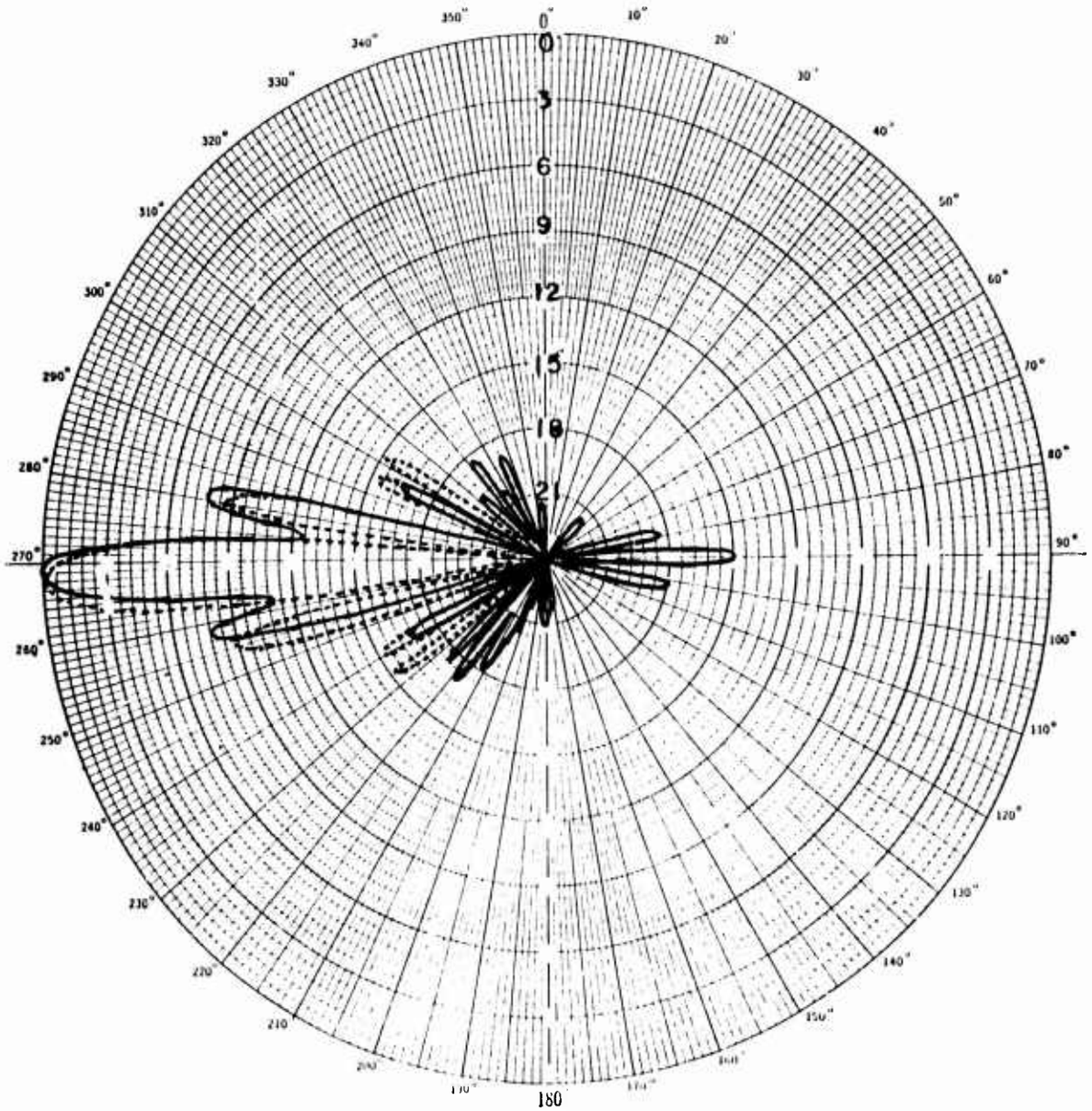

Figure III-22

WEST RHOMBIC
HORIZONTAL POLARIZATION

Elevation 4°

—— Experimental Freq. 20.052 MHz Pk = -.1 dB

---- Computed Freq. 20.0 MHz Pk = -.3 dB

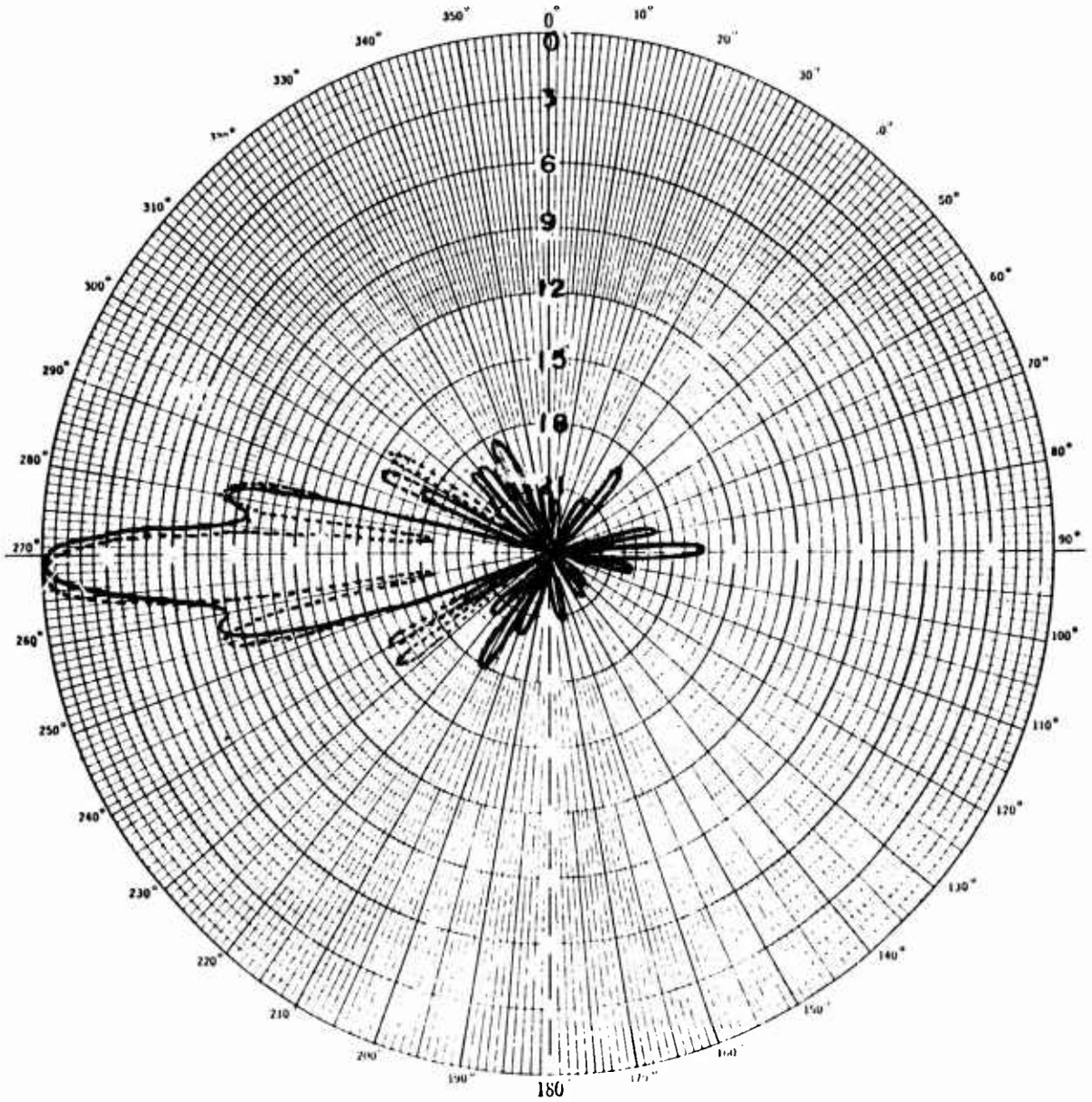

Figure III-23

WEST RHOMBIC
HORIZONTAL POLARIZATION

Elevation 6°

—— Experimental Freq. 20.052 MHz

Pk = 0 dB

---- Computed Freq. 20.0 MHz

Pk = 0 dB

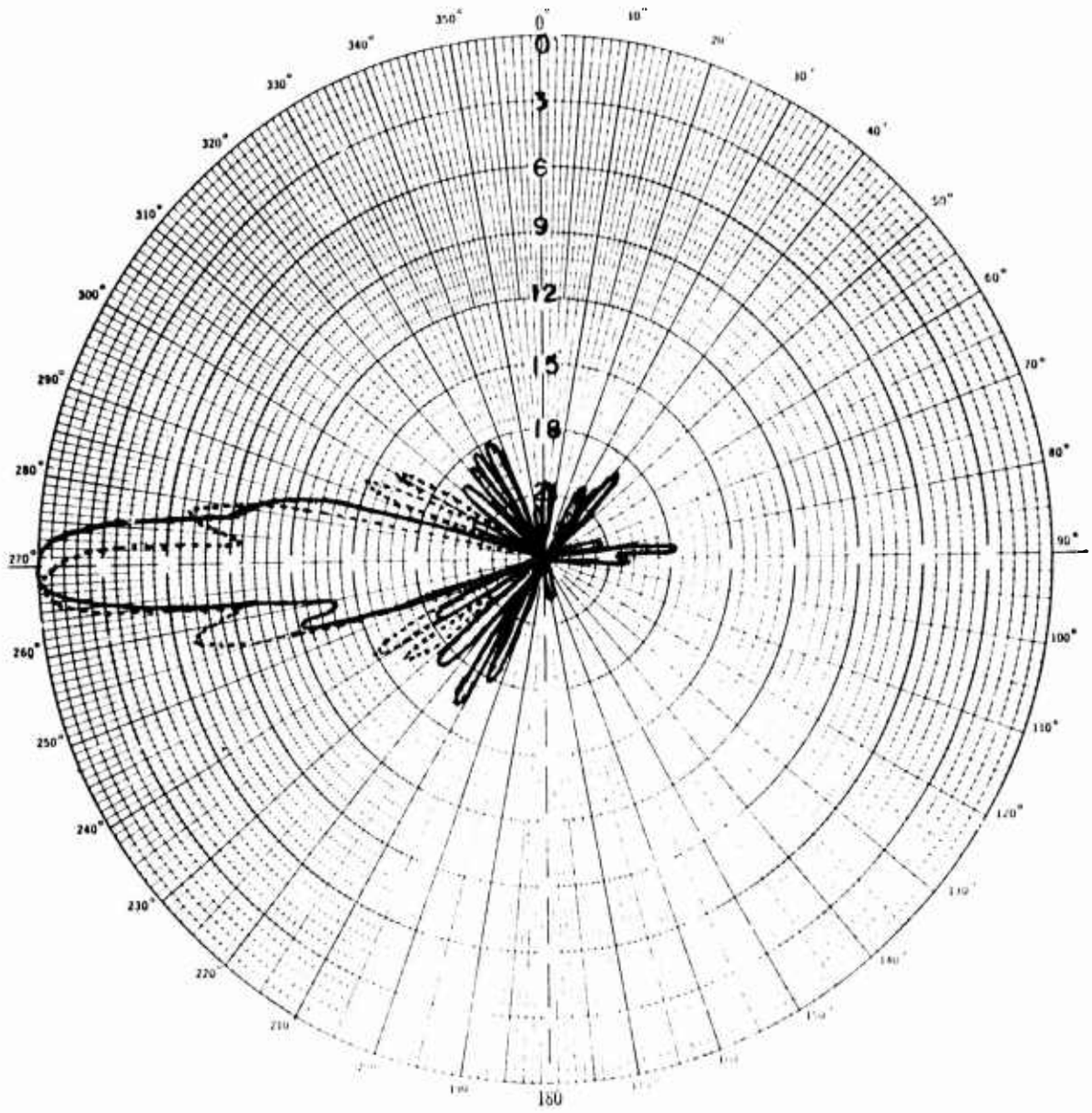

Figure III-24

WEST RHOMBIC
HORIZONTAL POLARIZATION

Elevation 8°

—— Experimental Freq. 20.052 MHz Pk = -.8 dB

---- Computed Freq. 20.0 MHz Pk = -1.7 dB

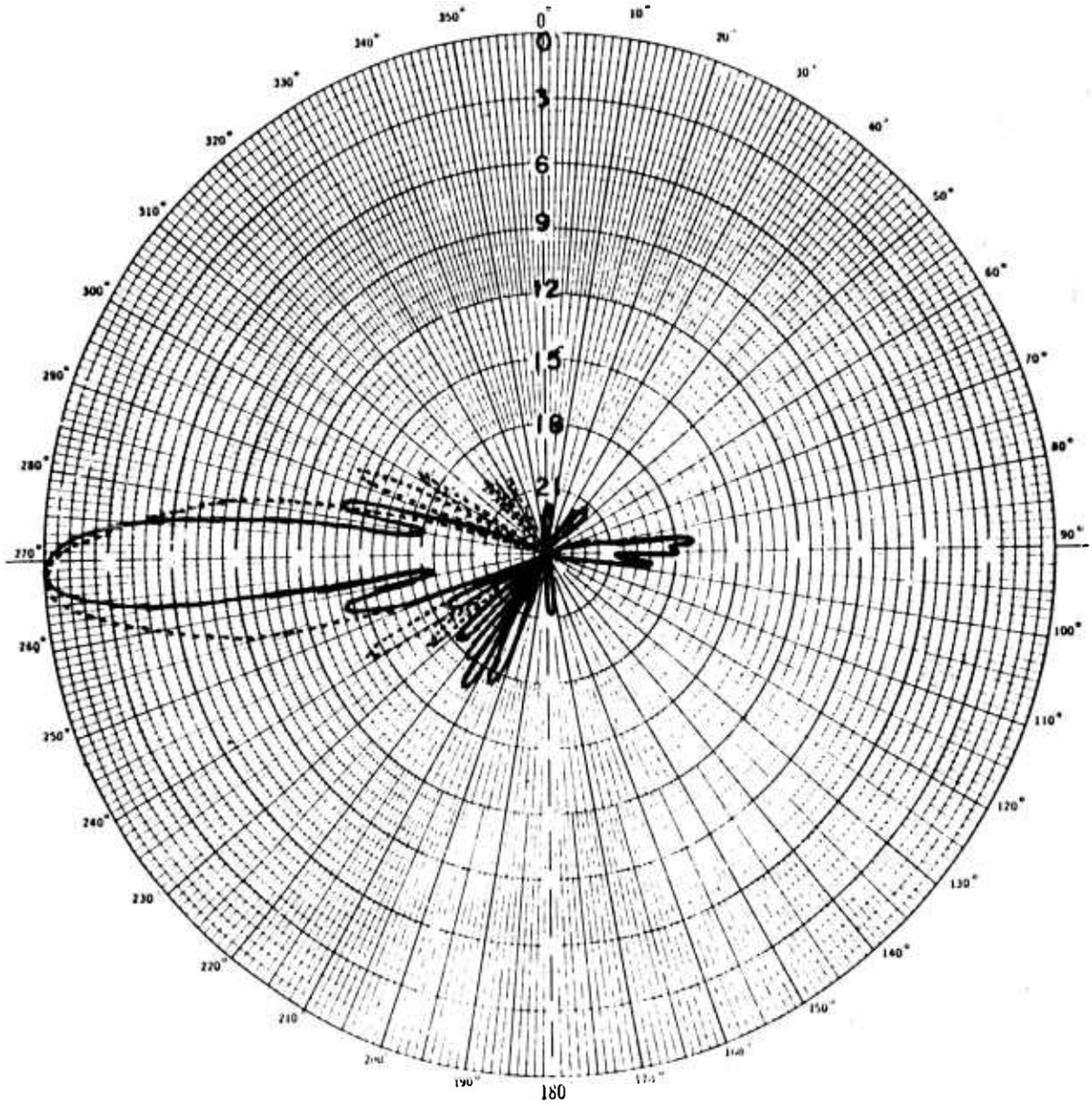

Figure III-25

WEST RHOMBIC
HORIZONTAL POLARIZATION

Elevation 10°

____ Experimental Freq. 20.052 MHz Pk = -1.2 dB

---- Computed Freq. 20.0 MHz Pk = -3.6 dB

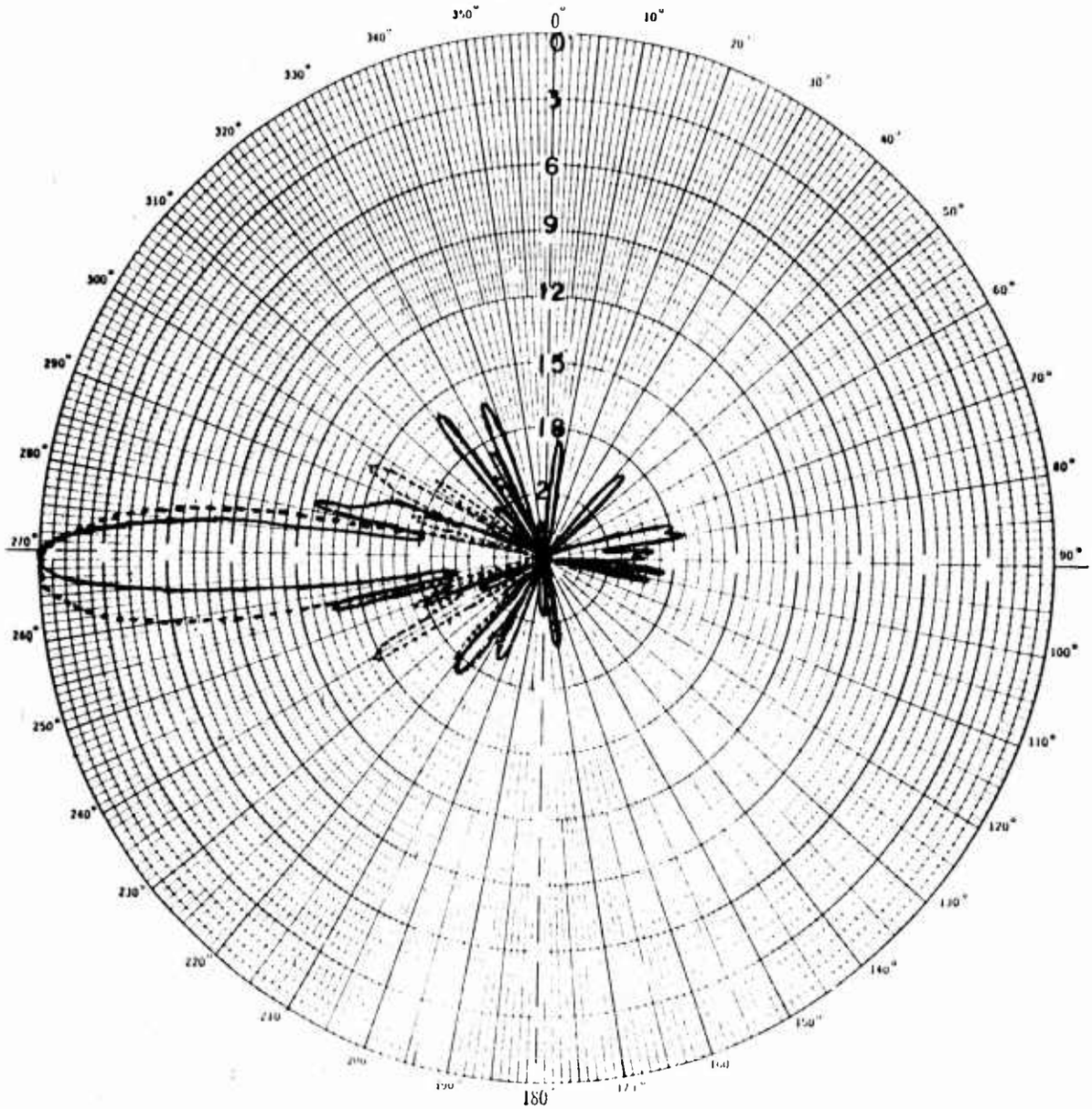

Figure III-26

WEST RHOMBIC
HORIZONTAL POLARIZATION

Elevation 12°

—— Experimental Freq. 20.052 MHz

Pk = -3.1 dB

---- Computed Freq. 20.0 MHz

Pk = -3.7 dB

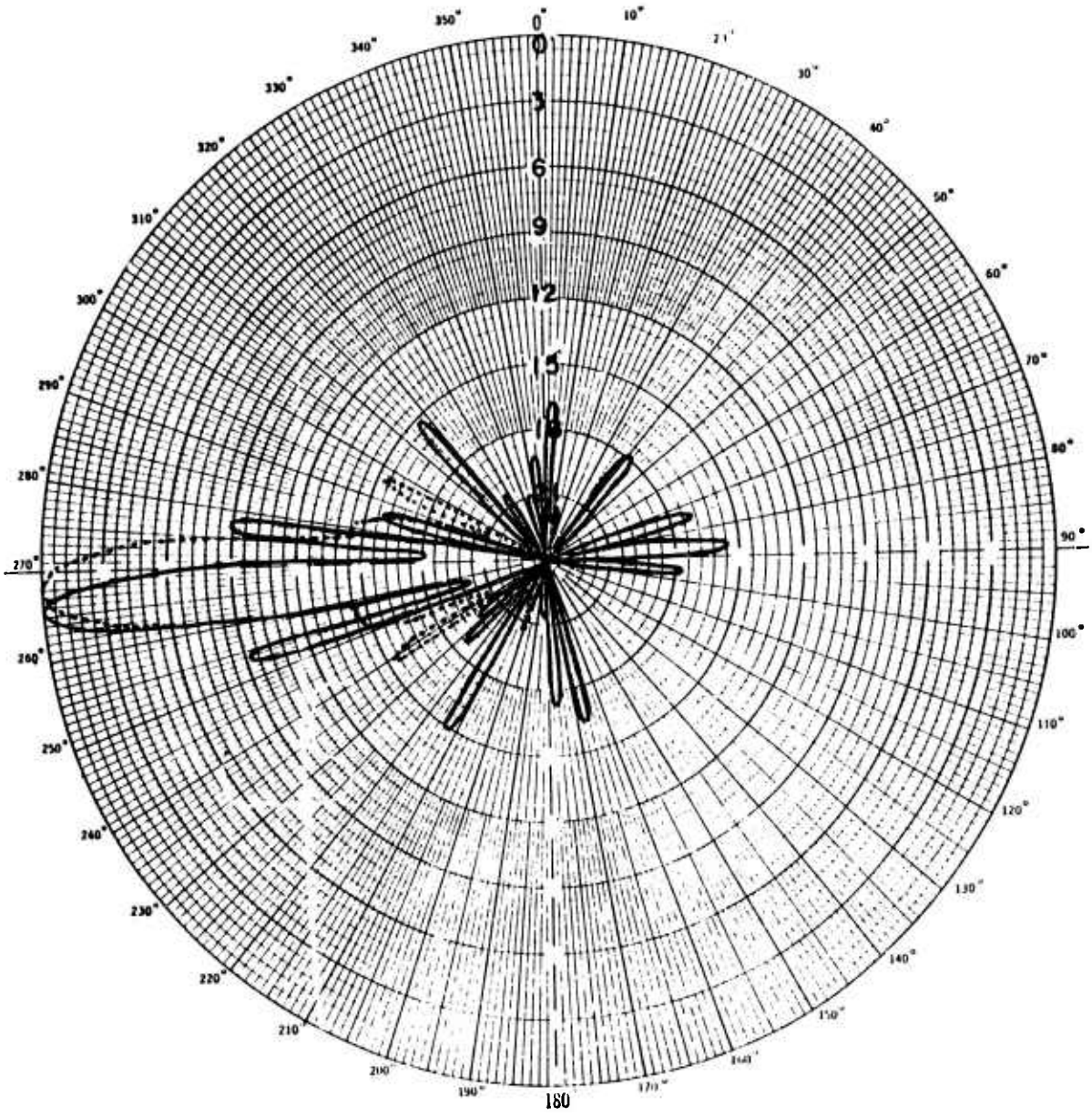

Figure III-27

WEST RHOMBIC
HORIZONTAL POLARIZATION

Elevation 14°

—— Experimental Freq. 20.052 MHz

Pk = -4.2 dB

---- Computed Freq. 20.0 MHz

Pk = -3.8 dB

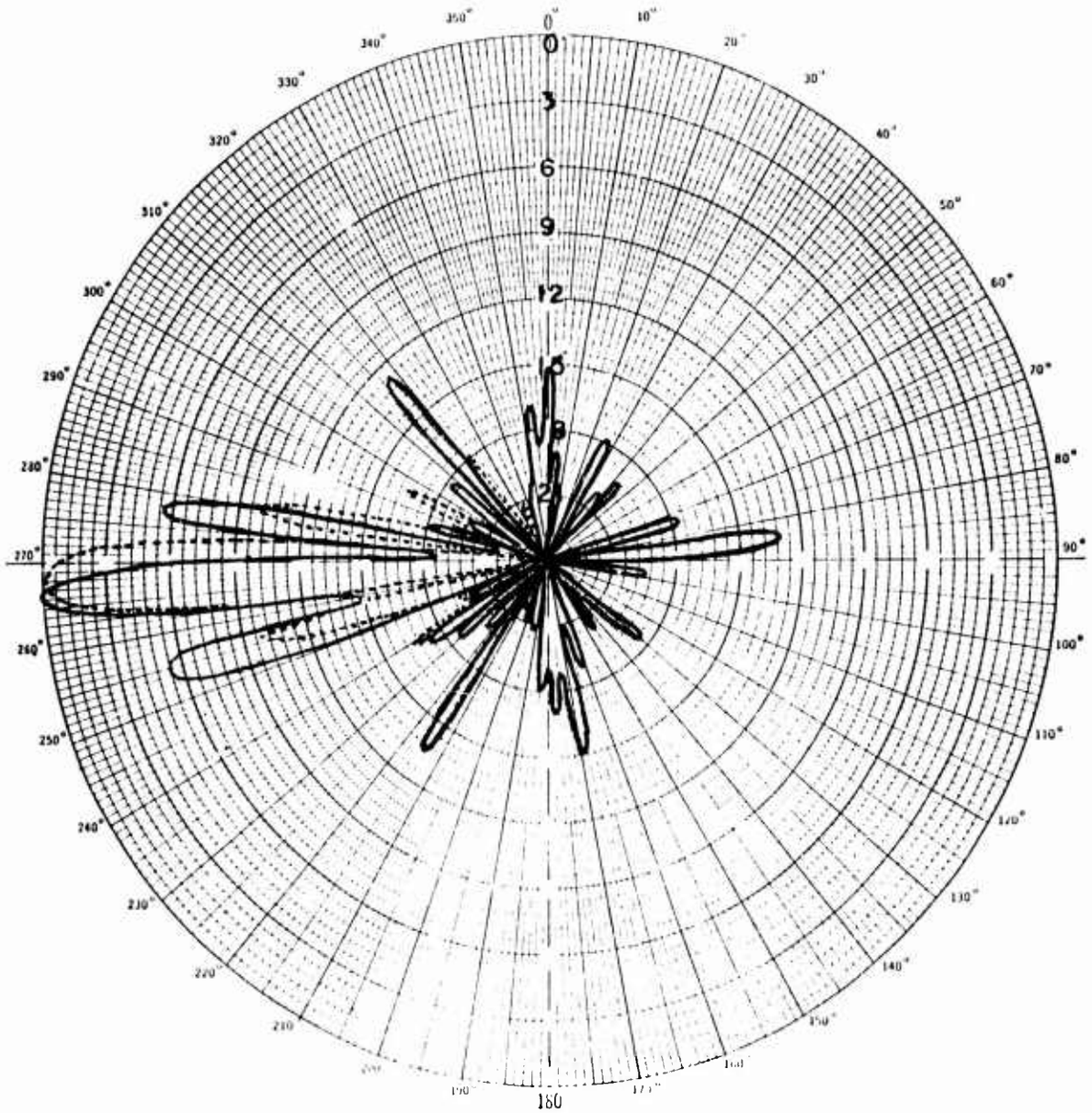

Figure III-28

WEST RHOMBIC
HORIZONTAL POLARIZATION

Elevation 16°

—— Experimental Freq. 20.052 MHz ---- Computed Freq. 20.0 MHz

Pk = -6.2 dB Pk = -4.0 dB

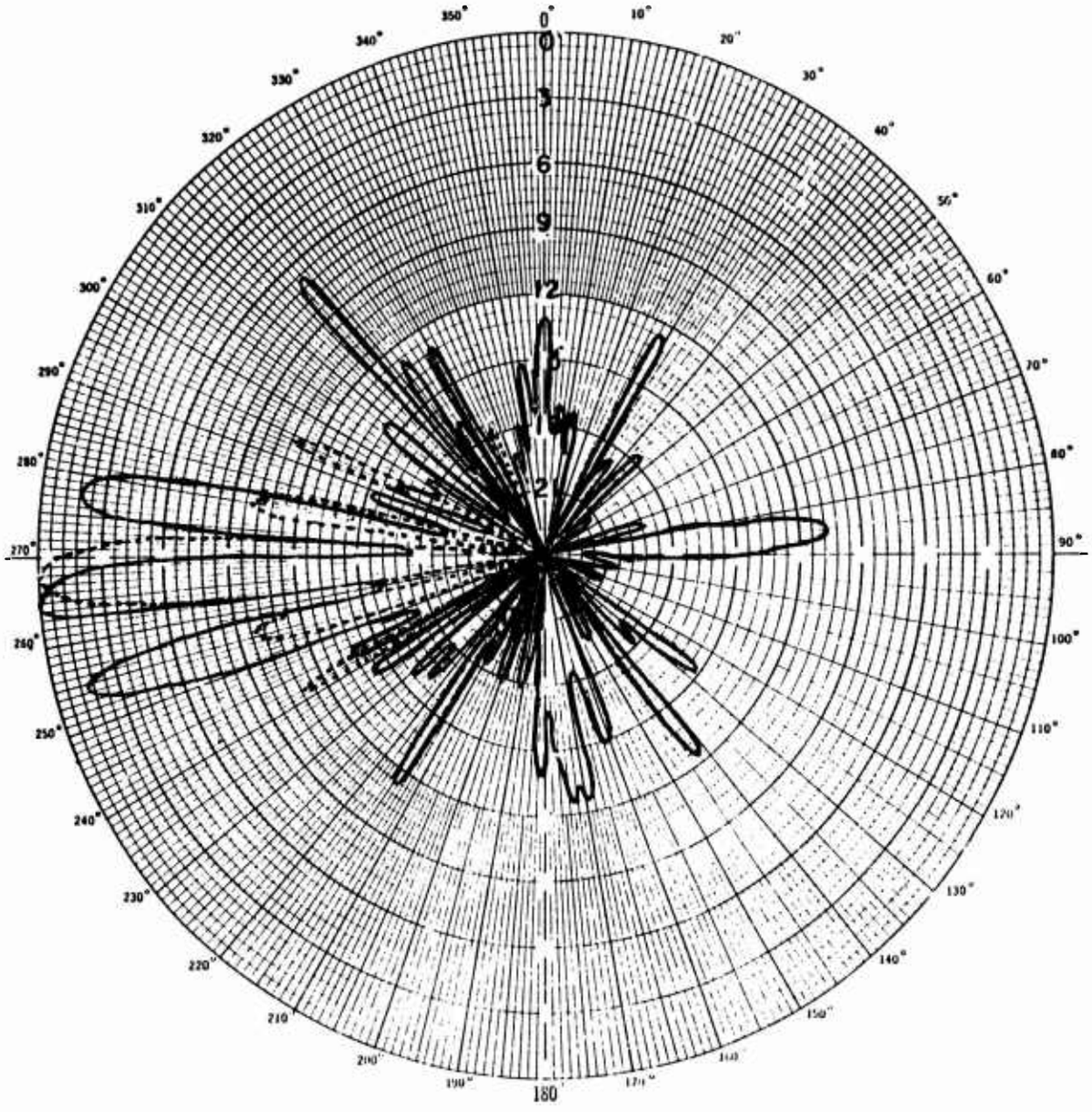

Figure III-29

WEST RHOMBIC
HORIZONTAL POLARIZATION

Elevation 18°

____ Experimental Freq. 20.052 MHz

Pk = -9.7 dB

---- Computed Freq. 20.0 MHz

Pk = -4.5 dB

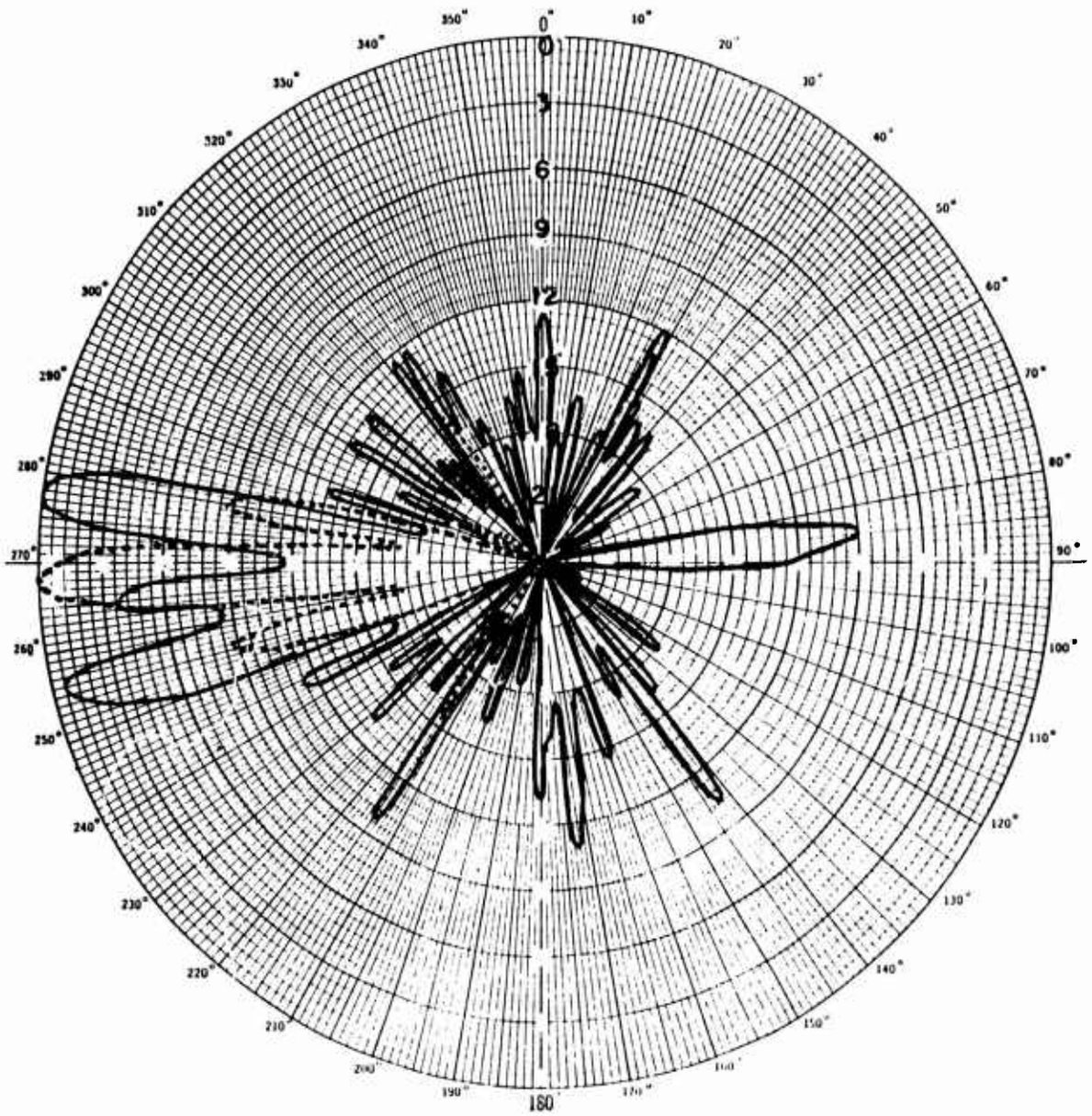

Figure III-30

WEST RHOMBIC
HORIZONTAL POLARIZATION

Elevation 20°

____ Experimental Freq. 20.052 MHz Pk = -15.2 dB

---- Computed Freq. 20.0 MHz Pk = -7.6 dB

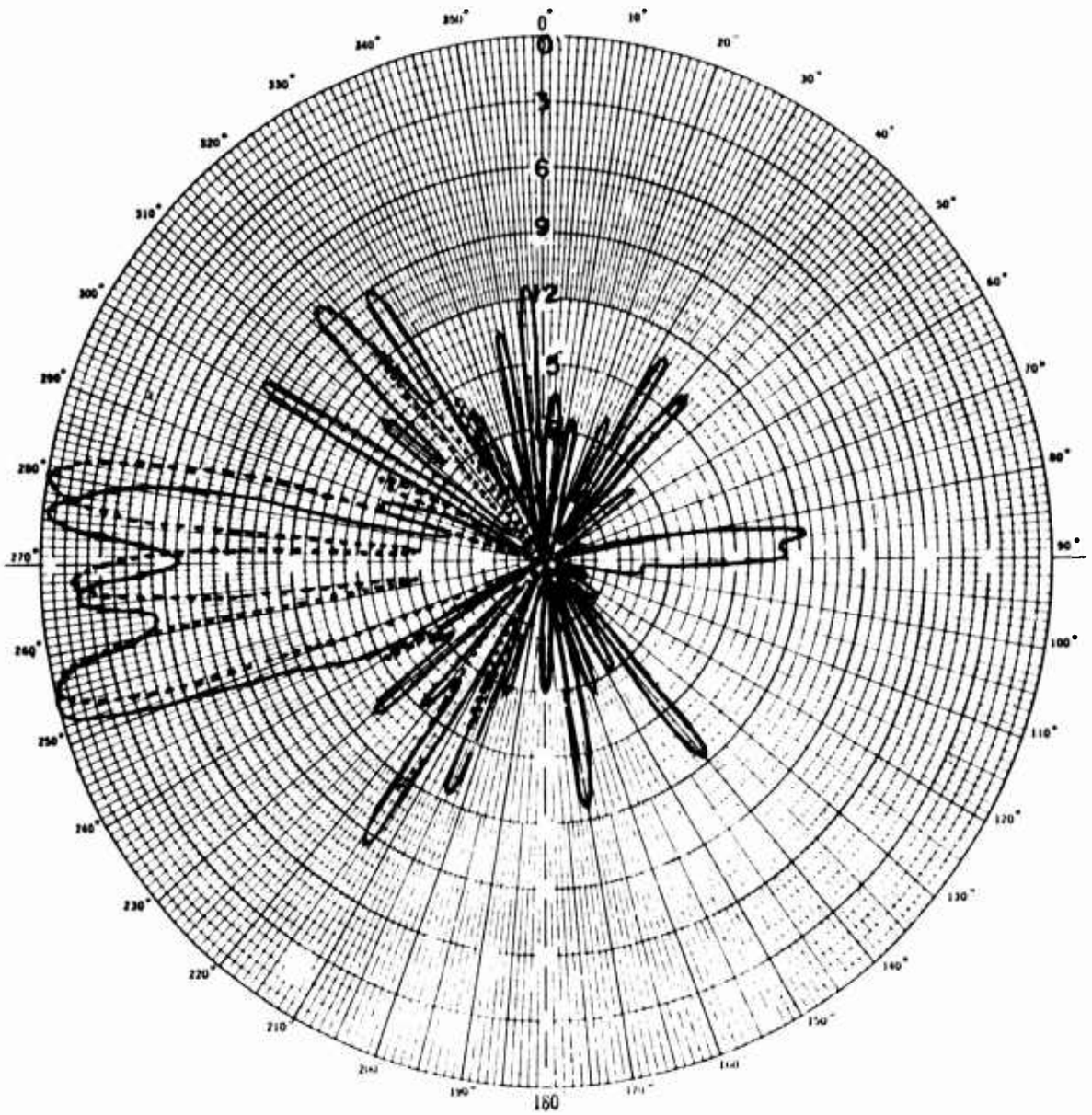

Figure III-31

WEST RHOMBIC
HORIZONTAL POLARIZATION

Elevation 22°

——— Experimental Freq. 20.052 MHz Pk = -13.7 dB

---- Computed Freq. 20.0 MHz Pk = -13.1 dB

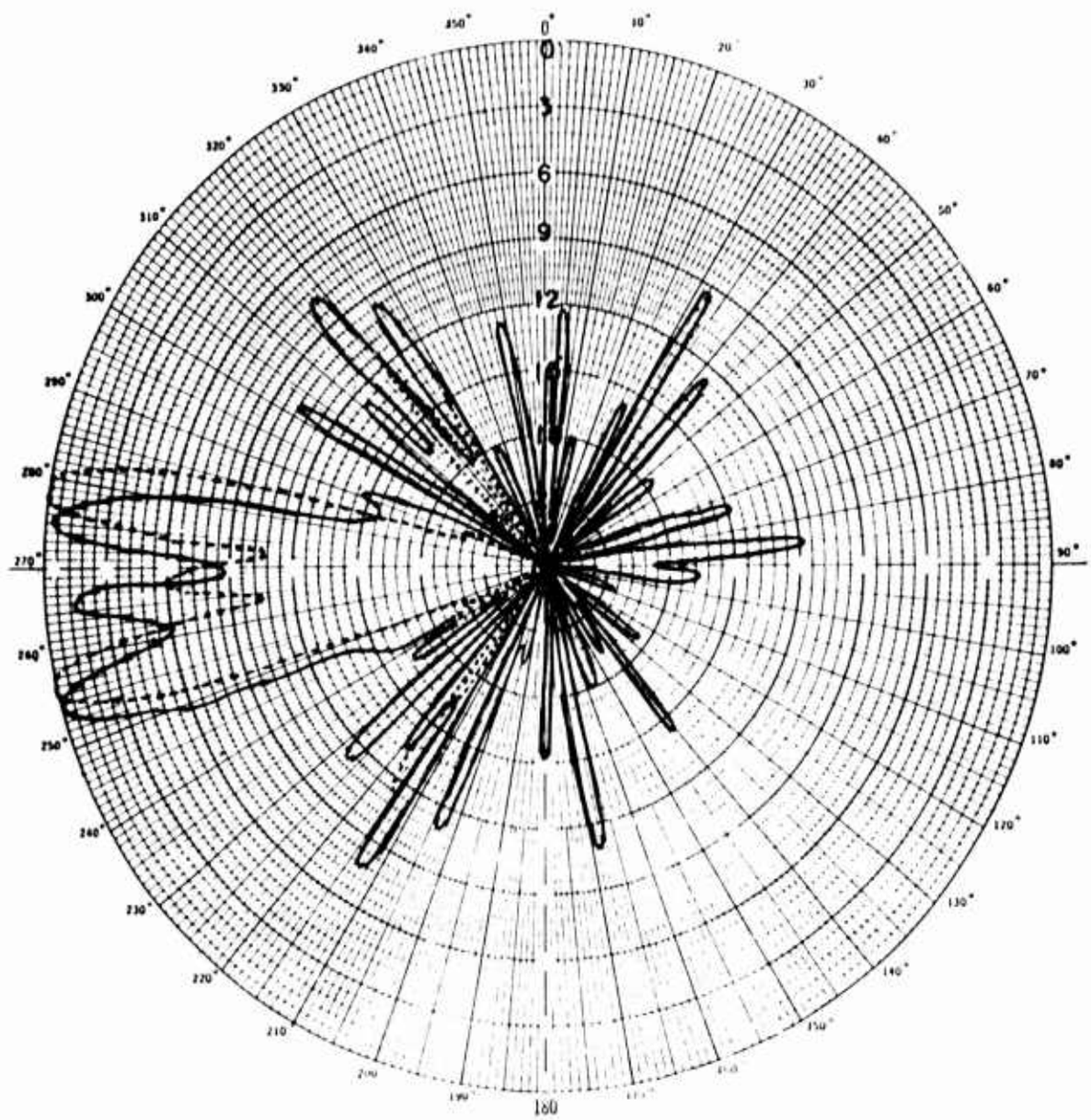

Figure III-32

WEST RHOMBIC
HORIZONTAL POLARIZATION

Elevation 24°

____ Experimental Freq. 20.052 MHz ---- Computed Freq. 20.0 MHz

Pk = -13.2 dB Pk = -14.4 dB

computed beam at 10.0 MHz is .9 dB below the peak of the computed vertical profile which lies between the 10° and 12° elevation plots of Figures III-5 and III-6. This apparent difference between the peak position in the vertical profile of the measured pattern data and the computed pattern data will be accounted for in the following paragraphs. The available experimental data of Figures III-1, III-32 indicate first side lobe levels from 8 to 10 dB down relative to the peak of the main beam, as compared to anticipated first side lobe levels of 5.5 dB using the horizontal configuration of Figure I-2.

It should be noted that the limited experimental data taken at 15.093 MHz resulted in the assumption that the peak of the experimental vertical profile was at 6° in elevation. This assumption was made with the knowledge of the experimental peak positions at frequencies of 10.5 and 20.052 MHz. The accuracy of this assumption is demonstrated when comparing the relative peak position of the computed at 15.0 MHz to that assumed for the experimental at an operating frequency of 15.093 MHz.

Figures III-33 through III-56 are plots of the measured antenna patterns with respect to the vertical profile peak position, for elevation angles of from 2° to 24°. These figures, III-33 through III-56 provide another means by which the data of Figures III-1 through III-32 can be represented. However, they allow one to more accurately visualize antenna pattern shape at various elevation angles as viewed from the peak of the vertical profile.

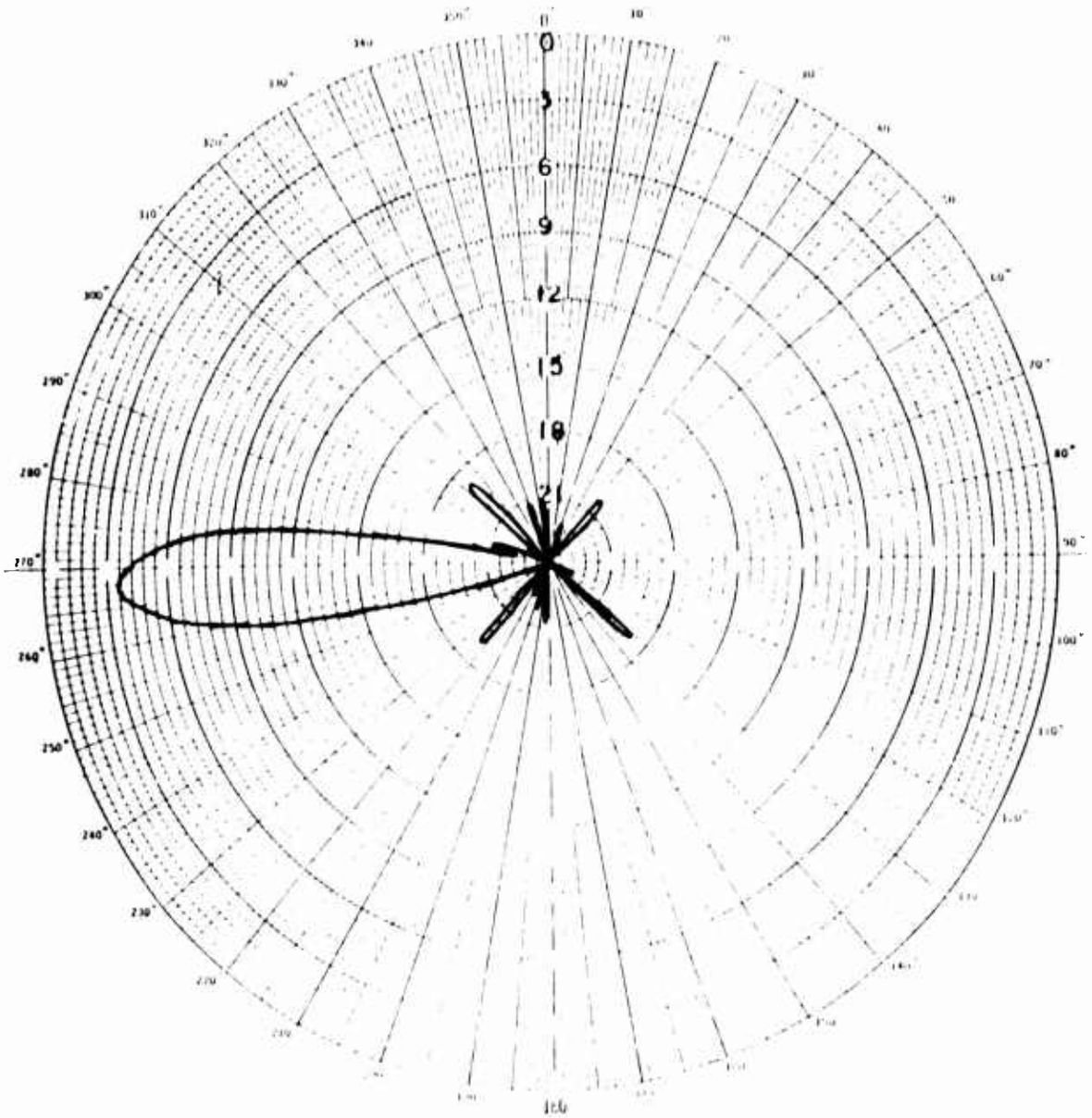

Figure III-33

WEST PHOMBIC
HORIZONTAL POLARIZATION

Frequency - 10.5 MHz

Elevation 2°

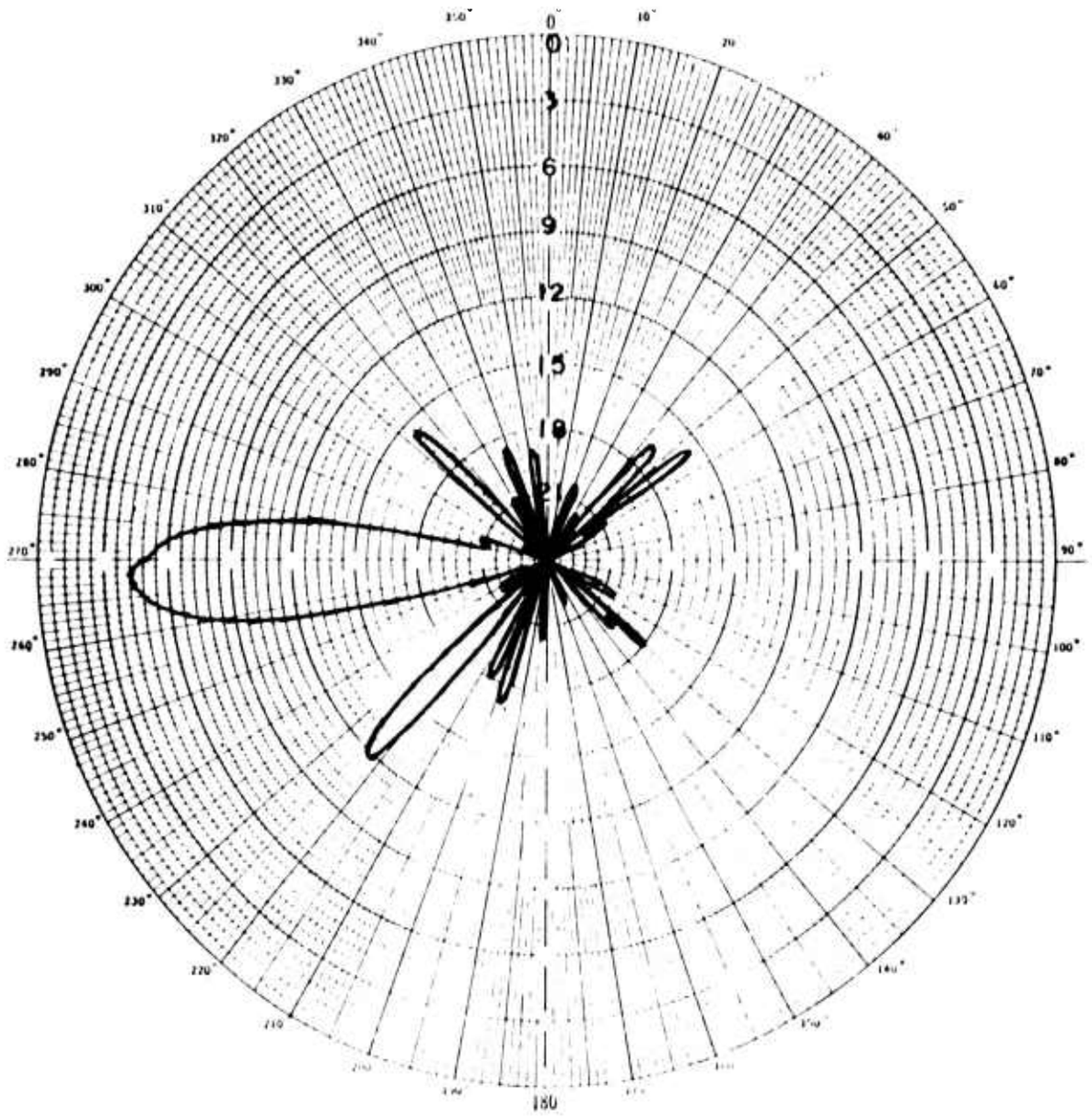

Figure III-34

WEST RHOMBIC
HORIZONTAL POLARIZATION

Frequency - 10.5 MHz

Elevation 4°

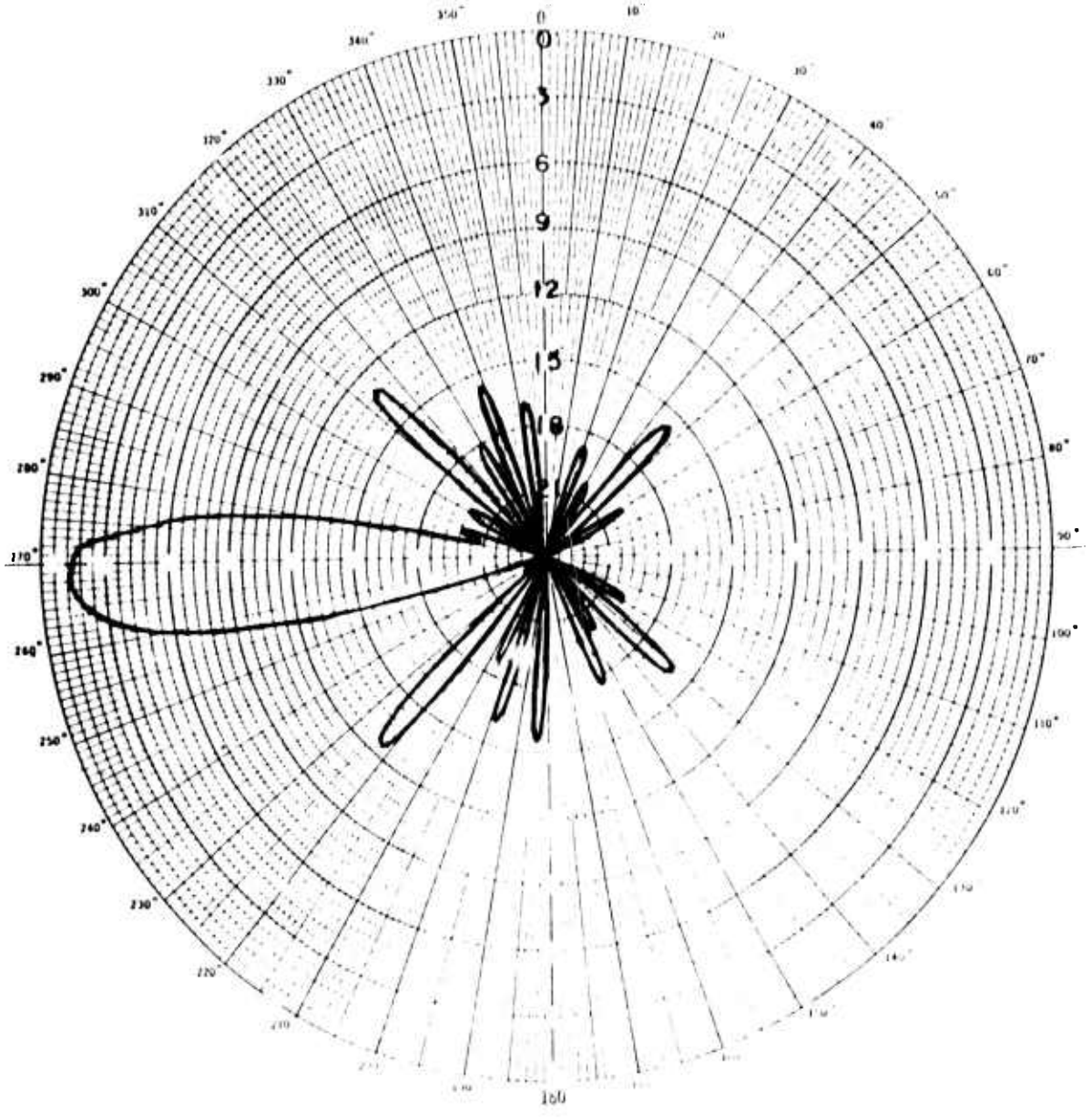

Figure III-35

WEST PHOMBIC
HOPIZONTAL POLAPIZATION

Frequency - 10.5 MHz

Elevation 6°

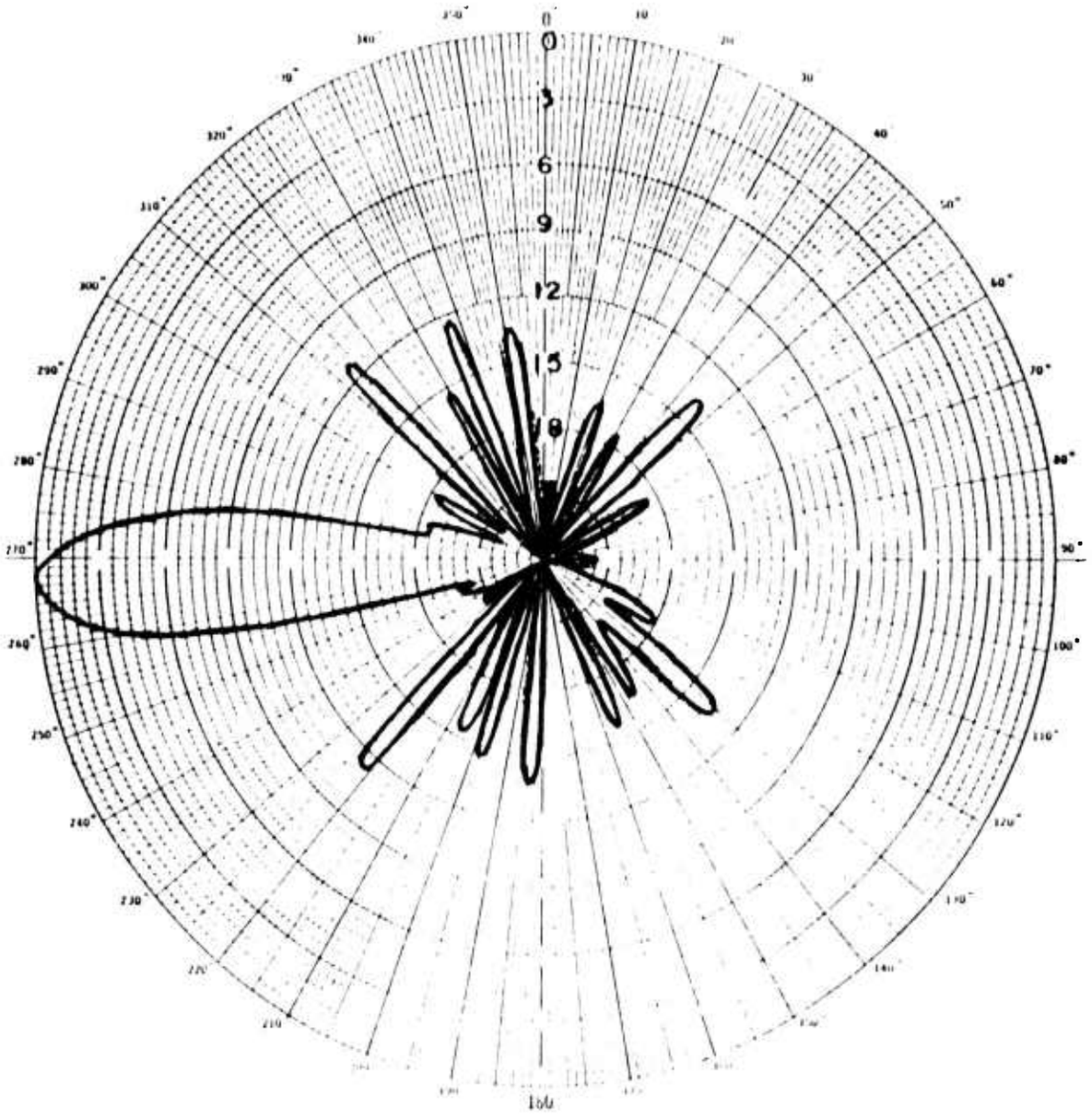

Figure III-36

WEST RHOMBIC
HORIZONTAL POLARIZATION

Frequency - 10.5 MHz

Elevation 8°

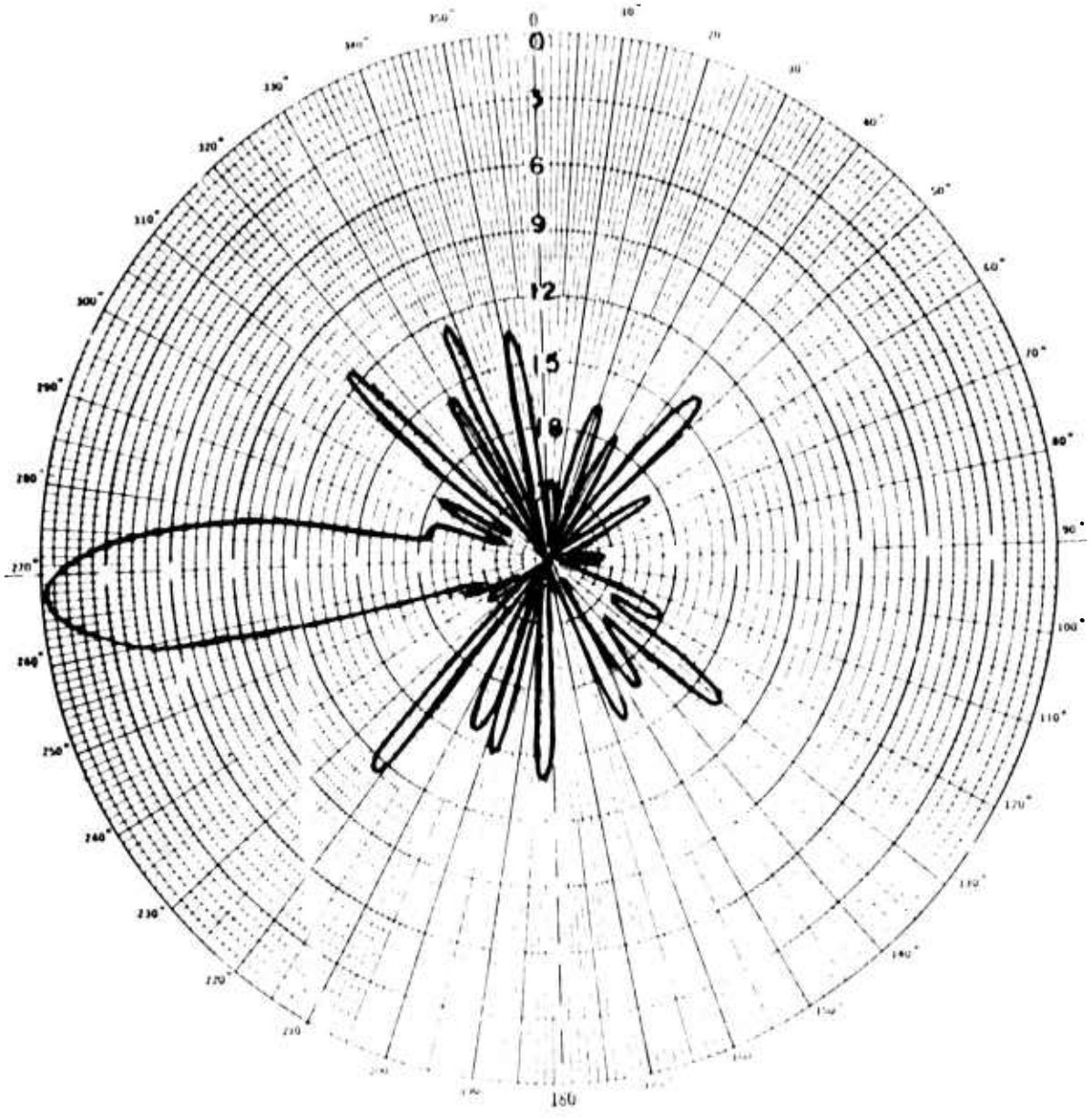

Figure III-37

WEST RHOMBIC
HORIZONTAL POLARIZATION

Frequency - 10.5 MHz

Elevation 10°

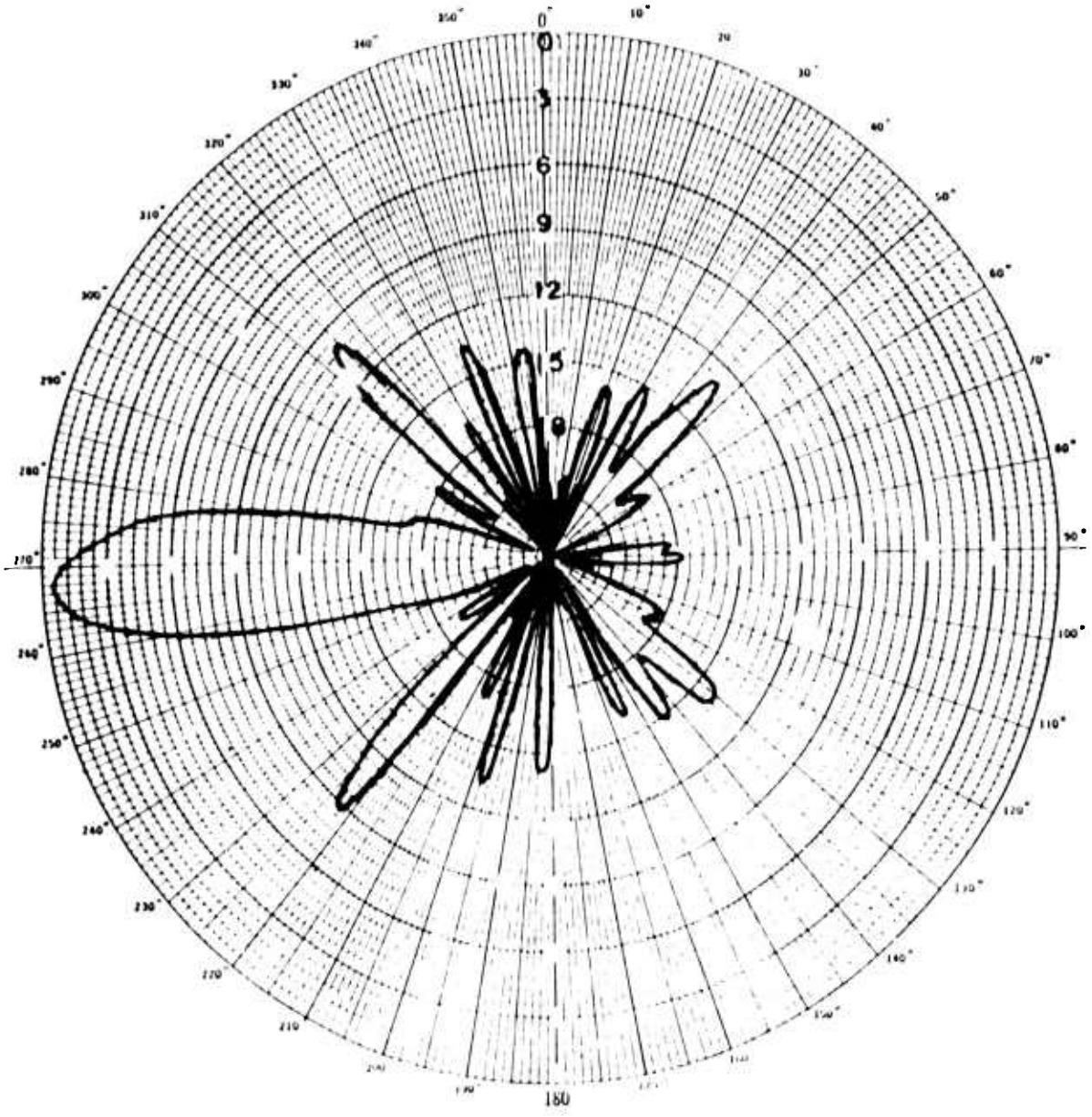

Figure III-38

WEST RHOMBIC
HORIZONTAL POLARIZATION

Frequency - 10.5 MHz

Elevation 12°

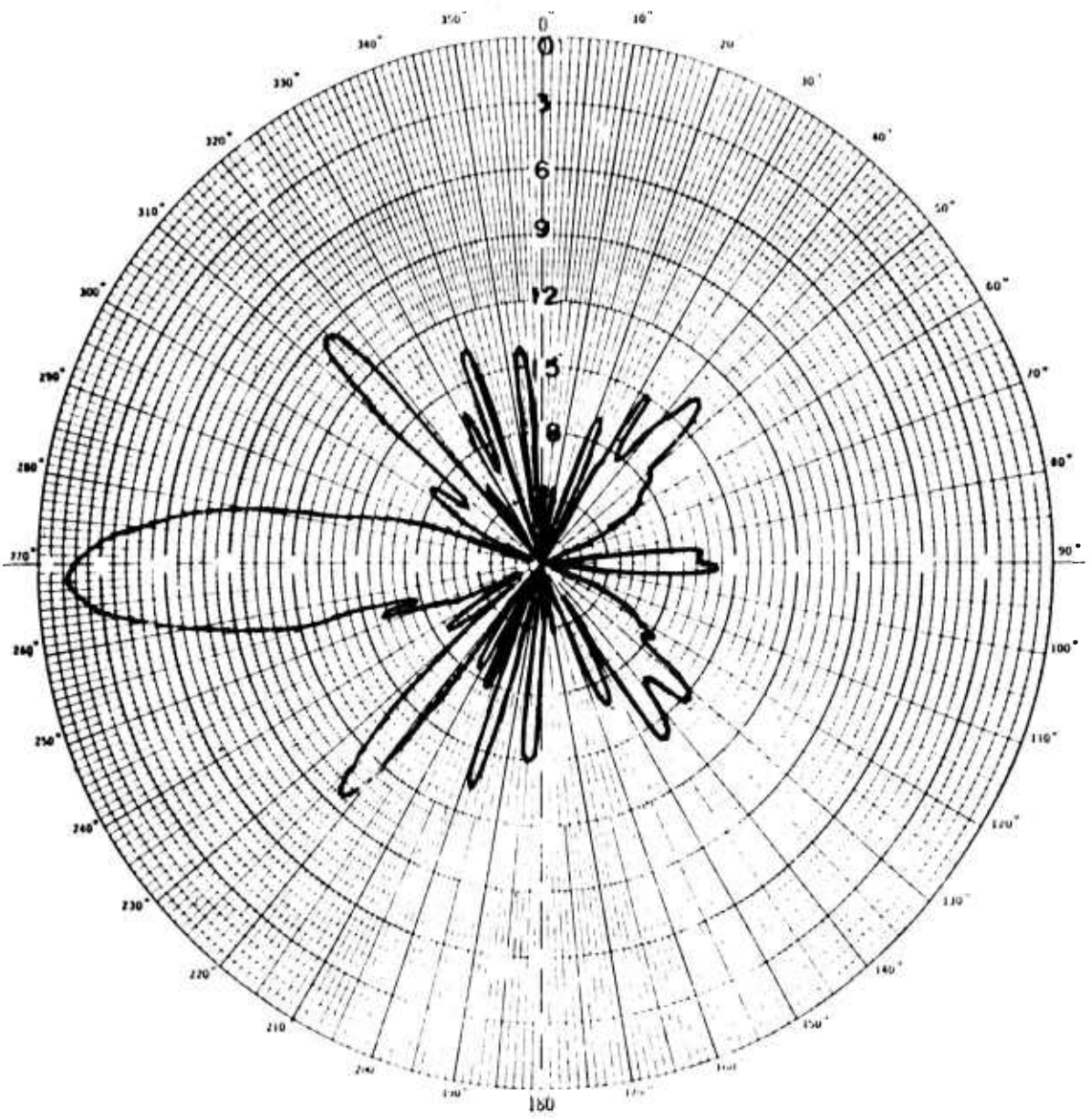

Figure III-39

WEST PHOMBIC
HORIZONTAL POLARIZATION

Frequency - 10.5 MHz

Elevation 14°

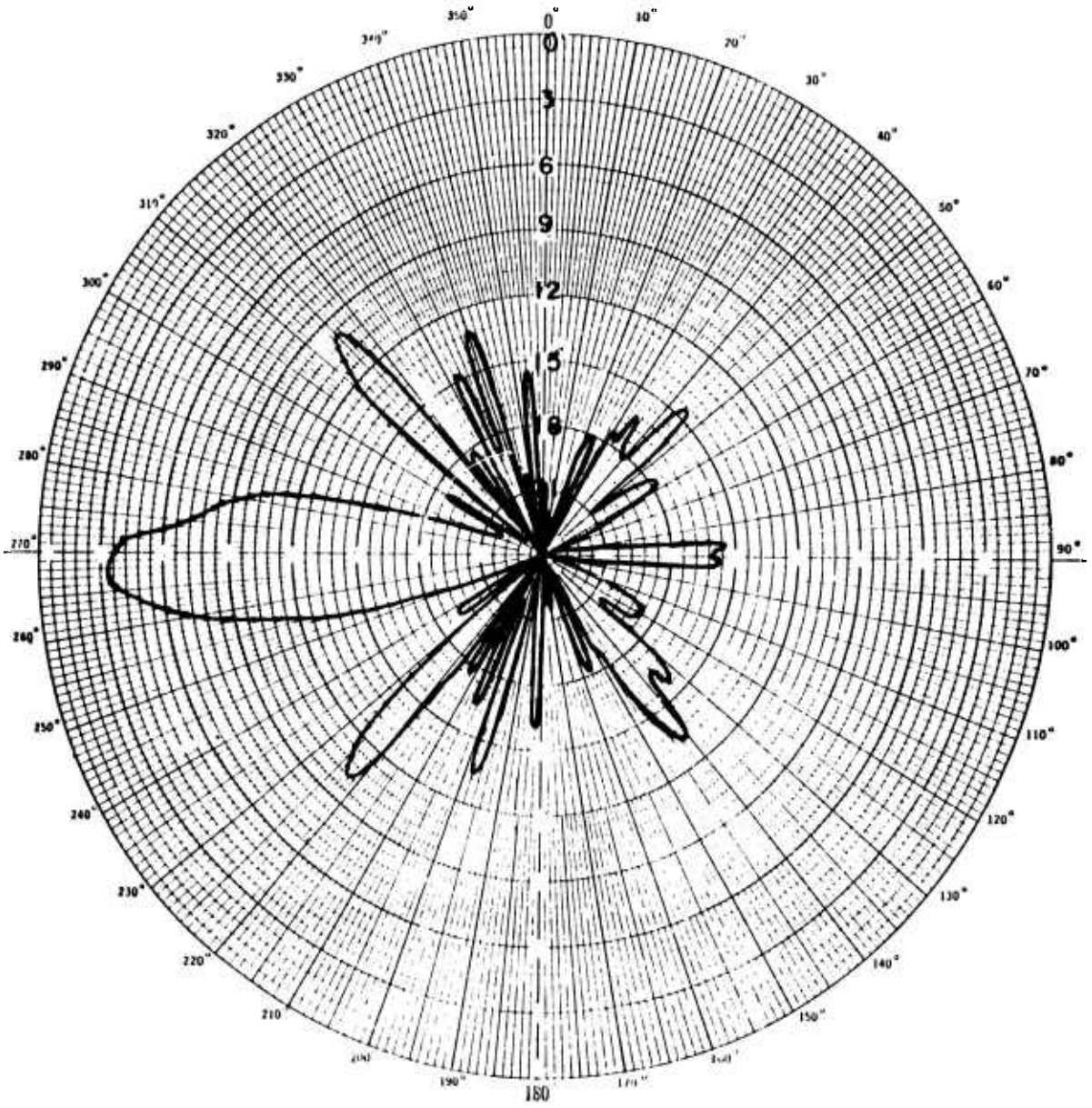

Figure III-40

WEST PHOMBIC
HORIZONTAL POLARIZATION

Frequency - 10.5 MHz

Elevation 16°

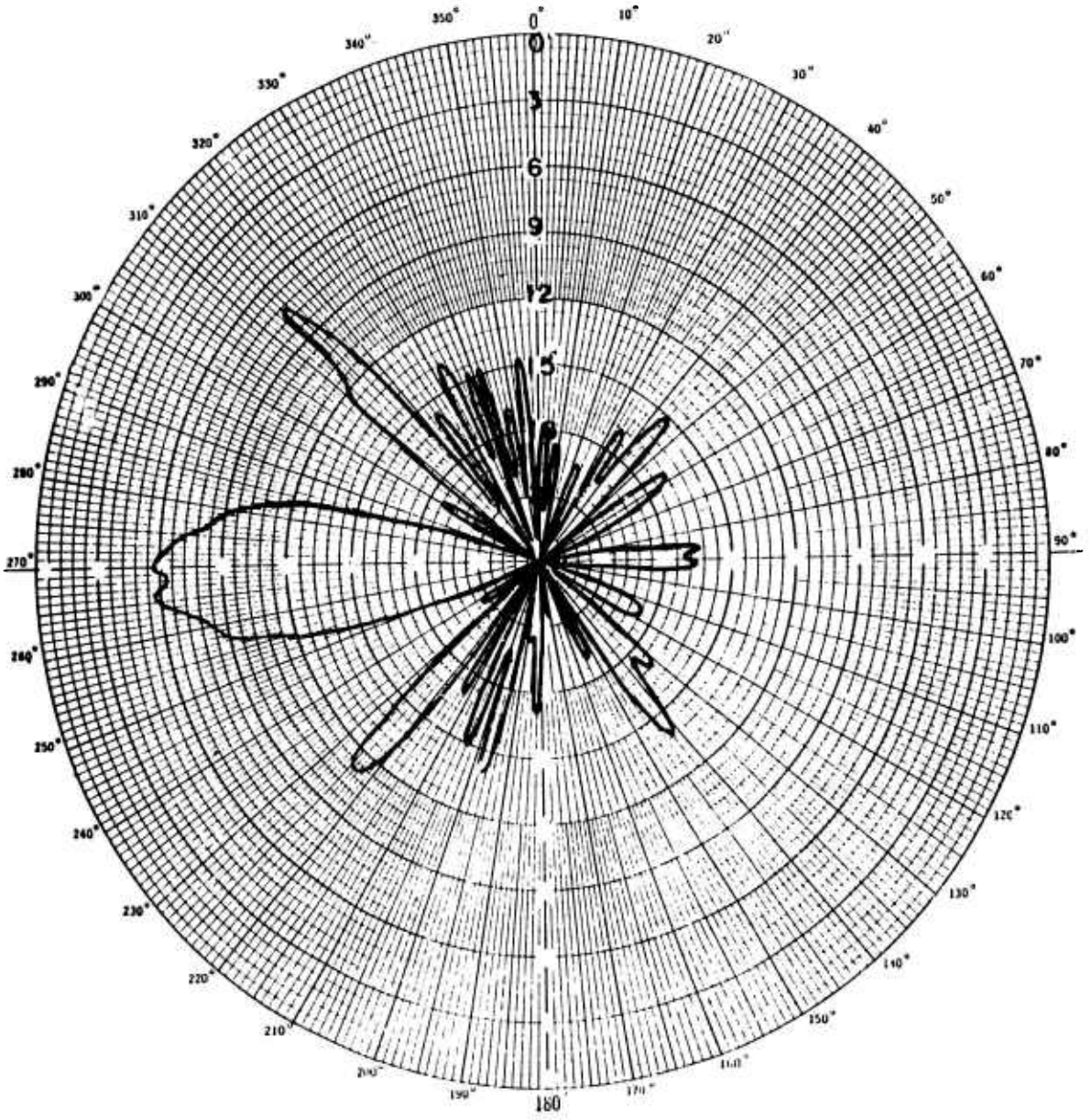

Figure III-41

WEST RHOMBIC
HORIZONTAL POLARIZATION

Frequency - 10.5 MHz

Elevation 18°

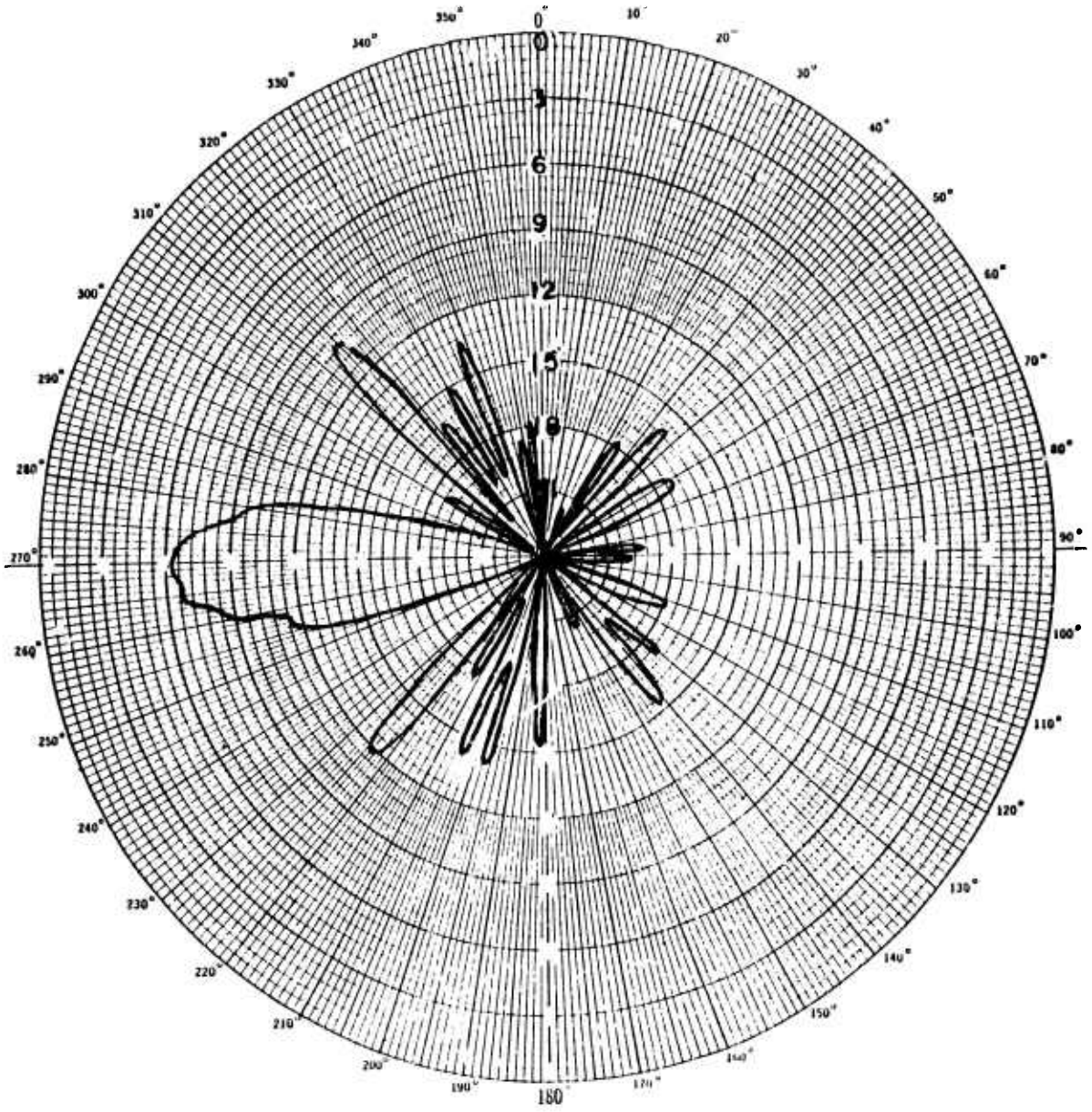

Figure III-42

WEST RHOMBIC
HORIZONTAL POLARIZATION

Frequency - 10.5 MHz

Elevation 20°

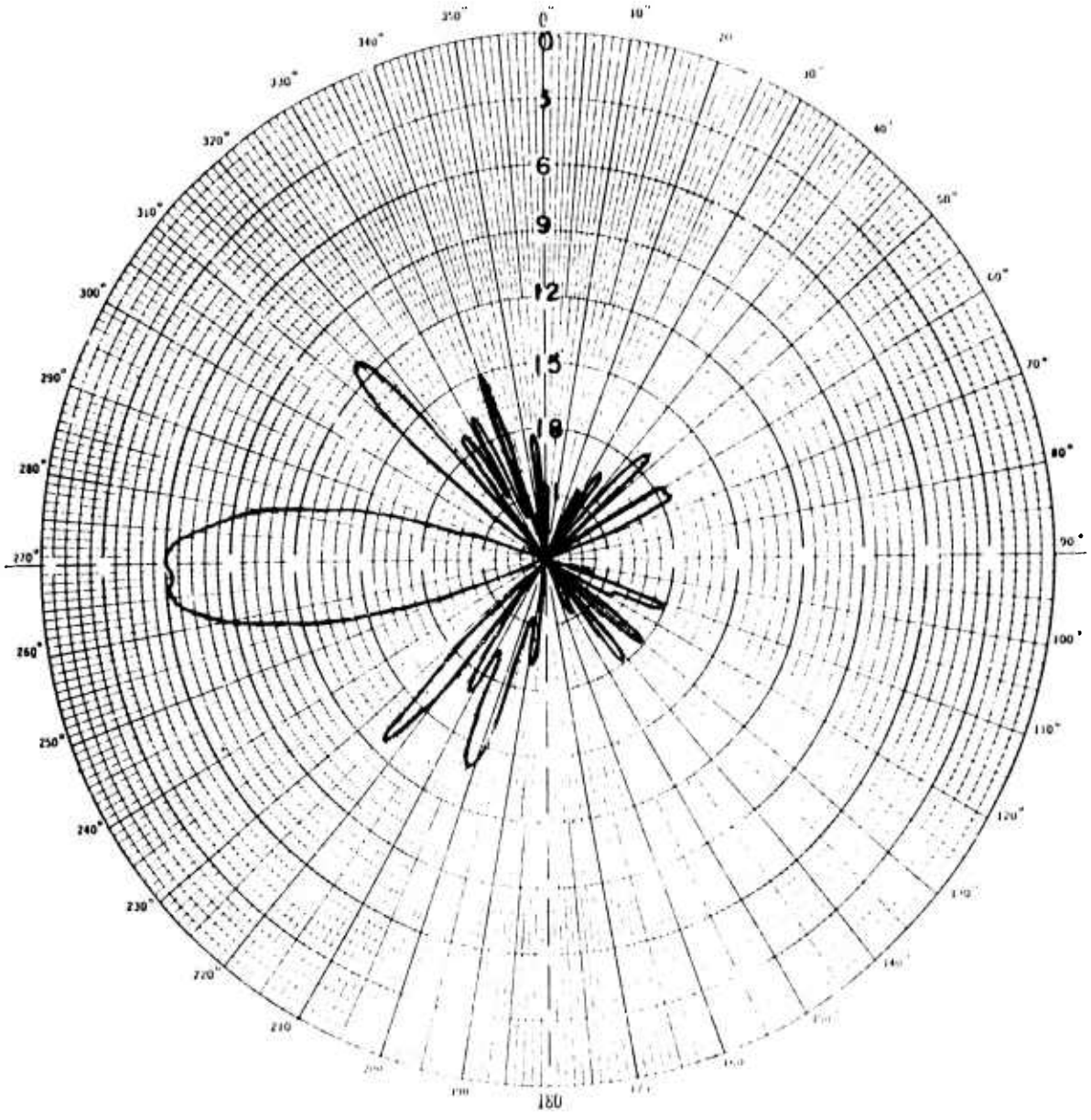

Figure III-43

WEST RHOMBIC
HORIZONTAL POLARIZATION

Frequency - 10.5 MHz

Elevation 22°

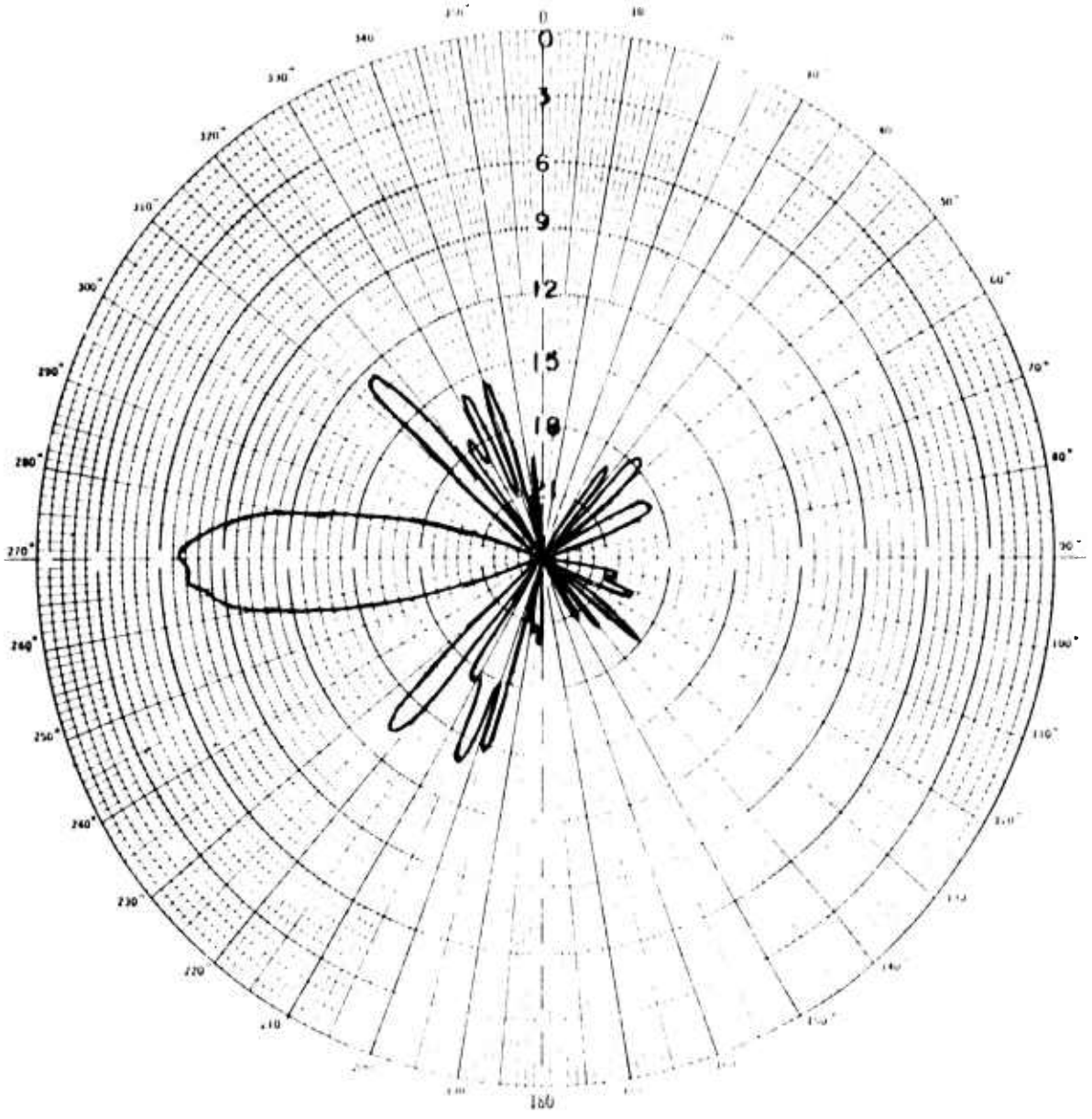

Figure III-44

WEST RHOMBIC
HORIZONTAL POLARIZATION

Frequency - 10.5 MHz

Elevation 24°

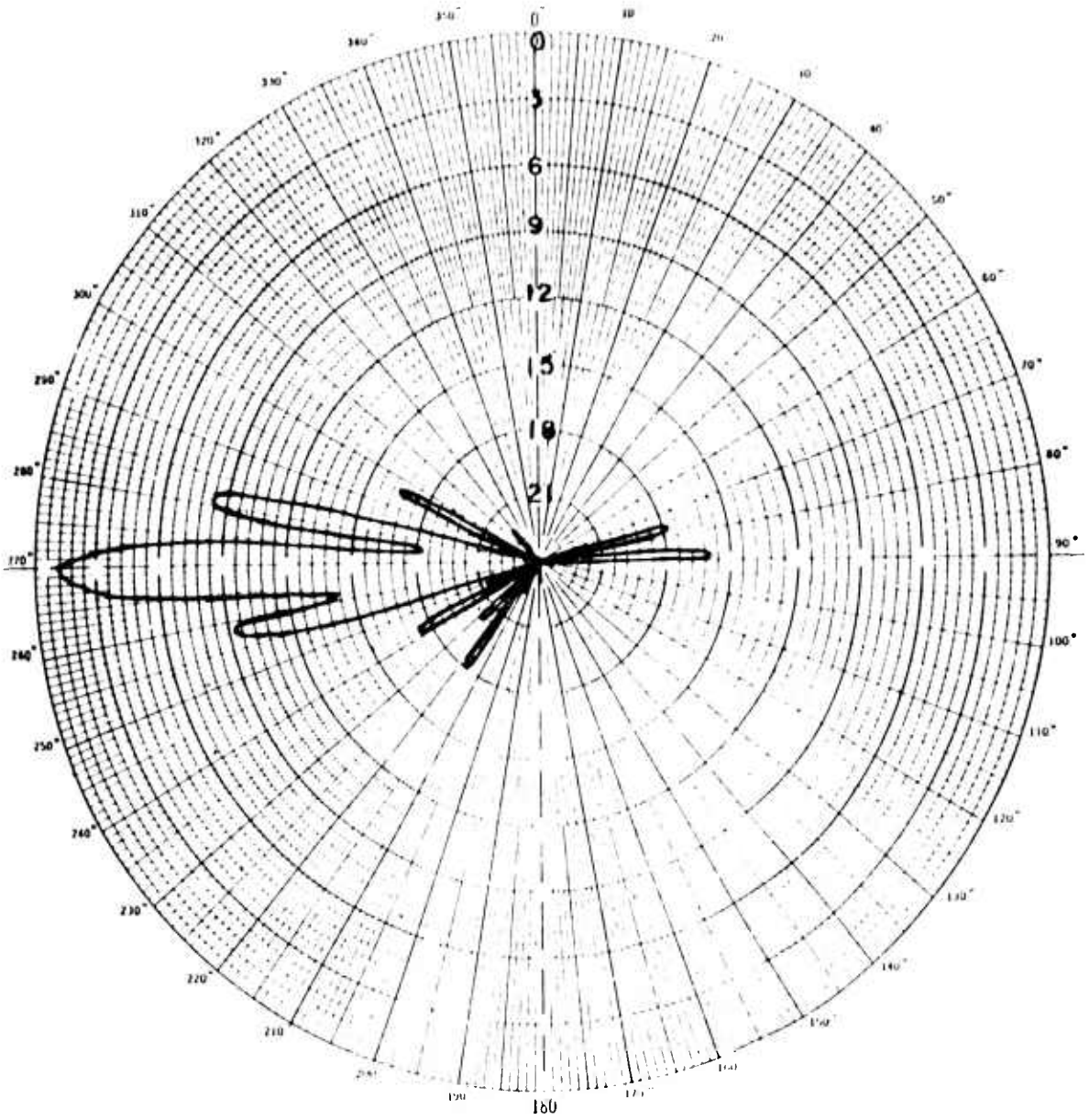

Figure III-45

WEST RHOMBIC
HORIZONTAL POLARIZATION

Frequency - 20.052 MHz

Elevation 2°

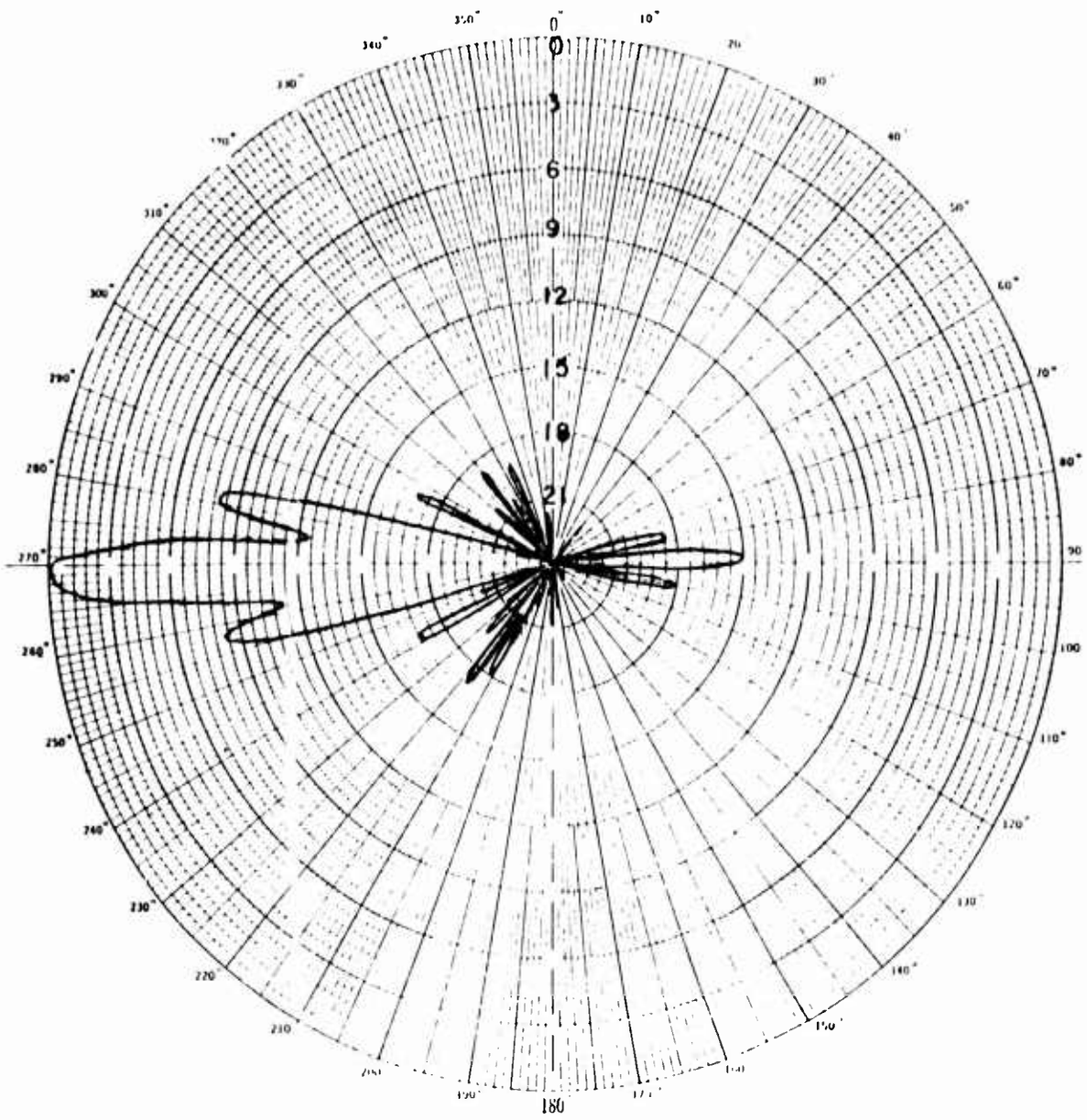

Figure III-46

WEST RHOMBIC
HORIZONTAL POLARIZATION

Frequency - 20.052 MHz

Elevation 4°

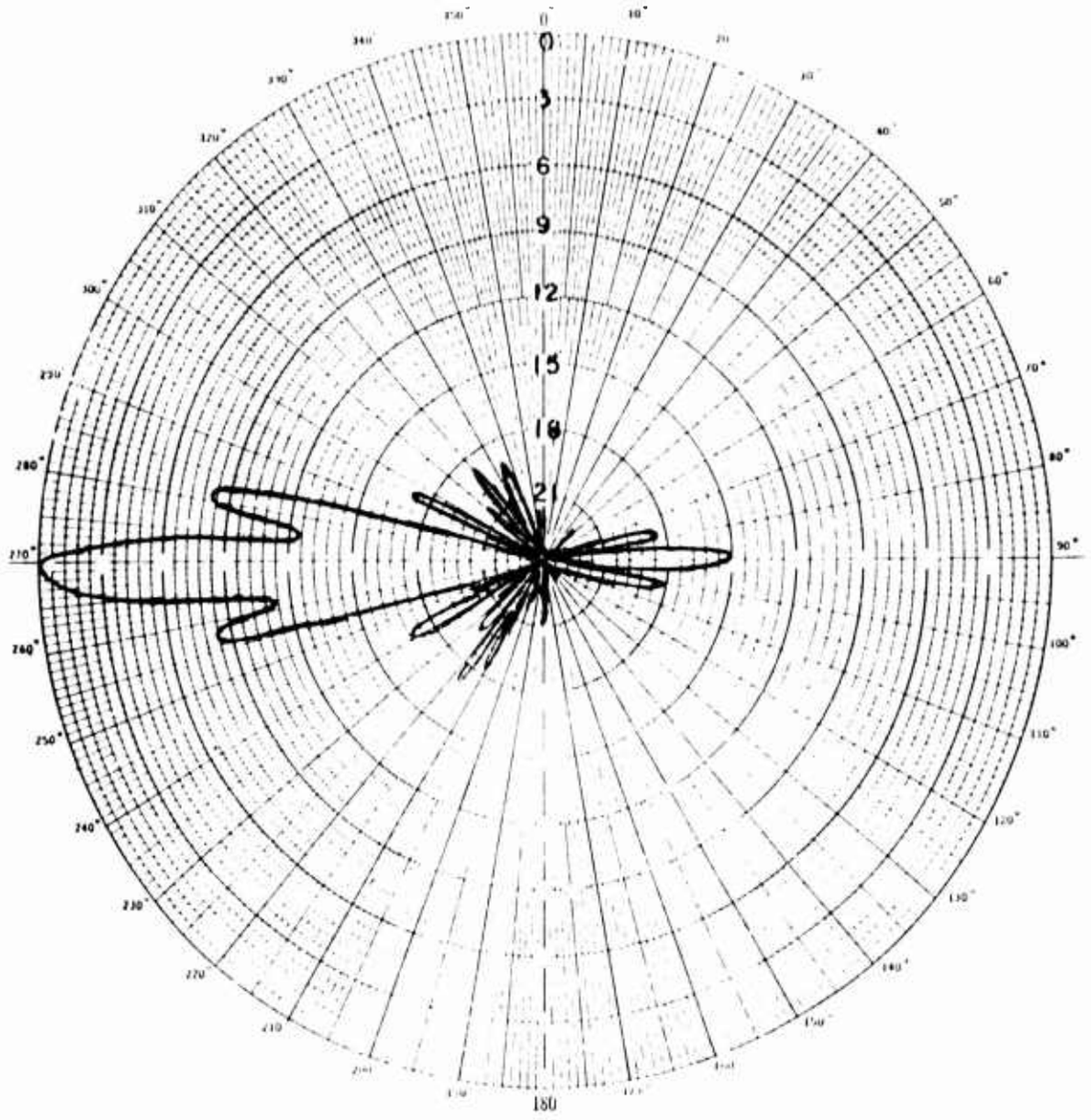

Figure III-47

WEST RHOMBIC
HORIZONTAL POLARIZATION

Frequency - 20.052 MHz

Elevation 6°

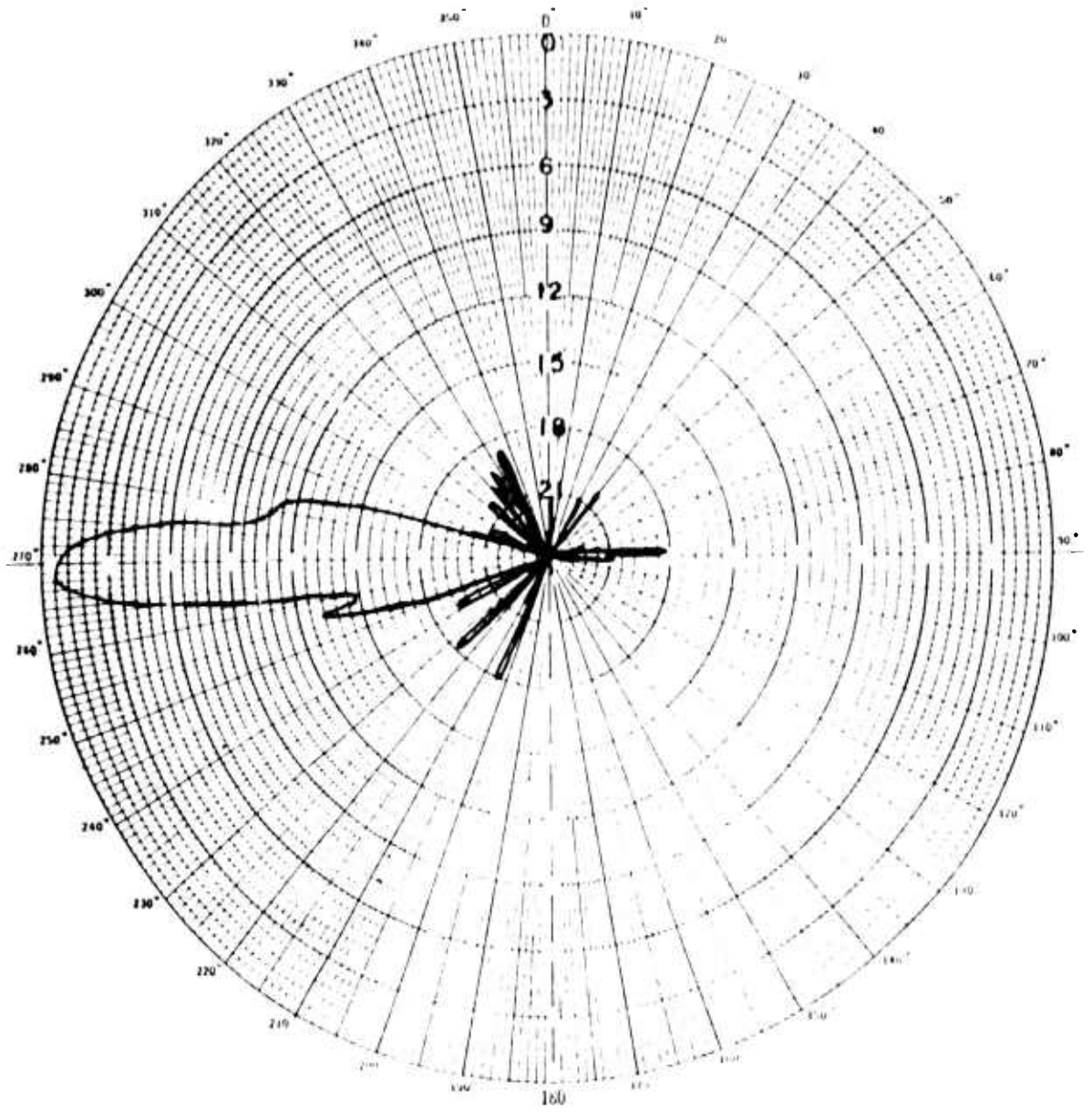

Figure III-48

WEST RHOMBIC
HORIZONTAL POLARIZATION

Frequency - 20.052 MHz

Elevation 8°

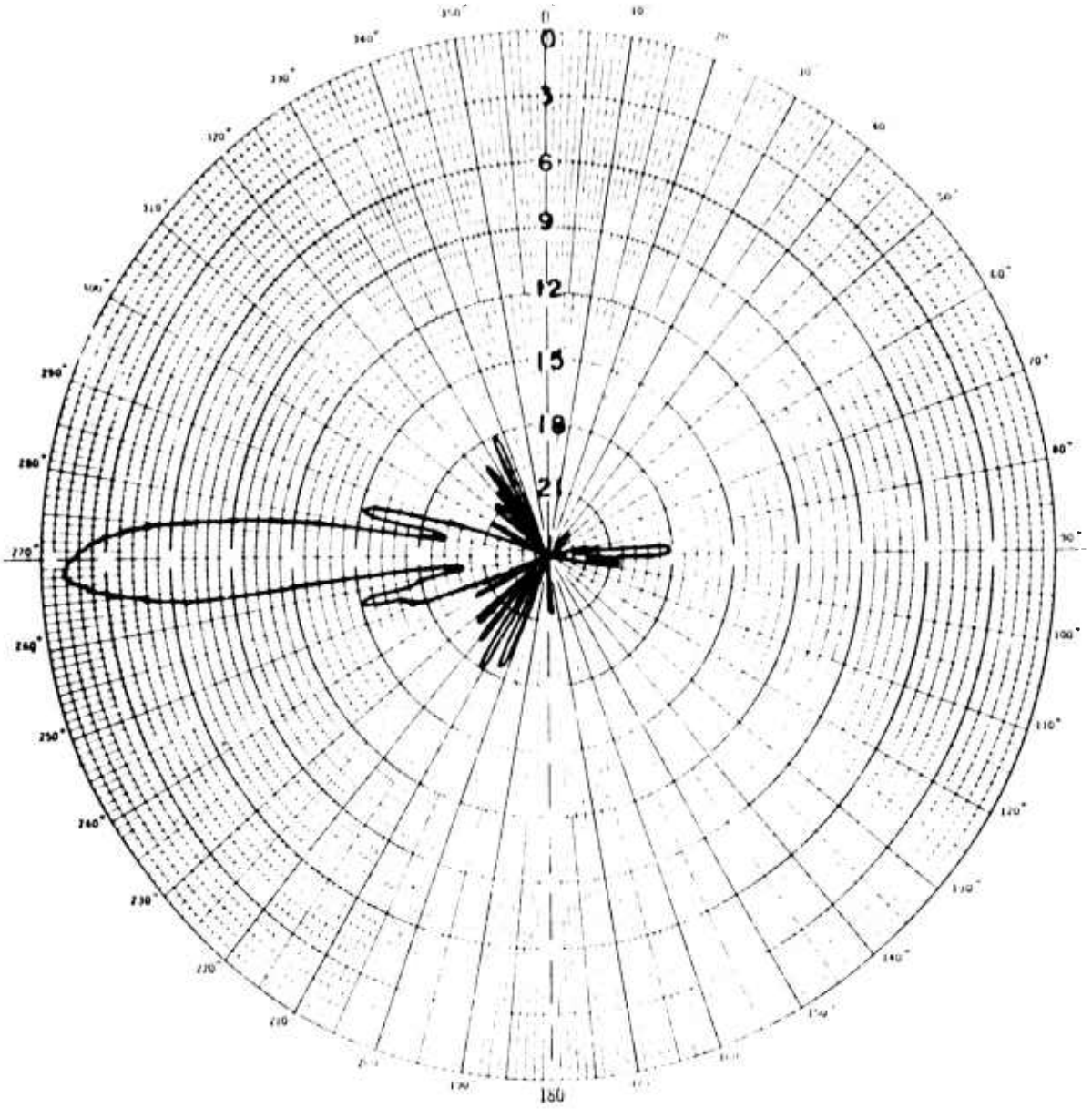

Figure III-49

WEST RHOMBIC
HORIZONTAL POLARIZATION

Frequency - 20.052 MHz

Elevation 10°

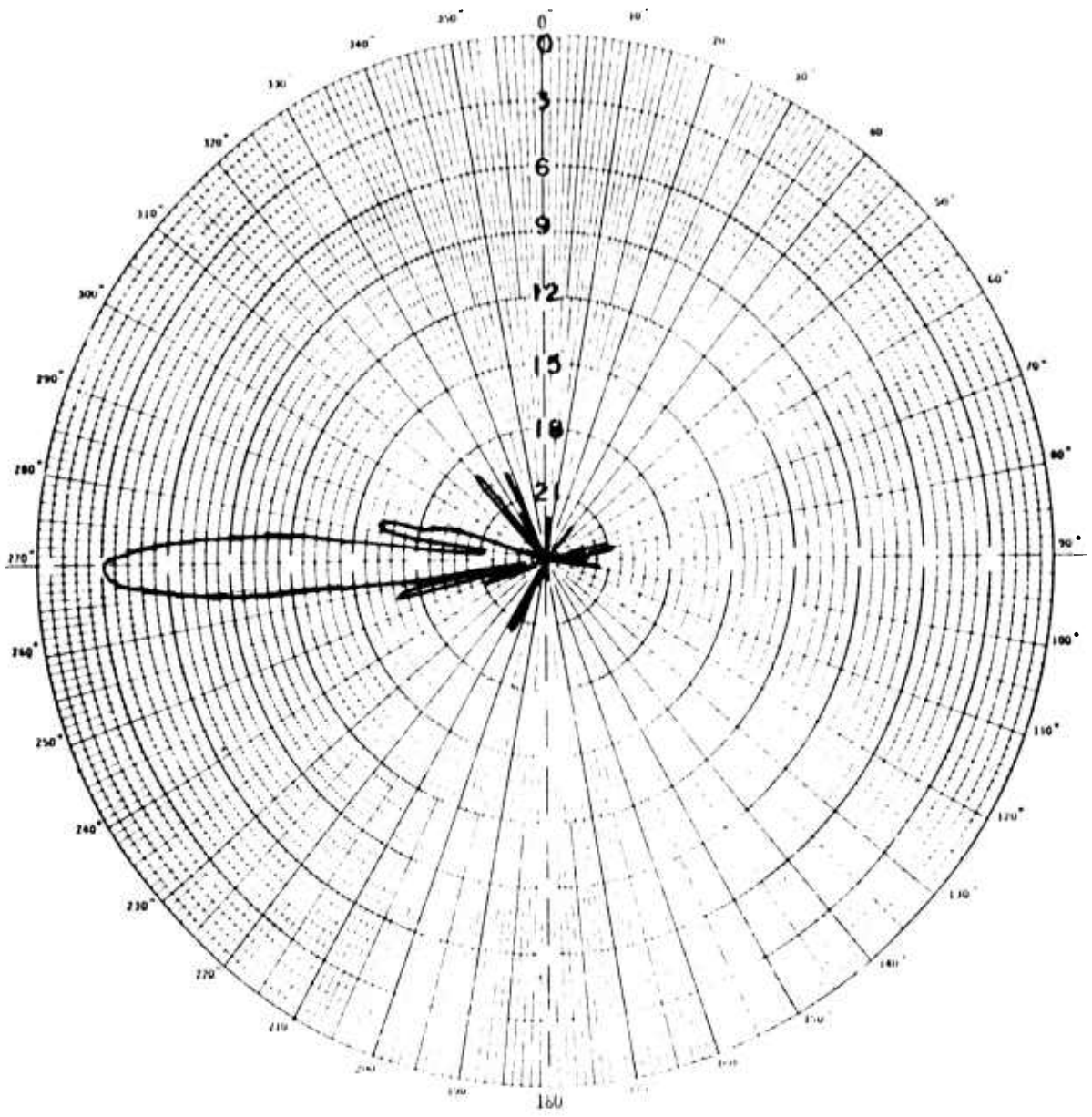

Figure III-50

WEST RHOMBIC
HORIZONTAL POLARIZATION

Frequency - 20.052 MHz

Elevation 12°

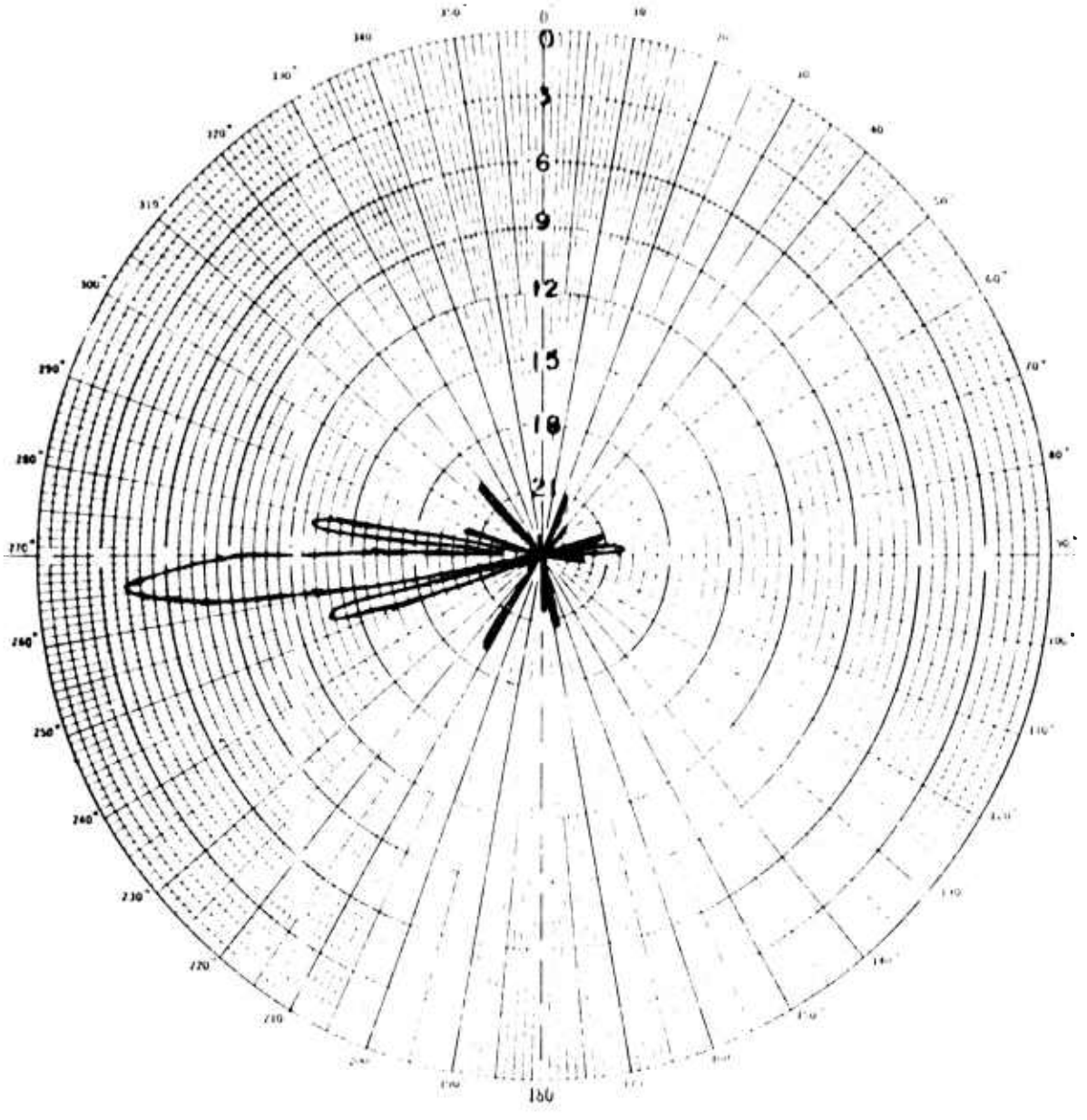

Figure III-51

WEST RHOMBIC
HORIZONTAL POLAPIZATION

Frequency - 20.052 MHz

Elevation 14°

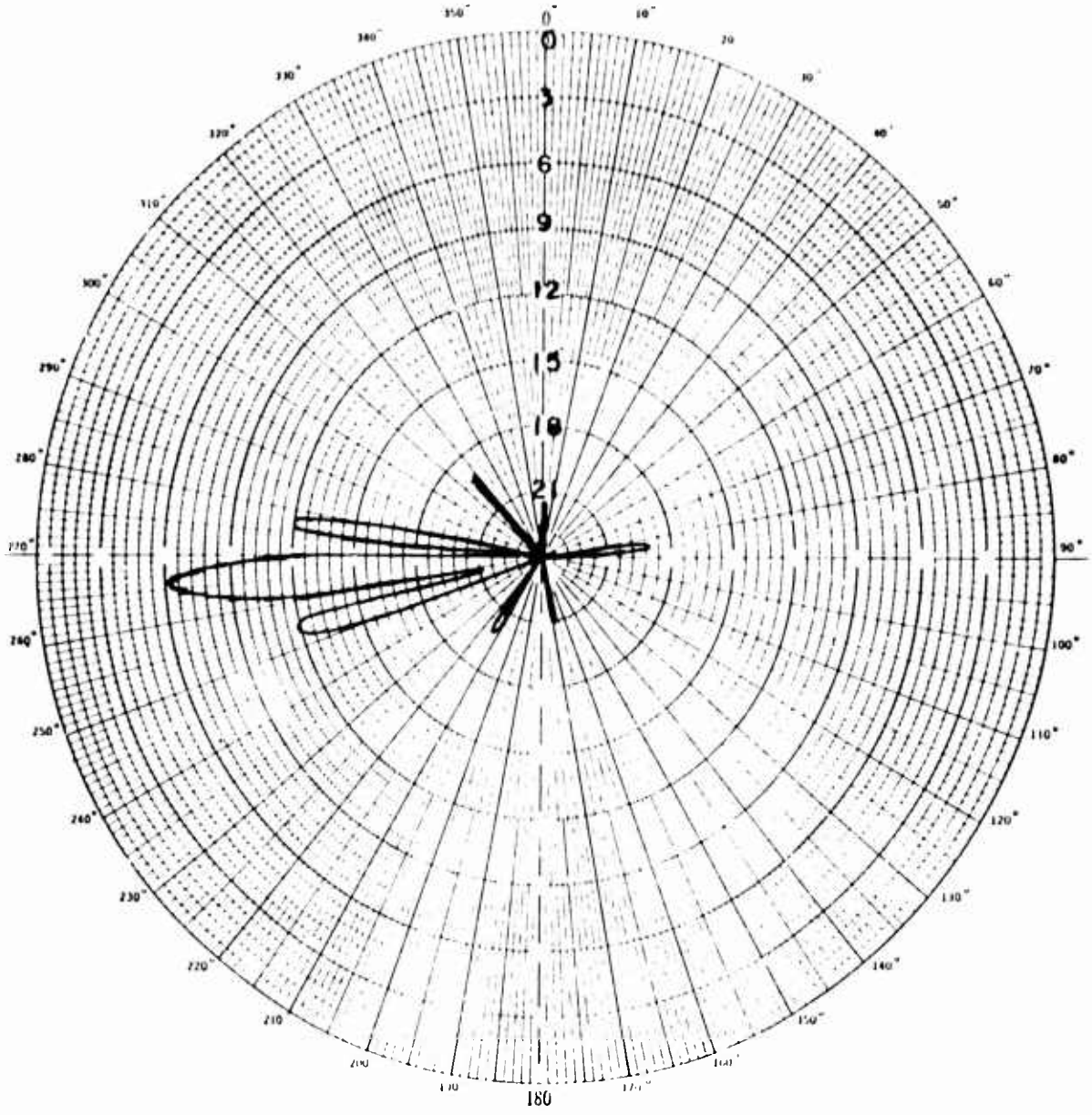

Figure III-52

WEST RHOMBIC
HORIZONTAL POLARIZATION

Frequency - 20.052 MHz

Elevation 16°

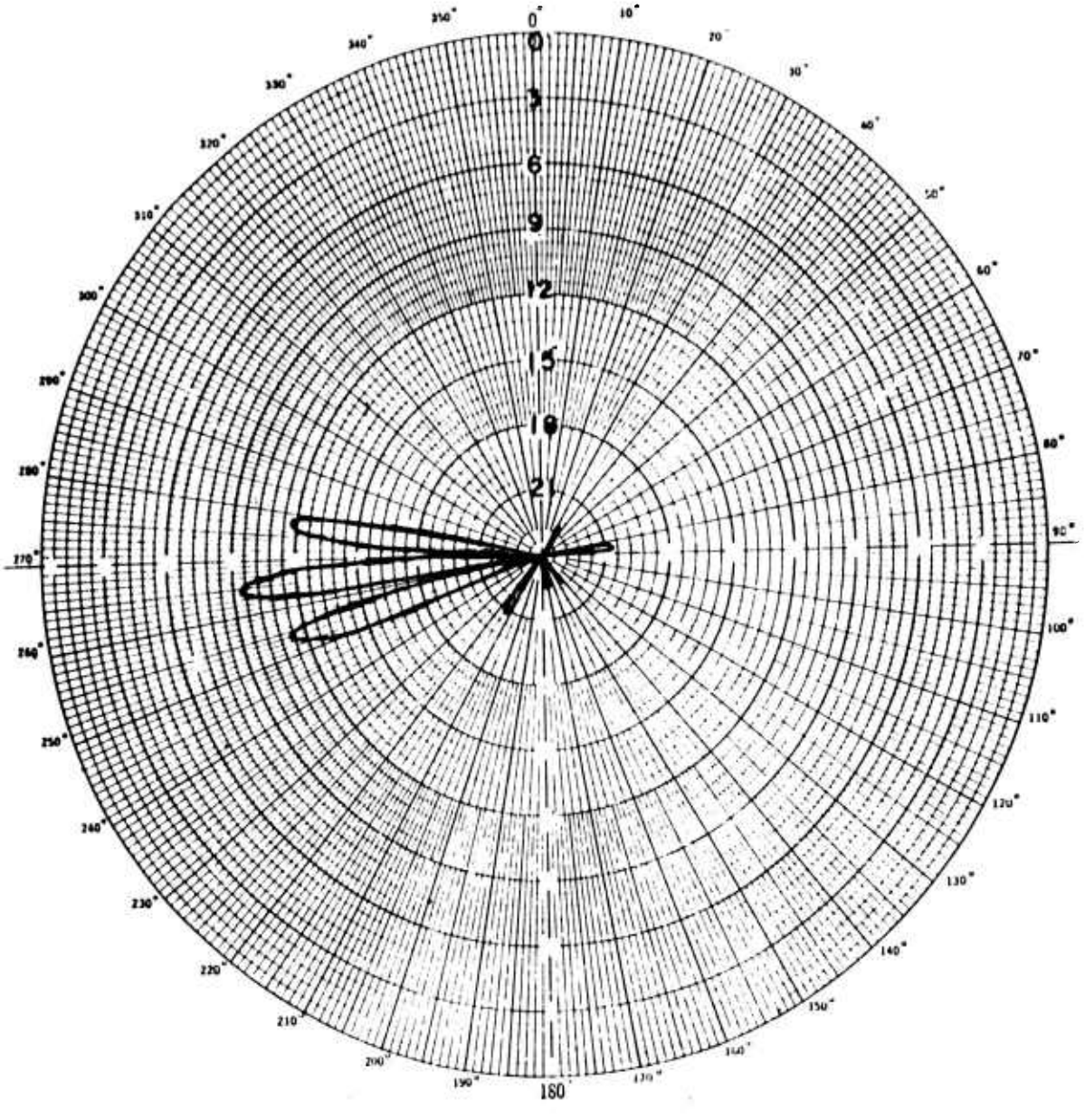

Figure III-53

WEST RHOMBIC
HORIZONTAL POLARIZATION

Frequency - 20.052 MHz

Elevation 18°

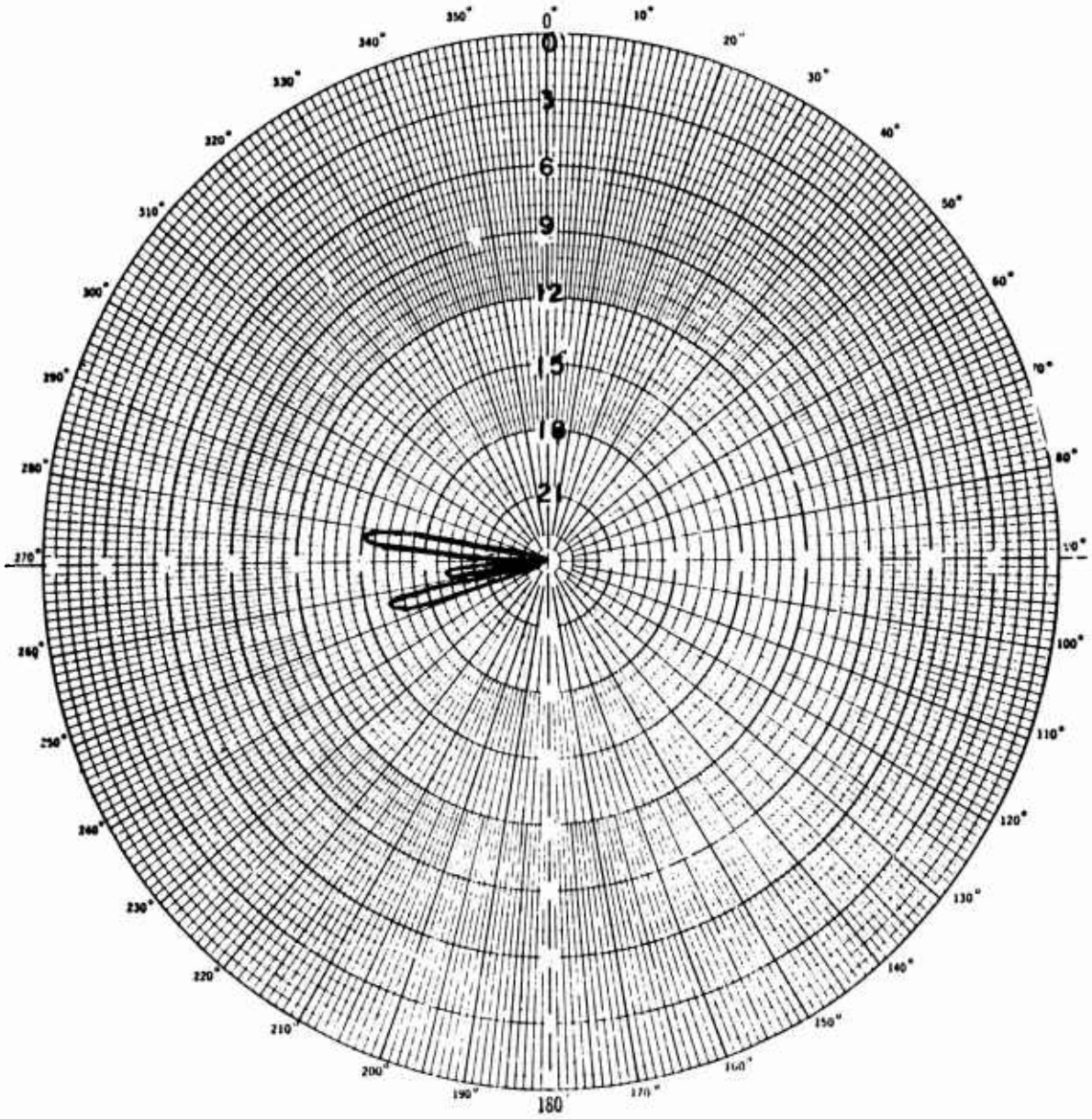

Figure III-54

WEST RHOMBIC
HORIZONTAL POLARIZATION

Frequency - 20.052 MHz

Elevation 20°

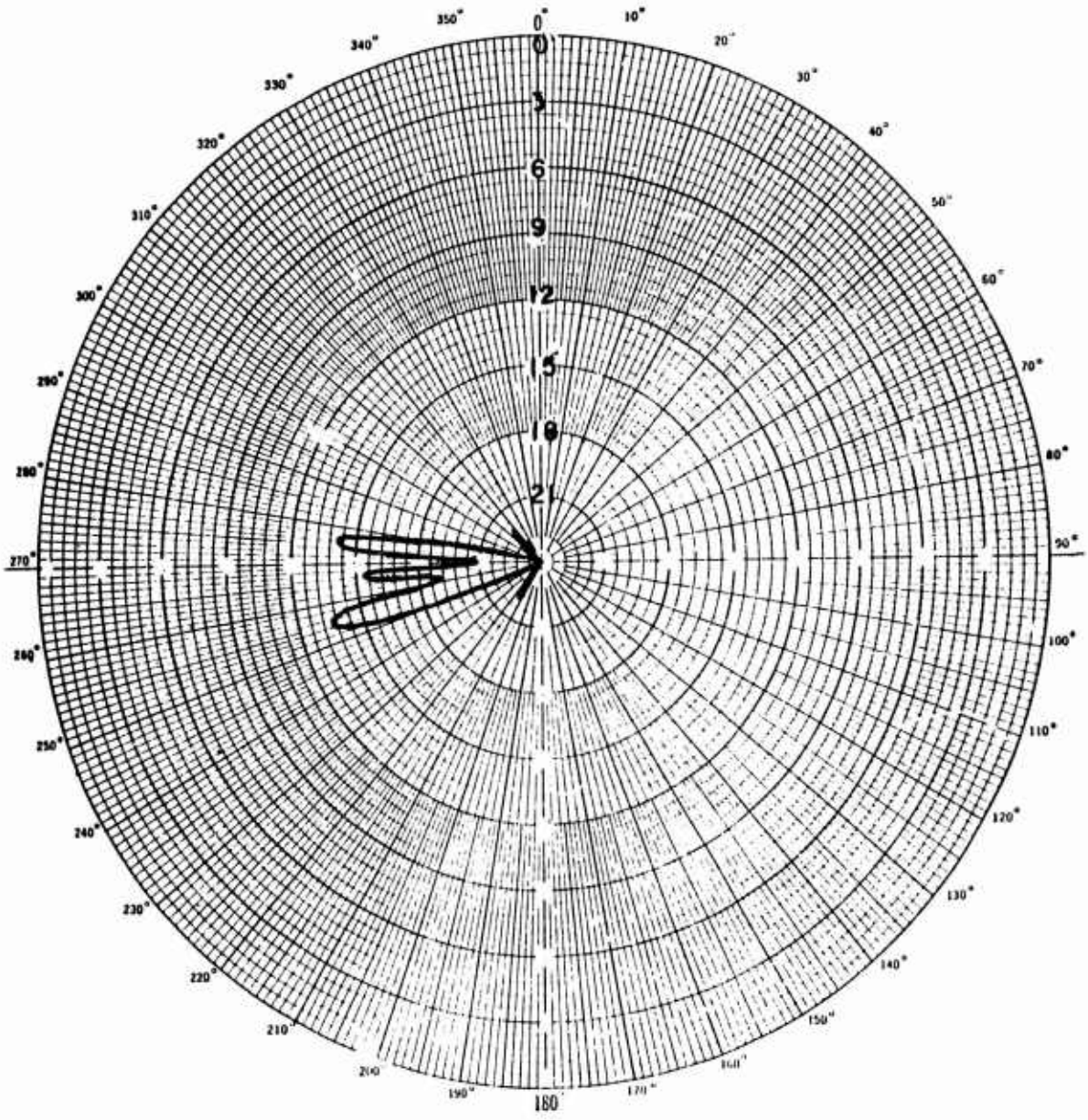

Figure III-55

WEST RHOMBIC
HORIZONTAL POLARIZATION

Frequency - 20.052 MHz

Elevation 22°

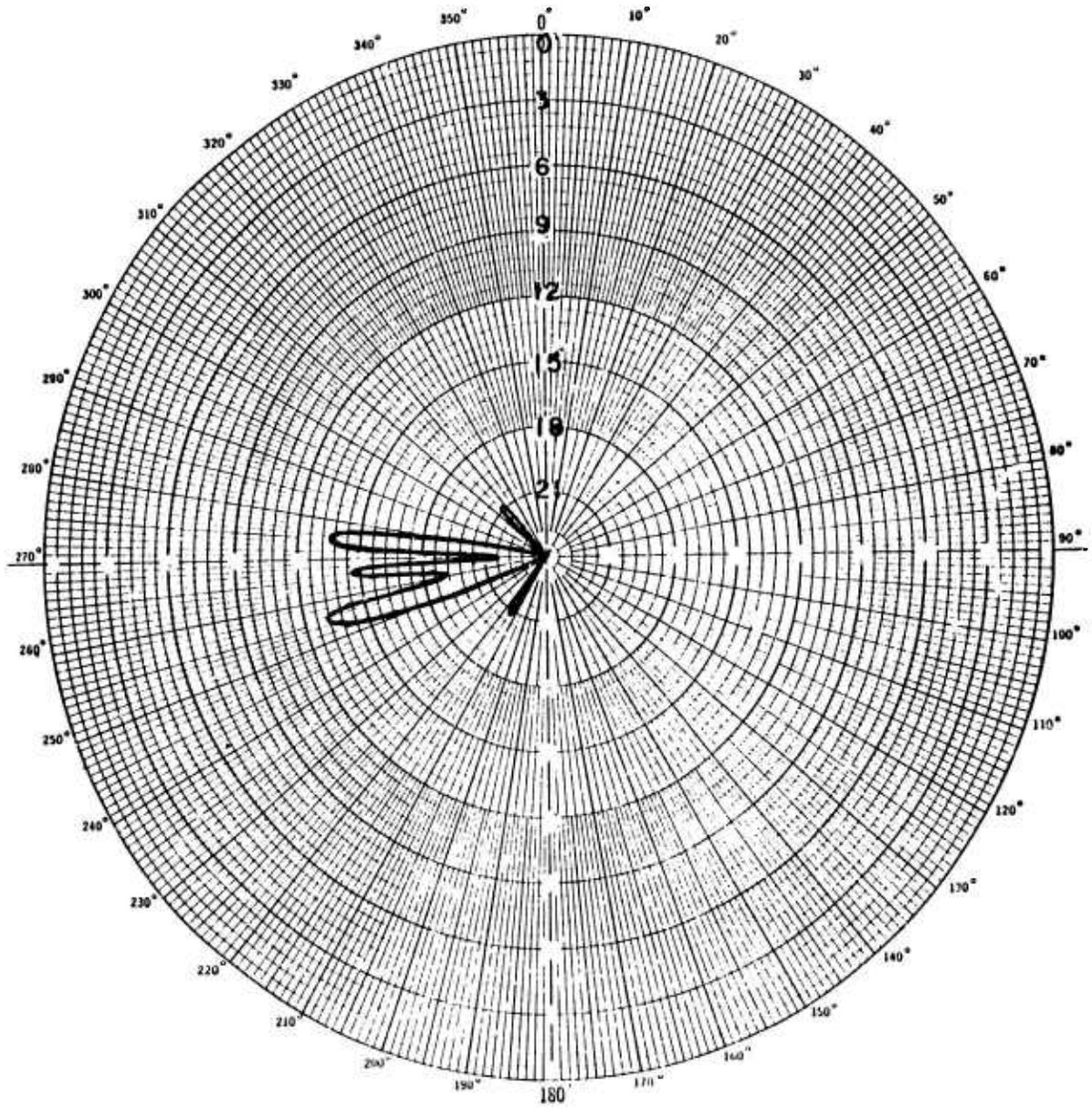

Figure III-56

WEST RHOMBIC
HORIZONTAL POLARIZATION

Frequency - 20.052 MHz

Elevation 24°

The polar plots shown in Figures III-1 through III-32 were used to plot Figures III-57a, III-57b, and III-58a, III-58b which respectively depict the computed and experimental horizontal beamwidths at 10, 15 and 20 MHz. Each of the individual plots provides both the 3 and 10 dB beamwidths as a function of elevation angles. It is readily apparent that discrepancies exist between the experimental and computed horizontal beamwidths at 15 MHz for elevation angles of 8°, 10°, 12° and 14°. In plotting the data at these particular elevation angles, only the values at 10 and 20 Mc were experimentally determined, because of limited experimental data at 15 MHz. Therefore only the 10 and 20 MHz points were used to plot the 8° to 14° experimental elevation curves. It was assumed that the appropriate experimental points for 15 Hz lie on the line joining the two known points. The inaccuracy of this assumption is demonstrated in Figures III-58a and III-58b. Figure III-59 represents a compilation of all the data contained in Figures III-57 and III-58, i.e. horizontal 3 and 10 dB beamwidths, both experimentally and computed as a function of elevation angles at operating frequencies of 10, 15 and 20 MHz.

In order to make any meaningful comparison between the computed and experimental data of Figures III-57 and III-58 reference must be made first to Figure III-60. This figure was extrapolated directly from Figures I-5 and I-6 and depicts the vertical profile beamwidth and peak positions as a function of frequency. It should be observed in Figure III-60 that the peak of the experimental vs the peak of

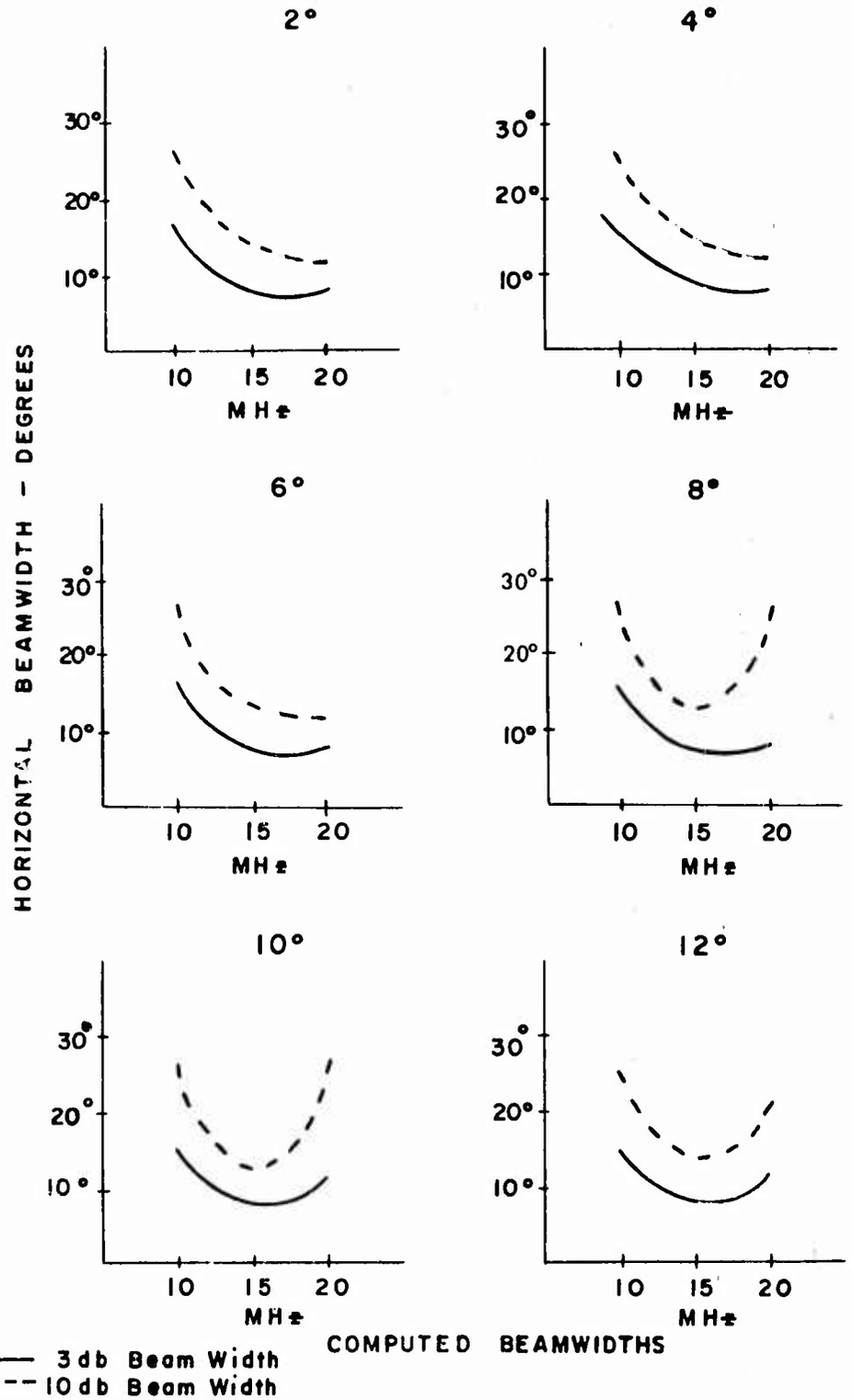

Figure III-57a

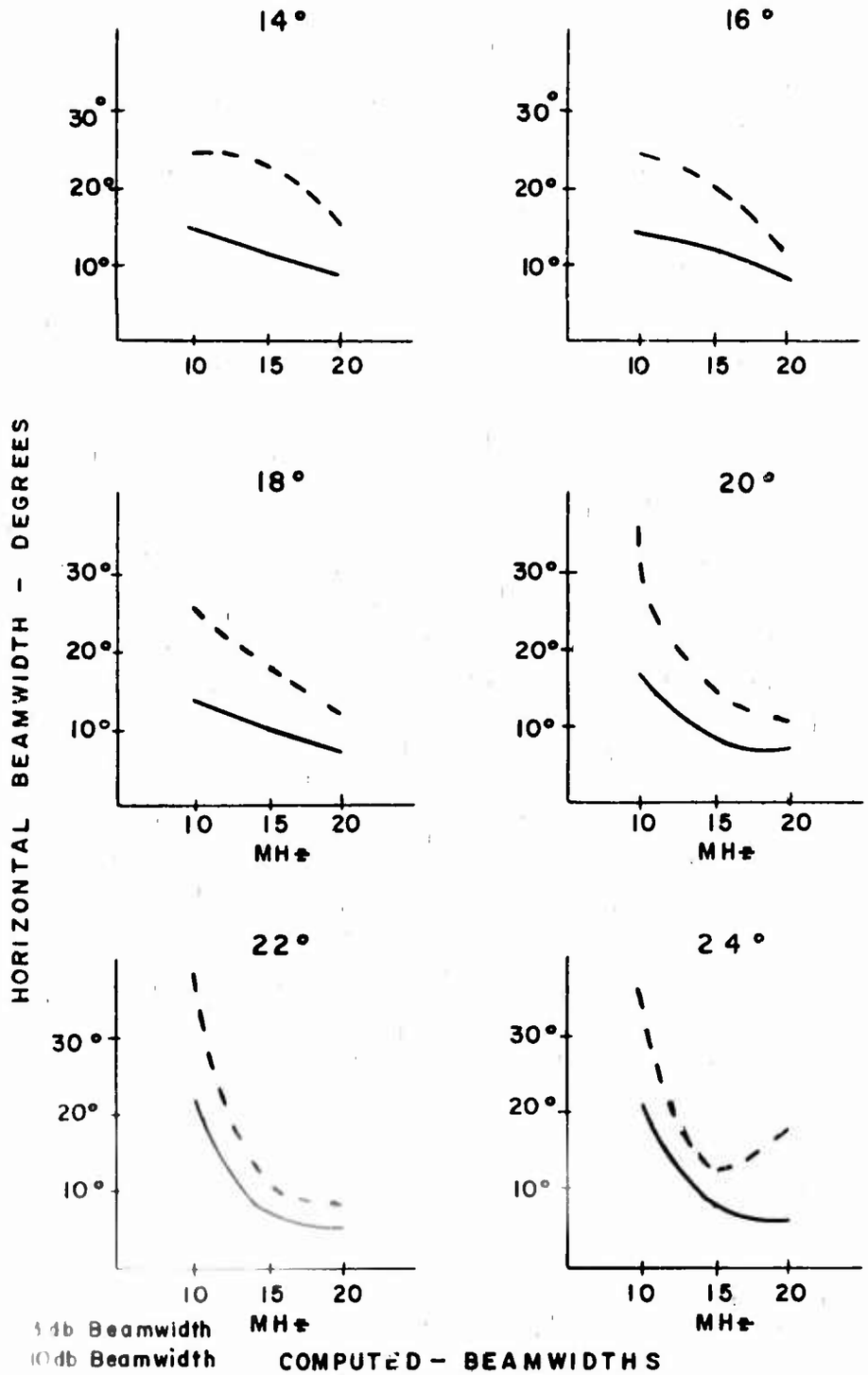

Figure III-57b

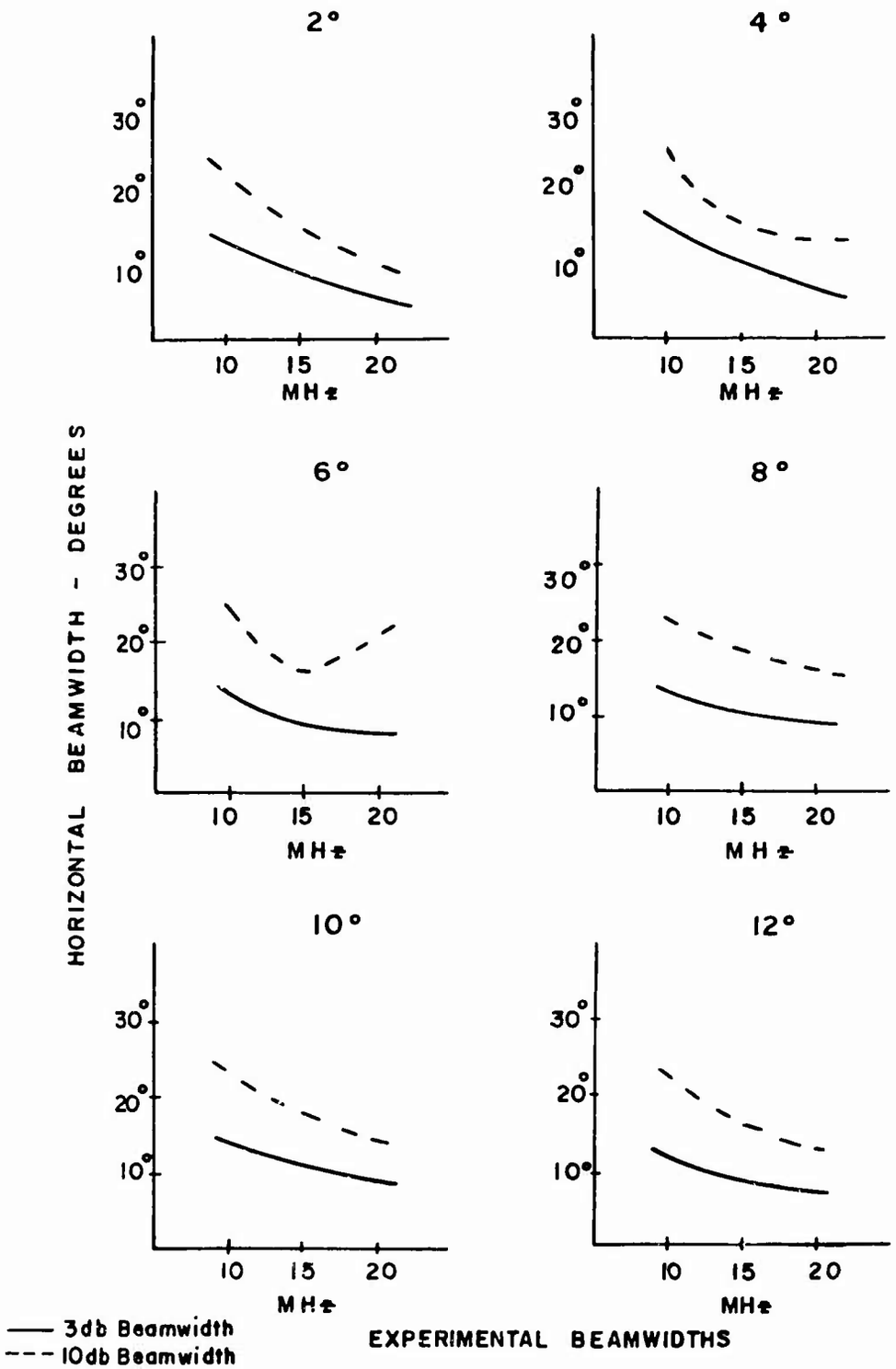

Figure III-58a

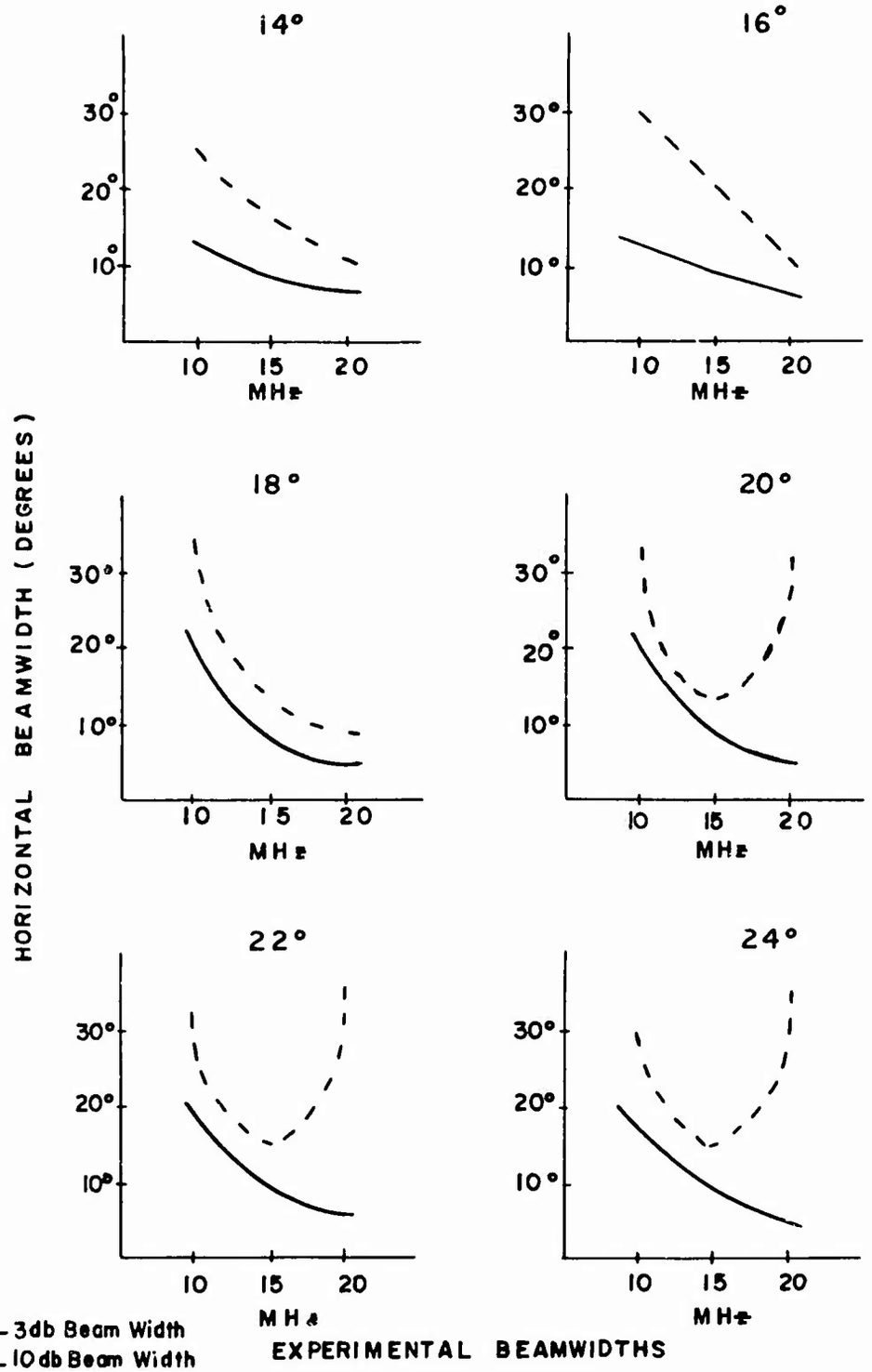

Figure III-58b

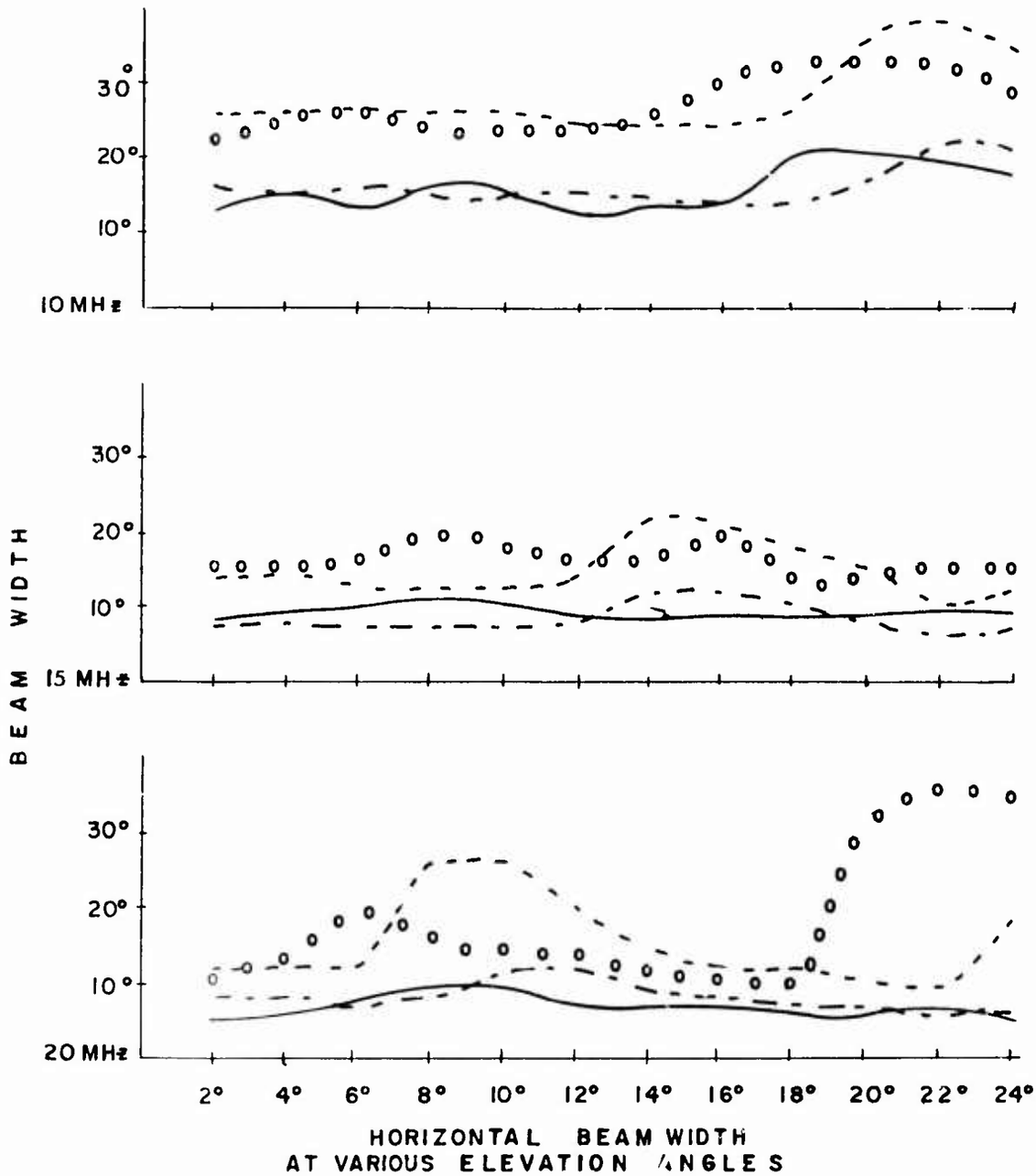

Figure III-59

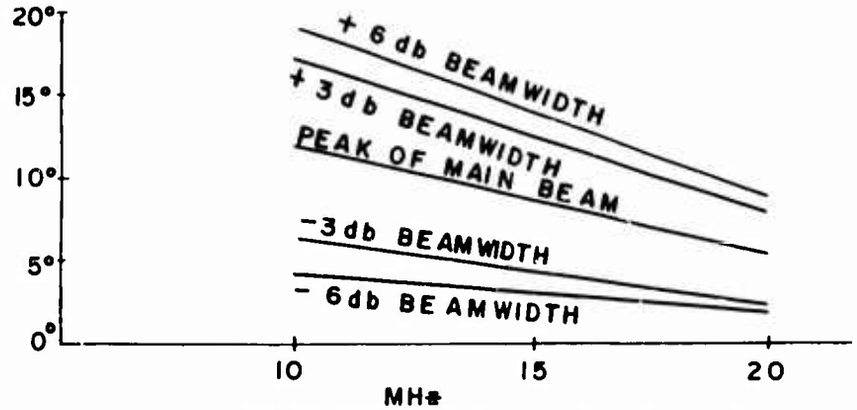

COMPUTED BEFORE MODIFICATION

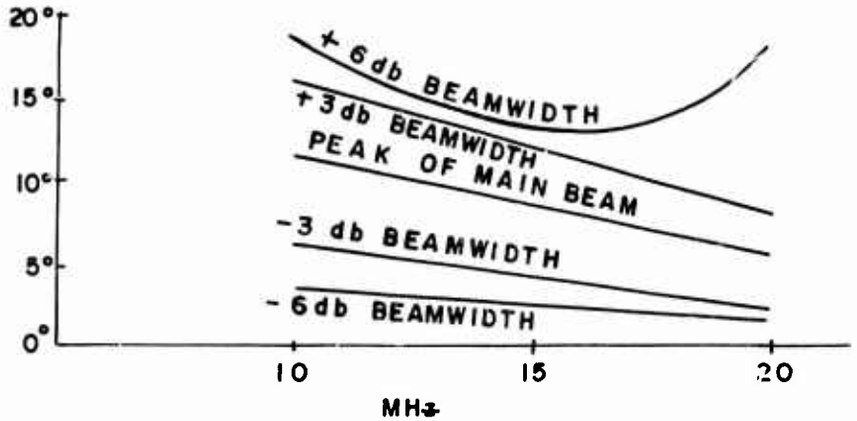

COMPUTED AFTER MODIFICATION

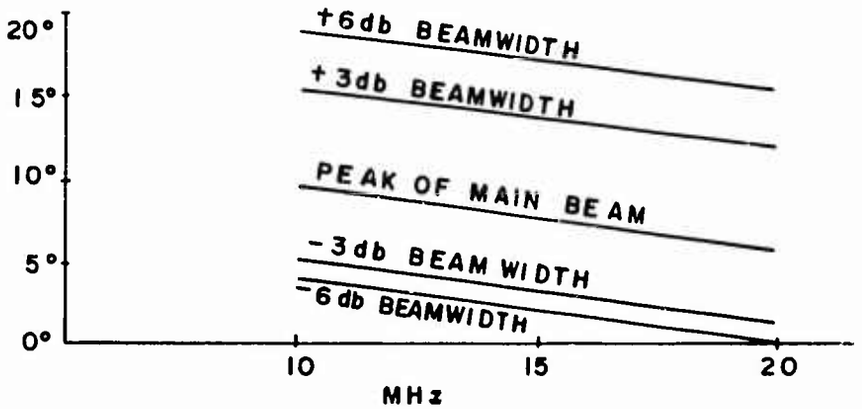

EXPERIMENTAL AFTER MODIFICATION

VERTICAL-PROFILE: BEAMWIDTH VS FREQUENCY

Figure III-60

computed after modification, at a particular frequency of operation, are not exactly coincident. This can be attributed to two possible causes. First, in the computed data, consideration was given to ground irregularities which might alter the apparent height of the antenna above ground and consequently its vertical profile. However, it is quite difficult to accurately approximate these effects; therefore the possibility of inadequate compensation is a very probable source of error. Secondly, the difference of .5 MHz between the computed and experimental frequencies at 10.0 MHz would account for a difference in the vertical profile peak position of 1° 39'. Correspondingly, the difference of 0.052 MHz between the computed and experimental frequencies at 20.0 MHz would account for a difference in the vertical profile peak position of 0° 26'. These values were obtained using the following equation from Williams.*

$$F_1 \ (H \ \Delta) = \sin (BH \sin \Delta)$$

where $B = \frac{2\pi}{\lambda}$

H = Antenna Height.

The above equation was solved for Δ when

F = 10 MHz,	H = 1.286 λ	to obtain	Δ =	11°	12'
F = 10.5 MHz	H = 1.507 λ	to obtain	Δ =	9°	33'
F = 20.0 MHz	H = 2.572 λ	to obtain	Δ =	5°	36'
F = 20.052 MHz,	H = 2.771 λ	to obtain	Δ =	5°	10'

It should be noted that these theoretical differences in peak position due to differences in frequency of operation are precisely those

*See Appendix

observed in Figure III-60. When comparing vertical experimental to computed beamwidths, the difference in relative peak positions should be taken into consideration. For example, in Figure III-60 the 10 MHz experimental pattern peaks at 10° and the computed at 12°. Therefore, when comparing the computed data of Figures III-57a and III-57b to the experimental data of Figures III-58a and III-58b, the 10° elevation pattern of Figure III-58a should be compared to the 12° computed elevation of Figure III-57a in order to make a valid comparison. Correspondingly the 12° and 14° experimental plots of Figures III-58a and III-58b should be compared respectively to the 14° and 16° plots of Figure III-57b.

Figure III-61 lists the experimental and computed 3 dB and 10 dB horizontal beamwidths at operating frequencies of 10 and 20 MHz. A close examination of this figure indicates a mean variation of 2.5° between the computed and experimental beamwidths.

SECTION IV

CONCLUSIONS

The experimental and computed data discussed, reflects a considerable degree of success in achieving the two primary objectives of this program. The first was to make the vertical antenna pattern frequency insensitive, i.e. to reduce the undesirable deep nulls in the vertical pattern profile and second, to reduce the first side lobe levels in the horizontal plane, to minimize the interference effects. It is well-known that increasing the antenna height will increase the

HORIZONTAL - BEAMWIDTH

EXPERIMENTAL Vs COMPUTED

	Freq. = 10 MHz				Freq. = 20 MHz			
Elevation Angle	Exp. 3 dB BW	Comp. 3 dB BW	Exp. 10 dB BW	Comp. 10 dB BW	Exp. 3 dB BW	Comp. 3 dB BW	Exp. 10 dB BW	Comp. 10 dB BW
2°	13°	15°	22°	25°	7°	8°	10°	12°
4°	14.5°	16°	25°	25°	6°	7°	13°	12°
6°	14°	15°	24°	25°	8°	8°	20°	24°
8°	13°	14°	23°	25°	9°	11°	16°	24°
10°	14°	15°	23°	24°	9°	12°	14°	20°
12°	12°	15°	22°	24°	7°	9°	13°	15°
14°	13°	14°	25°	24°	7°	8°	11.0°	11.5°
16°	13°	14°	30°	26°	6°	7°	10°	12°
18°	20°	17°	31°	32°	5°	7°	9°	10.8°
20°	20°	22°	31°	35°	5°	5°	28°	9°
22°	18.5°	21°	30°	35°	6°	6°	30°	18°

Figure III-61

number of nulls in the vertical pattern and hence reduce the reception of available propagating modes. The results of inclining the antenna allow for the reception of a greater number of propagating modes and the end-fire array reduces the high azimuth side lobe interference problems associated with a single horizontal rhombic antenna.

APPENDIX

Derivation of equations defining the height factor for both vertical (positive image) and horizontal (negative image) radiating elements.

In calculating height factors reference is made to Williams.

The resultant field at a point due to n coplanar elements is given by

$$E = k \sum_{1}^{n} I_n \angle \left[360° \left(\frac{dn}{\lambda} \right) \cos (\theta + \alpha n) + \beta_n \right] \qquad (1)$$

where

k = a constant depending on the distance to a field point and the frequency of radiation

I_n = current in antenna n

d_n = distance of antenna n from origin

α_n = angular position of antenna

β_n = relative phase of antenna current

θ = exploring angle of the polar diagram.

In calculating height factors for both vertical radiating elements (positive image) and horizontal elements (negative image), the following two special cases of the above equation are considered:

Positive images: Referring to Figure 1a the first case is obtained by putting $\alpha_1 = \beta_1 = 0°$ therefore

$$\left.\begin{array}{l} \alpha_1 = 0 \quad \beta_1 = 0 \\ \alpha_2 = \pi \quad \beta_2 = 0 \end{array}\right\} \text{ Cophasal for positive image case.}$$

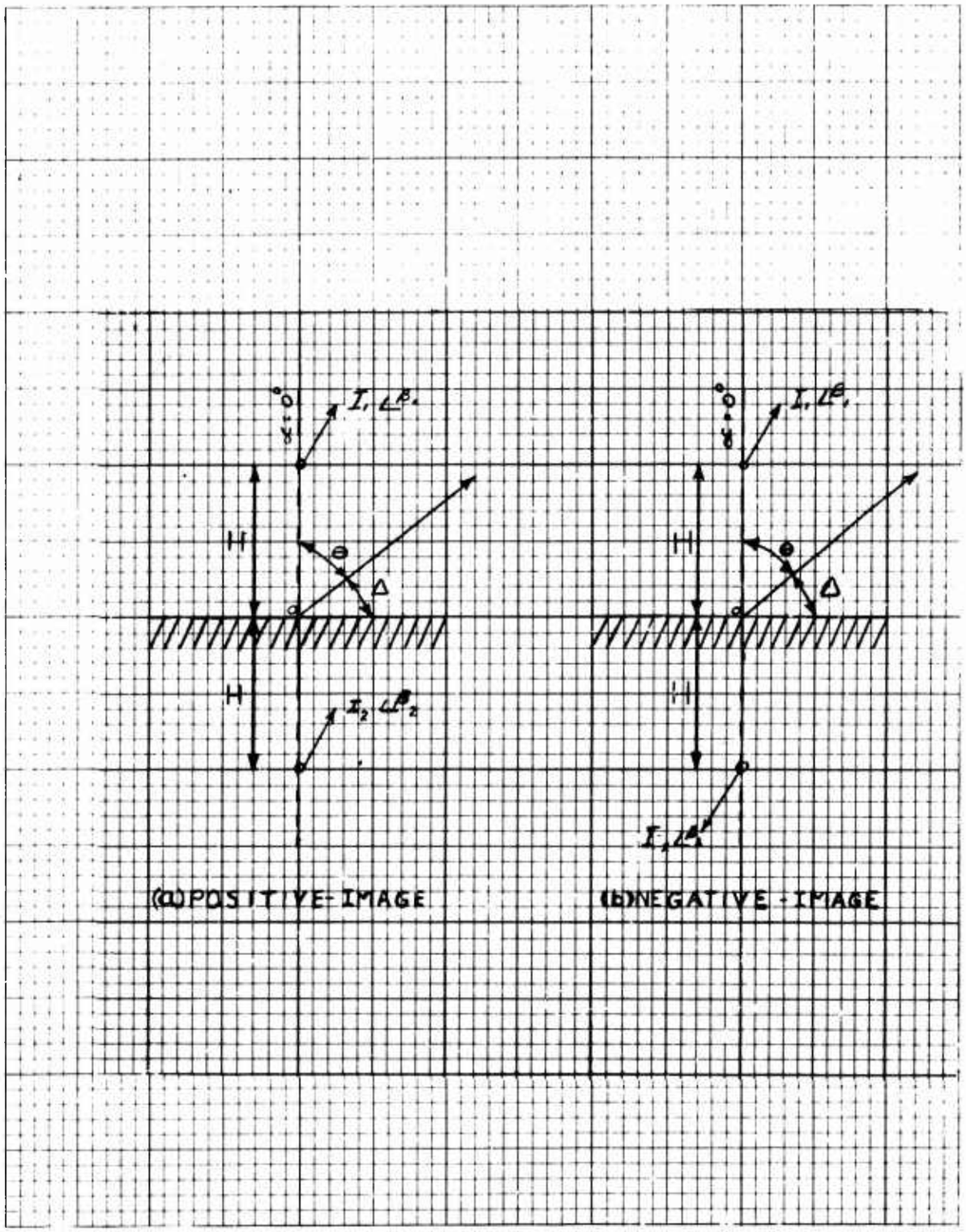

Figure 1a

Substituting the above values into Equation (1) and using radians instead of degrees, i.e. $\beta = \frac{2\pi}{\lambda}$ to turn lengths into radian measure, Equation (1) becomes:

$$E = k \left[I_1 \angle \left\{ 360° \left(\frac{d_1}{\lambda} \right) \cos (\theta + \alpha_1) + \beta_1 \right\} + I_2 \angle \left\{ 360° \left(\frac{d_2}{\lambda} \right) \cos (\theta + \alpha_2) + \beta_2 \right\} \right]$$

$$E = k \left[I_1 \angle \left\{ 360° \left(\frac{d_1}{\lambda} \right) \cos (\theta + 0) + 0 \right\} + I_2 \angle \left\{ 360° \left(\frac{d_2}{\lambda} \right) \cos (\theta + \pi) + 0 \right\} \right]$$

$$E = k \left[I_1 \angle \{ \beta H (\cos \theta) \} + I_2 \angle \{ \beta H \cos (\theta + \pi) \} \right].$$

where $\beta = \frac{2\pi}{\lambda}$ and $d_1 = d_2 = H$.

By use of the $\cos (\theta + \pi)$ trigonometric identity the above equation becomes

$E = k \left[I_1 \angle (\beta H \cos \theta) + I_2 \angle (- \beta H \cos \theta) \right]$ POLAR EQUATION.

This polar equation can be represented vectorally in the following way:

$E = k \left[I_1 \cos (\beta H \cos \theta) + I_1 \sin (\beta H \cos \theta) + I_2 \cos (-\beta H \cos \theta) + I_2 \sin (-\beta H \cos \theta) \right]$ VECTORIAL REPRESENTATION.

Simplifying and letting $I_1 = I_2$ we obtain:

$$E = 2k I_1 \cos (\beta H \cos \theta).$$

It is convenient to define a height function $F_1 (H, \theta)$ whose value gives the relative value of the polar diagram in a vertical plane. This may be done by putting $2KI$ equal to unity (normalizing) in the

above equation, which gives:

$$\left.\begin{aligned} F_1 (H, \theta) &= \cos (\beta H \cos \theta) \\ \text{or} \quad F_1 (H, \Delta) &= \cos (\beta H \sin \Delta) \end{aligned}\right\} \text{POSITIVE IMAGE}$$

where Δ = elevation angle,

Referring to Figure Ib, the second case, for horizontal elements (negative image), is obtained by again putting $\alpha_1 = \beta_1 = 0$ therefore

$$\left.\begin{aligned} \alpha_1 &= 0 \quad \beta_1 = 0 \\ \alpha_2 &= \pi \quad \beta_2 = \pi \end{aligned}\right\} \text{Antiphasal for negative image case.}$$

Proceeding as before:

$$E = k \left[I_1 \angle \{360° \left(\frac{d_1}{\lambda} \right) \cos (\theta + \alpha_1) + \beta_1\} + I_2 \angle \{360° \left(\frac{d_2}{\lambda} \right) \cos (\theta + \alpha_2) + \beta_2\} \right]$$

$$E = k \left[I_1 \angle \{360° \left(\frac{d_1}{\lambda} \right) \cos (\theta + 0) + 0\} + I_2 \angle 360° \left(\frac{d_2}{\lambda} \right) \cos (\theta + \pi) + \pi\} \right]$$

$$E = k \left[I_1 \angle \{\beta H \cos \theta + I_2 \angle \{ \beta H \cos (\theta + \pi) + \pi\} \right]$$

where $\beta = \frac{2\pi}{\lambda}$, $d_1 = d_2 = H$.

Again using the trigonometric identity the above equation becomes:

$$E = k [I_1 \angle(\beta H \cos \theta) + I_2 \angle(-\beta H \cos \theta + \pi)] \text{ POLAR EQUATION.}$$

This polar equation can be represented vectorially in the following way:

$$E = k [I_1 \cos (\beta H \cos \theta) + I_1 \sin (\beta H \cos \theta) + I_2 \sin (\pi - H \cos \theta) + I_2 \cos (\pi - H \cos \theta)],$$

Simplifying and letting $I_1 = I_2$ we obtain

$$E = 2kI_1 \sin (\beta H \cos \theta).$$

Normalizing as before, we obtain:

$$\left.\begin{aligned} F_1 (H, \theta) &= \sin (\beta H \cos \theta) \\ F_1 (H, \Delta) &= \sin (\beta H \sin \Delta) \end{aligned}\right\} \text{NEGATIVE IMAGE}$$

where Δ = angle of elevation.

References

Terman F. E., Radio Engineering, McGraw-Hill Book Company, Inc., New York (1947)

USAF Contract AF30(602)-1924 "Antenna Pattern Analyzer - Group AN/ASM-13" performed by Bendix Radio, Balt. MD.

Barnes C., "Full Scale HF Antenna Pattern Measurements Made with Transmitter Towed by Aircraft" Research Memorandum 9 to Contract DA-36-039-SC-87197 performed by Stanford Research Institute, Menlo Park, Calif. for USAERL Laboratory, Ft. Monmouth, NJ.

Barnes C., "Antenna Pattern Measurements of a Full-Scale Rhombic Antenna", supplement 2 to Research Memorandum 9 of Contract DA-36-039-SC-87197 performed by Stanford Research Institute, Menlo Park, Calif., for USAERD Laboratory, Ft. Monmouth, NJ.

Kraus J. D., Antennas, McGraw-Hill Book Company, Inc., NY (1950).

Final Report, USAF Contract AF30(602)-2881, "Rhombic Antenna Techniques" performed by Sanders Associates, Inc., Nashua, NH.

Williams, H. P., Antenna Theory and Design, Volume II, Sir Issac Petman and Sons, Ltd, London.